SYNTHESIS AND BIOLOGICAL EVALUATION OF PYRIMIDINE BRIDGED BIPHENYLS AS PUTATIVE LIGANDS TO TARGET PARKINSON'S DISEASE

A thesis submitted to the Central University of Punjab

For the Award of

Master of Pharmacy

In

Medicinal Chemistry

By

Manu Bala

(Reg. no. 16mpharm09)

Supervisor

Dr. Vinod Kumar

Department of Pharmaceutical Sciences and Natural Products

School of Basic and Applied Sciences

Central University of Punjab, Bathinda

June, 2018

DECLARATION

I declare that the thesis entitled **"SYNTHESIS AND BIOLOGICAL EVALUATION OF PYRIMIDINE BRIGDED BIPHENYLS AS PUTATIVE LIGANDS TO TARGET PARKINSON'S DISEASE"** has been prepared by me under the guidance of Dr. Vinod Kumar, Assistant Professor, Department of Pharmaceutical Sciences and Natural Products, School of Basic and Applied Sciences, Central University of Punjab, Bathinda. No part of this thesis has formed the basis for the award of any degree or fellowship previously.

Manu Bala
Department of Pharmaceutical Sciences and Natural Products,
School of Basic and Applied Sciences,
Central University of Punjab,
Bathinda – 151001
Date:

CERTIFICATE

I certify that Manu Bala has prepared her dissertation entitled **"SYNTHESIS AND BIOLOGICAL EVALUATION OF PYRIMIDINE BRIGDED BIPHENYLS AS PUTATIVE LIGANDS TO TARGET PARKINSON'S DISEASE"** for the award of M. Pharmacy (Medicinal Chemistry) degree from the Central University of Punjab, under my guidance. She has carried out this work at the Department of Pharmaceutical Sciences and Natural Products, School of Basic and Applied Sciences, Central University of Punjab, Bathinda.

Dr. Vinod Kumar
(Research Supervisor)
Assistant Professor
Department of Pharmaceutical Sciences and Natural Products,
School of Basic and Applied Sciences,
Central University of Punjab,
Bathinda- 151001
Date:

ABSTRACT

"SYNTHESIS AND BIOLOGICAL EVALUATION OF PYRIMIDINE BRIGDED BIPHENYLS AS PUTATIVE LIGANDS TO TARGET PARKINSON'S DISEASE"

Name of student	:	Manu Bala
Registration Number	:	16mpharm09
Degree for which submitted	:	M. Pharmacy (Medicinal Chemistry)
Supervisor	:	Dr. Vinod Kumar
Centre	:	Department of Pharmaceutical Sciences and Natural Products
School of Studies	:	Basic and Applied Sciences

MAO inhibitors have been explored as therapeutic agents for the treatment or management of PD. A series of 2,4,6-trisubstituted pyrimidine derivatives incorporating a propargyl moiety were synthesized and screened for their MAO inhibition potential using Amplex® Red assay. All the compounds showed good inhibitory activity for MAO-B. The structure-activity relationship profile has been developed with number of electron releasing and electron withdrawing substituents attached to the pyrimidine nucleus. **MV7** was found to be the most potent MAO-B inhibitor with IC_{50} value of 0.44 ± 0.02 µM. From molecular docking studies, it was found that compounds fit well in the active site of MAO-B isoform near FAD cofactor. Thus, the active compound **MV7** obtained in this series can act as promising lead for the development of effective and potent MAO-B inhibitor for the treatment of Parkinson's disease.

Manu Bala Dr. Vinod Kumar

ACKNOWLEDGEMENTS

First and the foremost I thank my Sai baba ji for his grace and mercy towards me and helping me at every stage of my work.

A very special thanks to my parents **Mr Kapoor Singh** and **Mrs Suman** for their love,support and sacrifices throughout the life for my studies and everything. I am very blessed to have such a lovely and supporting parents. I would also like to thank my brother **Mr. Vikrant** and sister **Miss. Anuradha** for their love and support.

I wish to express my warm and sincere thanks to **Prof. (Dr.) R.K. Kohli, Vice Chancellor and Prof. (Dr.) P. Ramarao, Dean Academic Affairs, Central University of Punjab, Bathinda**for his cooperation and allowing me to avail the essential infrastructure and library facilities and providing all the necessary facilities for carrying out the research work.

I would foremost like to express my heartfelt indebtness to my supervisor **Dr. Vinod Kumar**, Assistant Professor, Department of Pharmaceutical Sciences and Natural Products, for his patient guidance,constructive criticism, encouragement and valuable advices throughout my research and thesis writing.

I would also like to thank **Dr.Rajkumar Sir** and **Dr.Vikas Jaitak Sir**, **Dr.Pardeep kumar Sir**, **Dr.Venkat Rao Kaki Sir** ,Department of Pharmaceutical Sciences and Natural Products for their help and support through throughout my dissertation work.

I would like to thank my seniors **Ashish sir, Bhupinder Sir, Heena Ma'am, Gaurav Sir, Amit Sir, Sourav Sir,and Vijay Sir** for helping and supporting me throughout my M.Pharm.

I love to thank all my friends **Sachin, Amandeep, Arvind, Vishakha, Haris, Poornima, Neha, Aditi, Diksha, Partha, Souvik, Ashima, Sahil, Azhar** for the beautiful time we have shared throughout M.Pharm.

A sincere thanks and respect to **Mr. Rajesh Tiwari**, Junior Technical Assistant and **Mr. Reddy** for their generous help during my research period. The good wishes of all my well-wishers are gratefully acknowledged and sincere thanks to all the fellows who have helped me directly or indirectly.

MANU BALA

Dedicated to My Parents

And

my Sai Babaji

TABLE OF CONTENTS

LIST OF TABLES

LIST OF FIGURES

LIST OF SCHEMES

LIST OF APPENDICES

LIST OF ABBREVIATIONS

S. No.	Full Form	Abbreviation
1.	Monoamine oxidase	MAO
2.	Flavin Adenine Dinucleotide	FAD
3.	Parkinson's Disease	PD
4.	1,2,3,6-methyl-phenyl-tetrahydropyridine	MPTP
5.	Hydrogen peroxide	H_2O_2
6.	Amyotrophic Lateral Sclerosis	ALS
7.	Tyrosine	TYR
8.	Acetylcholinesterase	AChE
9.	Butyrylcholinesterase	BuChE
10.	Blood Brain Barrier	BBB
11.	Protein Data Bank	PDB
12.	Root Mean Square Deviation	RMSD
13.	Molecular Operating Environment	MOE
14.	Reactive oxygen species	ROS
15.	Dopamine	DA
16.	Nerve Growth Factor	NGF
17.	Glial cell line derived neurotropic factor	GDNF
18.	Brain derived neurotropic factor	BDNF
19.	Glyceraldehydes-3-phosphate dehydrogenase	GADPH
20.	Superoxide dismutase	SOD
21.	B-cell leukemia/lymphoma	BCL
22.	5-Hydroxytryptamine	5-HT
23.	Structure activity relationship	SAR
24.	Dimethyl sulfoxide	DMSO
25.	High Resolution Mass Spectroscopy	HRMS
26.	Nuclear magnetic resonance	NMR
27.	Gas chromatography-Mass spectrometry	GC-MS
28.	Thin layer chromatography	TLC

29.	Acetonitrile	ACN
30.	Potassium iodide	KI
31.	Potassium carbonate	K_2CO_3
32.	Dichloromethane	DCM
33.	Round bottom flask	RBF
35.	Dulbecco's modified Eagle's medium	DMEM
36.	Bovine serum albumin	BSA
38.	Doublet	d
39.	Singlet	s
40.	Multiplet	m
41.	Coupling constant	J

CHAPTER 1

INTRODUCTION

1. INTRODUCTION

The first clinical features of Parkinson's disease was described by a British surgeon, James Parkinson, in a monograph "An Essay on the Shaking Palsy", the first observations of patients affected by a disease he called "paralysis agitans"(Parkinson, 2002). Parkinson's disease (PD) is the second most common neurodegenerative disease. It is estimated that 1% of the individuals over the age of 65 are affected by Parkinson's disease. Worldwide incidence estimates of Parkinson disease range from 5 to >35 new cases per 100,000 individuals yearly.(Poewe et al., 2017)

Parkinson's disease (PD) is a chronic, slowly progressive, age-related neurodegenerative disease. It is characterized by tremor, rigidity, bradykinesia, akinesia and loss of postural reflexes. Some non-motor symptoms are also identified now which mainly occur at the very onset of disease.(Pandey, 2012). Although there are many motor symptoms that are taken as the main criteria for the diagnosis of PD , there are some non-motor symptoms such as impaired olfaction, sleep disorders ,constipation and some neuropsychiatric disorders like depression ,anxiety etc. which are prominent not only before but also during the onset of PD and its slowly progression(Chaudhuri & Schapira, 2009).

There are mainly two types of PD: sporadic (90-95%) and familial (5%).Familial PD is caused by rare highly age penetrant mutations inherited in an autosomal, recessive or dominant way. The biological effect of these mutations are enough for the development of this disease to occur. Sporadic PD is a complex disease in which various genetic variants all together with other genes play cumulative effect that causes the development of the disease(Sassi, 2011).

The pathological hallmark of Parkinson's disease is the loss of dopaminergic neurons in the substantia nigra pars compacta that lead to depletion of dopamine level in striatum and presence of Lewy bodies in other cells. (Hatano & Hattori, 2011).These intracytoplasmic inclusions are found in some other brain regions too such as the locus cerulus, cerebral cortex, and hypothalamus and nucleus basalis.

The major neuronal loss is still seen in SNpc which considerably lead to P.D(Feng, 2003). Within the substantia nigra, the ventrolateral neuronal cell groups are damaged the most, while dorsal and medial neuronal cells groups are resistant to the damage. The natural reason for specific damage of dopaminergic neurons may live in pacemaker-like properties of these cells, which leads to frequent intracellular calcium drifters. Calcium buffering is less in ventrolateral cells neurons than dorsal and medial cells neurons that leads to disruption of cellular homeostasis due to increased cellular stress. Cell death occurs due to interruption in normal virtue of nuclear membrane releasing some pro-aggregate nuclear factors (as histones) that triggers the α-synuclein aggregation. This aggregation further spreads to other cells by various means(Dickson, 2017).

The etiological factors in PD has changed surprisingly from one of a simply sporadic premise to the view that both environmental and genetics factors contribute to the onset of the illness to a point now where increasingly genetic predisposition is seen as a major contributor to the disease (Schapira & Jenner, 2011).

1.1 Environmental factors and PD

There are number of factors that causes development of PD such as exposure to various pesticides, herbicides, well water, industrial chemicals, living in rural environment, some exogenous toxins such as cyanide, trace metals, organic solvents, carbon monoxide and carbon sulphide. The most common environmental factor in P.D found to be 1,2,3,6-methyl-phenyl-tetrahydropyridine (MPTP). MPTP is a byproduct of synthetic narcotic meperidine analog(Olanow & Tatton, 1999). MPTP is highly lipophilic in nature and easily cross blood brain barrier, once it enters the brain MPTP gets converted to 1-methyl-4-phenyl-2, 3-dihydropyridinium (MPDP+) by enzyme MAO-B and then further into 1-methyl-4-phenylpyridium (MPP+) which is a toxic compound. MPP+ gets transported to dopamine neurons via DAT and exerts its toxic effect to dopaminergic neurons. MPP+ also inhibits mitochondrial transport chain component complex due to its accumulation in mitochondria (Przedborski & Vila, 2003).The inhibition of this complex leads to reduction of cellular

ATP which is the source of energy for the cells. Loss of cellular energy through various pathways lead to formation of superoxide radicals which likely causes the dopaminergic neuronal damage(Smeyne & Jackson-Lewis, 2005).

Another such factor is exposure to pesticides. Epidemiological studies have suggested that pesticides such as rotenone is a highly potent, lipophilic and high affinity specific inhibitor of complex 1. A continuous infusion of these toxic agents induced dopaminergic neuronal cell death and Lewy bodies in rodents which are similar to the P.D patients(Betarbet et al., 2000).

1.2 Genetic factors and PD

Numerous studies have focused on genetic factors associated with the P.D. Several genes have been identified that causes monogenic familial forms of P.D. The genetics of P.D are quite unpredictable with contribution of both Mendelian e.g. SNCA, LRRK2, PINK1 and non-mendelian factors e.g. single nucleotide polymorphisms. SNCA was the first identified gene in a familial form of PD that is located in the chromosome 4. Further, six point mutations were identified and described A53T, E46P, A30P, H50Q, G51D and A53E.These mutations intensify the natural tendency of alpha-synuclein to form fibrils which are toxic species. Parkin and PTEN-induced putative kinase 1PINK1 is another such mutated gene in early autosomal recessive PD. DJ1 i.e. Daisuke-Junko-1 when gets mutated leads to alteration in mitochondria shape and increase in ROS level. Vacuolar protein sorting 35 (VPS35) accounts for nearly 1% of familial PD. The major mutation among this is D620N (Delamarre & Meissner, 2017). Leucine rich repeat kinase 2 (LRRK2) is the gene that has 51 exons encoding LRRK2 or dardarin, a 2527 amino acid protein. Around 40 variants have been recognized in the gene and 16 among these are identified as pathogenic. Missense mutations among these genes have found to be the reason behind Mendelian PD so far. Studies among populations showed that LRRK2 mutations have been carried by 5-15% of autosomal dominant PD families.G2019S mutations is the most common mutation responsible for 7% familial

PD and also in 1-2% sporadic PD.Another mutation identified in LRRK2 is G2385R(Sassi, 2011).

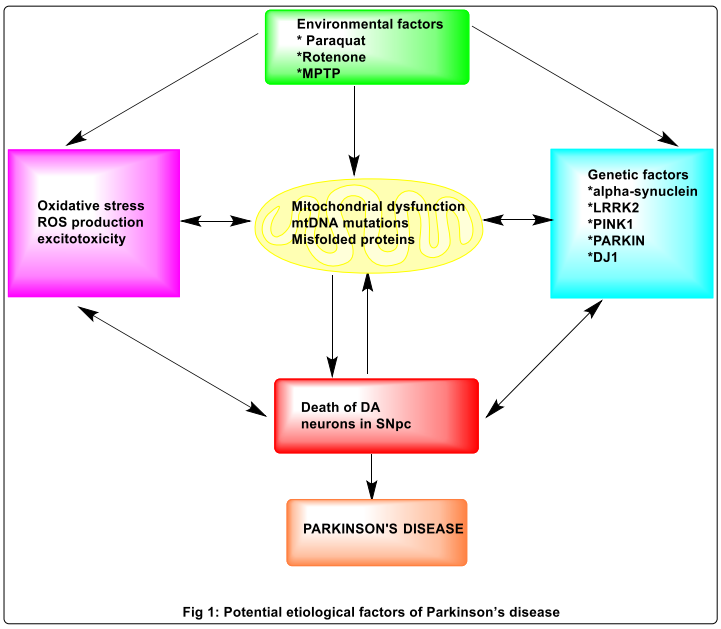

Fig: 1.1.0 Potential etiological factors of PD(Thal, 2015)

CHAPTER 2

REVIEW OF LITERATURE

2. REVIEW OF LITERATURE

2.1 Pathogenesis

2.1.1 Oxidative stress

Intracellular ROS is mainly generated by the mitochondrial electron transport chain and thus it became an important target for deleterious effects of ROS. Any damage to the mitochondrial respiratory chain effect the cell's ability to work as cellular metabolism depends upon the ATP supplied continuously through the mitochondrial respiratory chain. Mitochondria has its defense system that protects the cells by neutralizing the ROS and repairing the damage caused by ROS.ROS along with some proapoptotic proteins released from inter membrane space of mitochondria could prompt the activation of various cell death pathways (Gogvadze, Orrenius, & Zhivotovsky, 2006). There is increased generation of ROS due to redox cycling of catechol which causes oxidative stress in nigrostriatal dopaminergic neurons which are affected in PD(Dauer & Przedborski, 2003). Glutathione level is decreased in SNpc (substantia nigra pars compacta) of pre symptomatic PD that shows that oxidative stress takes place before the neuronal loss (Dexter et al., 1994).Mitochondrial complex I dysfunction due to reduction in the glutathione level SNpc depicts an interplay between mitochondrial functional impairment and oxidative stress(Chinta & Andersen, 2006). Redox environment can also be induced by DA in some specific regions of brain 6-hydroxydopamine, a derivative of DA (Dopamine agonist) is used experimentally to injure dopaminergic neurons. (Dauer & Przedborski, 2003).Selective susceptibility of dopaminergic neurons in SNpc can be due to the ability of DA to undertake oxidative stress itself. As DA is very reactive, it can be certainly oxidized and react further with the cellular components to form highly toxic ROS species(Jenner, 2007).Furthermore, nitrosative stress have also been found in postmortem brain tissues of PD patients(Tsang & Chung, 2009).Although oxidative stress have been found as major mechanism in PD but till now no such antioxidant therapy has been found and proven to cure PD clinically.

Studies have found that antioxidant therapy in combination can be an effective treatment for PD(Singh & Dikshit, 2007).

2.1.2 Protein aggregation

Protein aggregation and misfolding have been found to be a significant mechanism in PD. Each proteins involved in this disorder is linked to a characteristic aggregate of misfolded protein which appear to have toxic properties(Yacoubian & Standaert, 2009).The pathological hallmark of PD involves aggregation of some proteins such as alpha-synuclein as Lewy bodies. Specific genes like leucine rich repeat kinase (LRRK2), PTEN-induced putative kinase 1 (PINK1), DJ-1, Parkin (PRKN), P-type ATPase gene-ATP13A2 are found to be mutated(Thomas & Beal, 2007).A recent study suggested that pathogenic misfolding of alpha-synuclein followed by its aggregation and accumulation are fundamental to the disease process(Jones et al., 2015).Parkin is a ubiquitin E3 ligase protein whose function is to protect the neurons against the mutated alpha-synuclein(Petrucelli et al., 2002).Any mutations in PINK1 gene prompt neuronal death, mitochondrial dysfunction and different cellular functions(Kim et al., 2016). Mutations in DJ-1,PINK,parkin are associated with recessive parkinsonism(Thomas & Beal, 2007).LRRK2 associated PD is not clearly understood but it has been found that mutation in LRRK2 causes deposition of aggregated protein and degeneration of neurons. Protein accumulation is regulated by the two intracellular protein clearance pathways (ubiquitin-proteasome system /UPS) and autophagy. Some studies have reported that accumulation of proteins is due to overexpression of LRRK2 and its interaction with UPS(Lichtenberg, Mansilla, Zecchini, Fleming, & Rubinsztein, 2011)

2.1.3 Mitochondrial dysfunction

Mitochondria are extremely dynamic organelles which accomplish a many functions such as energy metabolism, various cellular process like regulation of calcium homeostasis, stress response and cell death pathways(Winklhofer & Haass, 2010).Energy loss is one of the hallmark of neurodegenerative disorders. Mitochondria also called as power house of cell is responsible for generation of ATP

which is essential for cell's chemical energy. Mitochondrial dysfunction leads to reduced level of ATP thus resulting in impaired cell functioning that leads to ROS generation. Any dysfunction of mitochondria effects neuronal normal functioning also as neurons are very active and are reliant on aerobic metabolism for energy. Mitochondria are also important for regulation of apoptosis(Norberg, Orrenius, & Zhivotovsky, 2010). Reduction in mitochondrial complex 1 activity in SNpc of a PD patient has been reported(Mann et al., 1994).Various environment factors like pesticides exposure, urban wastes, environmental toxins are involved in pathogenesis of PD.MPTP, a meperidine analogue is converted to MPP+ by MAO-B in glial cells where it further get transported via DAT and damage dopaminergic neurons (Dauer & Przedborski, 2003).Also high levels of mtDNA deletions were found in nigral neurons of a PD patients that leads to mitochondrial dysfunction(Kraytsberg et al., 2006). PINK1 and parkin, two autosomal recessive PD gene products, have significant roles in mitophagy, a cellular process to clear injured mitochondria. PINK1 triggers parkin to ubiquitinate external mitochondrial membrane proteins to prompt a selective degradation of injured mitochondria by autophagy(Hu & Wang, 2016).A study suggested that dopamine and related catechol amines can intermingle with α-synuclein and stabilize the protofibril phase of aggregation signifying the augmented vulnerability of dopaminergic neurons to destruction(Conway, Rochet, Bieganski, & Lansbury, 2001).Furthermore ,there were report on high level of iron and α-synuclein SNpc of a PD patient which lead to disease development(Zecca, Youdim, Riederer, Connor, & Crichton, 2004).Iron along with α-synuclein leads to increased generation of ROS that causes more toxic effects(Turnbull et al., 2001).Any mutation occurred in α-synuclein causes mitochondrial faults as well as proneness to oxidative stress(Martin et al., 2006).Two mitochondrial respiratory chain function enhancers coenzyme Q10 and creatine are undertaking clinical phase trials for the treatment of PD as these approaches can enhance mitochondrial function(Kones, 2010).

2.1.4 Calcium homeostasis

There are diverse channels and pumps that are located on the plasma membrane to pump the calcium outside and inside the cell**.** Cell physiology functions are maintained by these channels and pumps and any abnormality in this regulation lead to altered calcium homeostasis which promotes commencement of death signaling pathways. Calcium channel blocker could avoid aggregation of alpha-synuclein which might be calcium dependent such as trimethadione. Cells have widespread physiological functions so they need to tightly regulate Ca^{2+} homeostasis to elude extreme conditions leading to cell death. Reports suggested that neurotoxic effects of calcium have been extensively involved in brain diseases. Some other studies showed the significant role of calcium homeostasis in pathogenesis of PD(Goswami, Joshi, & Singh, 2017).Some authors have shown that Ca^{2+} dysregulation and oxidative stress supportively stimulate α-synuclein aggregation(Rcom-H'cheo-Gauthier, Goodwin, &Pountney, 2014).Unnecessary calcium leads to cell death by various pathways such as oxidative stress, mitochondrial dysfunction, dysregulated calcium signaling and ER stress(Marambaud, Dreses-Werringloer, & Vingtdeux, 2009).Toxic metabolites of dopamine, endoplasmic reticulum stress and apoptosis are found to be some other mechanism that are involved in PD pathogenesis(Goswami et al., 2017).

2.2 Current approaches in the treatment of Parkinson's disease

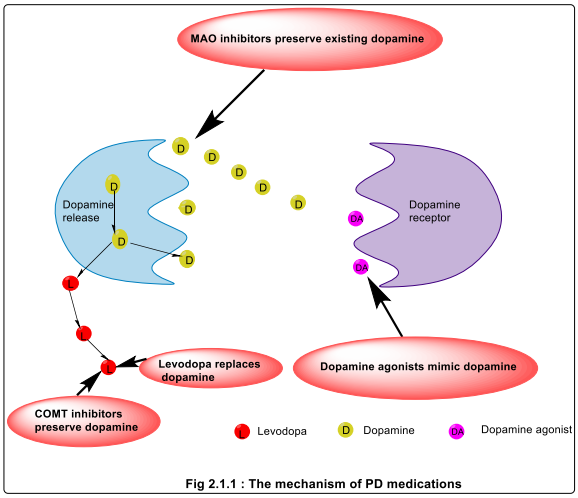

Fig 2.1.1 : The mechanism of PD medications

2.2.1 Dopamine precursor

Striatal dopamine insufficiency in Parkinson's disease (PD), first described in 1960, was a crucial event that led to the era of levodopa therapy. Since then it is an integral component of combination therapies. Levodopa (L-DOPA) that gets biosynthetically converted to dopamine by aromatic L-amino acid decarboxylase (AADC) is commonly given to enhance dopamine level in PD patients(Tolosa, Martí, Valldeoriola, & Molinuevo, 1998). Levodopa is likely to lose its efficacy over time with greater than 80% of patients on therapy for longer than 10years suffering dyskinesia and ‘on-off’ episodes. Carbidopa is frequently given in combination to decrease systemic metabolism of L-DOPA that helps to use low doses of L-DOPA while preserving efficacy and decreasing side effects like nausea(Ellis & Fell, 2017).

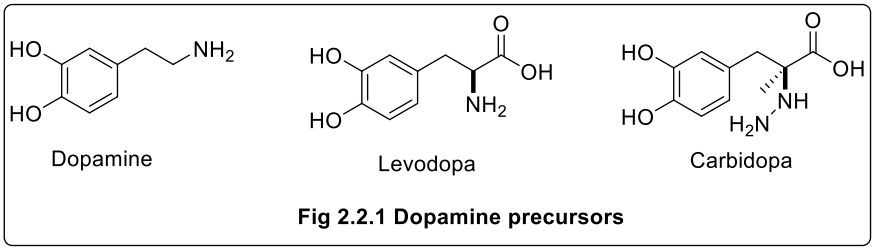

Fig 2.2.1 Dopamine precursors

2.2.2 MAO inhibitors

The monoamine oxidase (MAO) enzyme consist of two isoforms, MAO-A and MAO-B which are present in utmost human tissues comprising brain, liver and heart. These enzymes have vital roles in the metabolism of neurotransmitter amines and thus these are an important drug target for disease conditions that occur due to deficiency of these particular neurotransmitters. While reduction in central serotonin which is a substrate of MAO-A is linked with depression, Parkinson’s disease is associated with decrease in level of central dopamine, thus MAO-B inhibitors proved to be useful to inhibit dopamine metabolism, a strategy frequently combined with L-DOPA which is metabolic precursor of dopamine(Chirkova et al., 2016). Some approved MAO-B inhibitors include selegiline and rasagiline which are both irreversible inhibitors(Ellis & Fell, 2017).

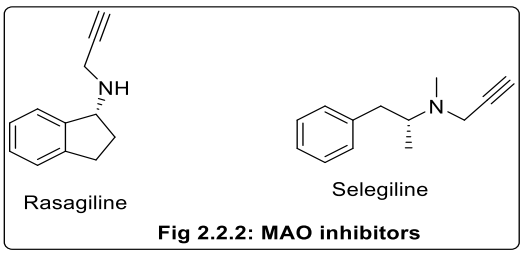

Fig 2.2.2: MAO inhibitors

2.2.3 COMT inhibitors

COMT is a broadly distributed enzyme in the brain, liver, kidney, gastrointestinal tract and erythrocytes. It is found in glial cells of brain but not in nigrostriatal dopaminergic neurons. Its function is not precise to dopamine system and also it not involved in peripheral metabolism of othercatecholamines(Encarnacion & Hauser, 2010). It catalyzes a corresponding pathway converting dopamine into 3-methoxytyramine which further get oxidized by MAO-B to produce homovanillic acid. Inhibition of COMT leads to an increase in dopamine level in brain that causes less motor symptoms and thus these have been used for PD management over the previous two decades in combination therapy.Entacapone and tolcapone are two popular approved COMT inhibitors used(Ellis & Fell, 2017).

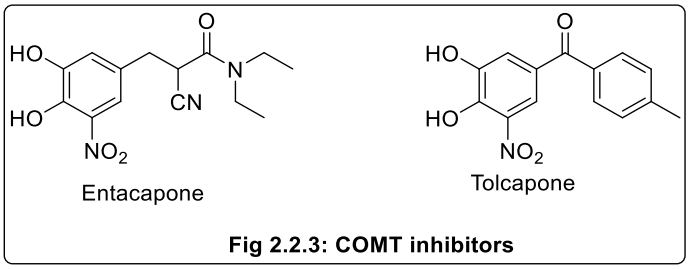

Fig 2.2.3: COMT inhibitors

2.2.4 Dopamine agonists

Dopamine receptors belong to two classes of GPCR i.e. G-protein coupled receptors, D1 and D2 classes. The organization of DA receptors was mainly based on their effects on adenylyl cyclase (AC) activity and cyclic adenosine monophosphate (cAMP) accumulation in the cells. The D1 receptor subtypes stimulate while the D2 subtypes inhibit AC activity and cAMP production. Studies showed that D1 and D2 constitutes two different classes of receptors also molecular

cloning confirmed this. Receptor subtypes have been allocated to the D1 receptor class (D1A/D1 and D1B/D5) of mammals despite the fact that other types (D1C and D1D) exist in non-mammalian vertebrates and similarly three types (D2, D3 and D4) of the D2 class have been isolated. The D1 and D2 receptors constitute the foremost DA receptor subtypes and they are differentially expressed in several areas of the human brain(Radad, Gille, & Rausch, 2005). Dopamine agonists are the agents that act on dopamine receptors to intensify the effects of dopamine. Some approved potent agonists are Apo morphine, bromocriptine, ropinorole, pramipexole and rotigotine. Each of these drugs are potent agonist of D2- like receptors with a number of having some balance of D1-like agonism(Ellis & Fell, 2017).

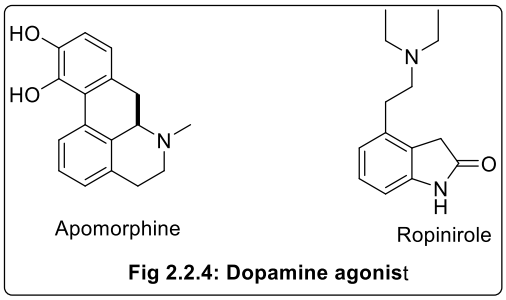

Fig 2.2.4: Dopamine agonist

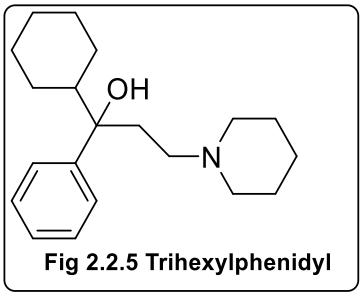

Fig 2.2.5 Trihexylphenidyl

2.2.5 Anticholinergics

Anticholinergics modify the activity of acetylcholine that is involved in regulation of movement, instead of acting directly on the dopaminergic system. This have beneficial impacts on tremor and dystonia in PD patients. Two approved drugs that decrease the activity of acetylcholine are benzatropine and trihexiphenidyl (Fig 2.2.5)(Ellis & Fell, 2017).Some other approved therapies include Amantadine, which is a NMDA glutamate receptor antagonist which is recommended for mitigation of dyskinesia in PD but its efficacy was questioned(Crosby, Deane, & Clarke, 2003).

2.3 MAO inhibitor as a target in Parkinson's Disease

Monoamine oxidase (MAO, EC 1.4.3.4) is a Flavin adenine dinucleotide dependent enzyme. It is mainly responsible for the deamination of monoamine neurotransmitters xenobiotics and endogenousaminesinthe Central and peripheral

nervous systems(Legoabe, Petzer, & Petzer, 2012).The MAO enzyme exist in two isoforms i.e. MAO-A and MAO-B where in MAO-A isoform is mainly present in liver, gut, skin and placenta whereas MAO-B is the key isoform in the brain. Human MAO-A and MAO-B isoforms comprises of amino acid sequences that are 70% identical, though, they differ in tissue distribution, inhibitor selectivity and substrate specificity. MAO-A has substrate specificity for the massive endogenous amines like serotonin, epinephrine and norepinephrine however MAO-B has substrate specificity for the small exogenous amines such as benzylamine, ß-phenyl ethylamine(Juárez-Jiménez et al., 2014). Dopamine and tyramine are mutual substrates for both the isoforms.

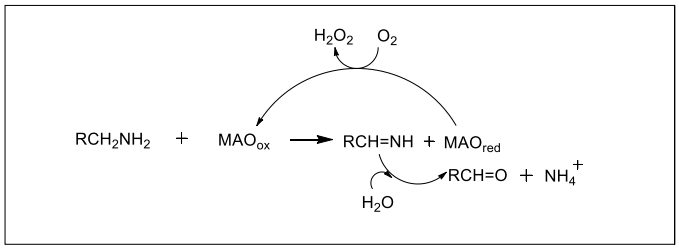

Fig 2.3.1 General mechanism of catalytic action of MAO enzyme.

MAO-B is the major isoform in the brain and with the aging its expression in the glial cell can rise up to four-fold. Parkinson's disease (PD) is linked with the affected basal ganglion are where MAO-B isoform appears to be expressively responsible for the metabolism of dopamine(Cerqueira, Netz, Diniz, do Canto, & Follmer, 2011). Thus, inhibitors of MAO-B isoform have been used in the management and treatment of PD.X-Ray co-crystal structure of two isoforms of MAO enzyme that areMAO-A and MAO-B are shown in Figure: Fig 2.3.2

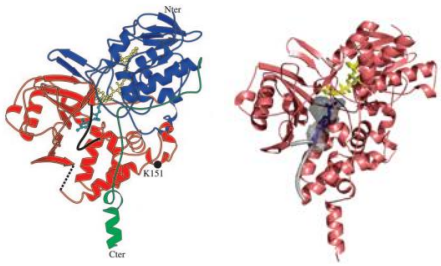

MAO-A (2BXR) MAO-B (2V5Z)

Fig 2.3.2: Crystal structures of both MAO-A and MAO-B

The MAO enzyme is bounded covalently to co-factor FAD at cysteine residue by an 8-alpha (s-cysteinyl) riboflavinlinkagewithhighlywell-maintainedstructure(Santana et al., 2006). The X-ray crystal structure studies showed that the human MAO-A exists as monomeric unit while MAO-B exist as dimeric unit(Sachs & Engelman, 2006). The MAO-A and MAO-B both isoforms have cavities with volumes of 400 A and ~700 A respectively.Further, MAO-B cavity is divided into two parts i.e. entrance cavity of volume 290 A and substrate cavity of volume ~400A(Zaib et al., 2015).The two cavities of MAO-B isoform are separated by Ile199 and Tyr326 side chains .There is difference in the structure of active site of human MAO-A and MAO-B isoforms which is due to the alteration in 7 out of 20 amino acid residues that line the active site of the enzyme and a change in the cavity shaping loop 210-216(Kumar, Prakash Gupta, & Kumar, 2017). Cavities of both the isoforms are hydrophobic in nature but MAO-B isoform comprises of a small highly preserved hydrophilic area in the entrance cavity (Kumar et al., 2017)

2.3.1 MAO-B inhibition and its role in neuroprotection

The MAO enzyme plays its major role in oxidative deamination of a extensive range of biogenic and xenobiotic amines, as well as DA, noradrenaline, adrenaline, tyramine, serotonin, ß-phenyl ethyl-amine, N-methylhistamine, benzylamine, also methoxy metabolites of the parent amines, such as metanephrine and normetanephrine. MAO inhibitors were initially clinically used in the treatment of depressive disease.(Deshwal, Di Sante, Di Lisa, & Kaludercic, 2017).MAO-B inhibitor's role in neuroprotection has been postulated to be multidimensional based on in vitro studies, and may comprise of inhibition of ROS production, increase of neurotrophic factors in neurons and glia, or up regulation of anti-apoptotic factors.(Pienaar, Dexter, & Burkhard, 2010) Another possibility is that activity of MAO-B rises certainly with age due to which there is increased oxidative stress which is a possible cause of neuronal dysfunctioning.(Herrera, Muñoz, Steinbusch, & Segura-Aguilar, 2017).By inhibiting hyperactive MAO-B enzyme and reducing its concentration may help in the neuroprotection and is able to lessen the Parkinson's affects.(Liu et al., 2017)

2.4 Recent advances in the treatment of Parkinson's Disease

Some recent identified promising MAO inhibitors are as follows:

In a recent study Wang et al synthesized a series of 31 compounds (Fig 2.4.1) and showed that most of the representative benzyloxy substituted derivatives possessed selective and potent MAO-B inhibitory activities as well as neuroprotective properties in a 6-OHDA and rotenone treated PC12 cells. Furthermore, the selected compounds showed no major cytotoxicity instead when they were evaluated for ADMET in silico properties they showed good oral absorption and BBB permeability. The compound 2.4.1b (Fig 2.4.1) showed most promising results with low toxicity. Based on these results they proved that compound 13 with IC_{50} 12.34 ± 1.62 in Nano molarand other benzyloxy substituted MAO-B inhibitors could be a promising drug candidate for the treatment of PD(Wang et al., 2016)

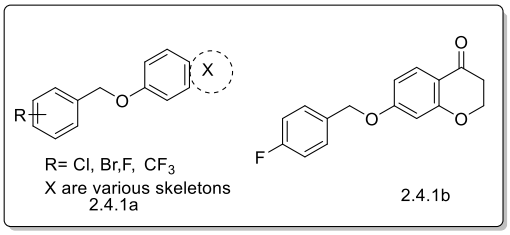

Fig: 2.4.1

Further, a recent study reported a series of 2H-1, 3-benzoxathiol-2-one analogues as potent MAO-B inhibitors with IC_{50} values ranging from 0.003 to 0.051 µM. Dialysis studies showed that two of this series analogues showed relatively potent MAO-A inhibition activity. Also it was observed that a selected analogue is a reversible MAO-A inhibitor. Compounds (Fig: 2.4.2) with dual MAO-A/B inhibition properties can be predominantly appropriate where depression is a comorbidity of PD(Mostert, Petzer, & Petzer, 2016).

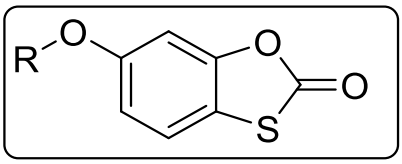

R		IC_{50} (µM)	
		MAO-A	MAO-B
1.	3-$Cl_6CH_4CH_2$	0.424 ± 0.0092	0.004 ±0.0003
2.	4-$Cl_6CH_4CH_2$	0.189 ± 0.012	0.003 ± 0.0001

Fig: 2.4.2

Van der's group reported and showed that for the first time a series of benzyloxynitrostyrene class of compounds that act as inhibitors of MAO-B and have good potencies when compared with reversible inhibitors as safinamide and the irreversible inhibitors selegiline and rasagiline. A series of novel 3-benzyloxy-β-nitrostyrenes were synthesized and were found to be highly potent MAO-B inhibitors with IC_{50} values in low nanomolar range 39-565nM. Among these compounds anIC_{50}= 0.039µM, the 4"-F substituted 3-benzyloxy-β-nitro styrene was identified as the most potent inhibitor (Fig: 2.4.3). These compounds exhibit similar binding modes to human MAO-B as safinamide due to their structural similarity with it. Further it was examined that substitution with bulky groups like Br, CF_3, and CH_3 led to lower MAO-B inhibition. Thus, they concluded this class can be a promising leads for development of reversible and selective MAO-B inhibitors for treatment of PD(Van der Walt, Terre'Blanche, Petzer, & Petzer, 2017).

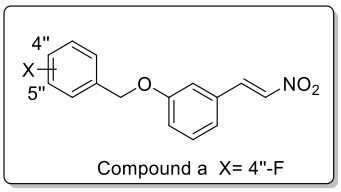

Fig: 2.4.3

Also, a study reported that chalcones which are well known for its MAO inhibition activity when incorporated with hetero aromatic substituents inhibit MAOs forming number of compounds that showed potent and specific MAO-B inhibition. The study investigated the MAO inhibitory properties of 2-heteroarylidene-1-indanone

derivatives and found that these were specific MAO-B inhibitors with two of the compounds showing potent activities. Further, these derivatives displayed reversible inhibition of MAOs (Fig: 2.4.4) Although the reversibility of the MAO inhibition was not tested but it was likely that 2-heteroarylidene-1-indanones are reversible MAO inhibitors since the related 2-benzylidene-1-indanones were already found to act reversibly(Nel, Petzer, Petzer, & Legoabe, 2016).

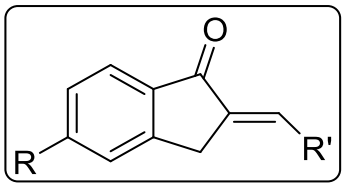

COMPOUND	R	R’	IC_{50} (µM)	
			MAO-A	MAO-B
1.	OCH_3	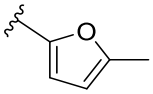	4.73 ± 0.190	0.026 ±0.005
2.	OCH_3	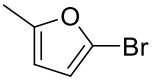	0.183 ± 0.038	0.0044 ± 0.0006

Fig: 2.4.4

Costas-Lago group synthesized compounds of hybrid structure pyridazine-coumarin, which were found to be potent, selective and reversible inhibitors of MAO-B. The compounds were synthesized following a multistep approach which based onKnoevenagel reaction and using pyridazinone as key intermediate. Among all, two compoundsboth substituted with a bromine atom in the pyridazinyl fragment were found to be the most promising and active compounds of the series synthesized, with IC_{50} values in the sub-micro molar range (Fig: 2.4.5a). Theoretical calculation of ADME properties of the compounds also proposed a good pharmacokinetic profile for both compounds(Costas-Lago et al., 2017).

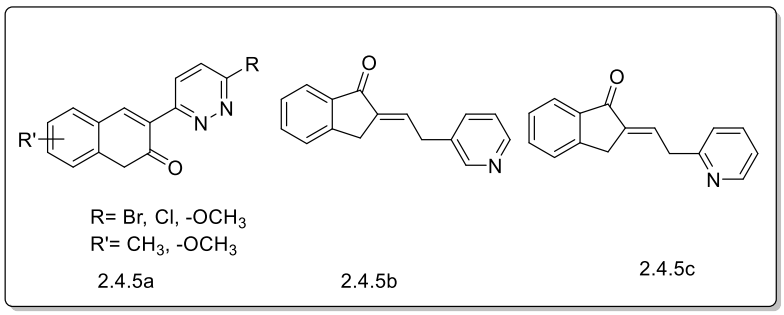

Fig: 2.4.5

Nel group synthesized a series of fifteen 2-heteroarylidene-1-indanone derivatives as monoamine oxidase (MAO) A and B inhibitors. Structurally these compounds are related to series of heterocyclic chalcone derivatives which have earlier been shown to act as MAO-B specific inhibitors. The 2-heteroarylidene-1-indanones are in vitro inhibitors of MAO-B, showing IC_{50} values of 0.0044–1.53 μM and mainly compounds 2.4.5b and 2.4.5cwere reported as the MAO-A isoform inhibitors with IC_{50} values 0.061±0.006μM and 0.853±0.051μM. (Nel et al., 2016)

Chen et al synthesized a series of novel and selective hMAO-B inhibitors with novel scaffold of tricyclic pyrazolo [1, 5-d] [1, 4] benzoxazepin-5(6H)-one. Compound 2.4.6a (IC_{50}=221 nM) exhibited the best inhibitory activity and isoform selectivity against hMAO-B which they found to be superior to selegiline (IC_{50}=321 nM), which is a commercially used in PD(Fig: 2.4.6).Also, their data supported further studies to assess rational design of more efficiently selective h-MAO-B inhibitors(R. Chen et al., 2016).

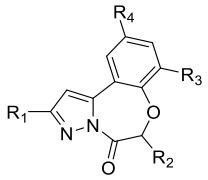

Compound	R_1	R_2	R_3	R_4	MAO-A (nM)	MAO-B (nM)
2.4.6a	4-F-Ph	CH_3	H	H	Inactive	221 ± 28

Fig: 2.4.6

Fioravanti group synthesized a series of 1-methyl-3, 5-diphenyl-4, 5-dihydro-1H-pyrazoles and assessed their inhibitory efficacy towards the two hMAO isoforms i.e. A and B. Most of the derivatives were found to be potent and selective hMAO-B inhibitors. In particular, derivative A showed greater hMAO-B affinity than selective inhibitor selegiline coupled with high selectivity index (SI = 145) (Fig 2.4.7). The most selective hMAO-B inhibitor was the 3-methyl analogue B with an SI higher than 909.(Fioravanti et al., 2013)

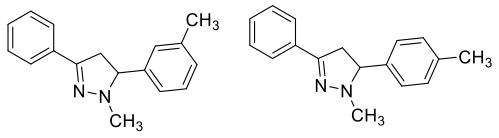

1.

2.

	SI	MAO-A (IC_{50} µM)	MAO-B(IC_{50} µM)
1	> 909	----------	0.11 ± 0.01
2	145	1.39 ± 0.07	0.0096 ± 0.0003

Fig 2.4.7

2.4.2 Pyrimidines derivatives as MAO inhibitors

Pyrimidine is an important six membered heterocyclic structure, present in various bioactive compounds(Fumagalli, Lecca, Abbracchio, & Ceruti, 2017).This scaffold was found to be a remarkable synthon and a variety of novel heterocycles with excellent pharmaceutical profile can be designed from this.(Jain et al., 2016).Mathew et al. synthesized a series of novel (1H)-benzimidazole bearing pyrimidine-trione (Fig2.4.8, a) based MAO-A inhibitors and screened in vitro for antidepressant activity,(Mathew, Suresh, & Anbazhagan, 2016). Altomare et al. reported condensed pyrimidines (Fig. 2.4.8, b and c) derivatives for their MAO-B inhibitory activity and found potent MAO-B inhibitors with little or no affinity for MAO-A isoform(Altomare et al., 1998).The same research group also reported on the synthesis of new pyridazine-, pyrimidine- and 1,2,4-triazine-containing tricyclic derivatives (Fig. 2.4.8, d and e) as potential MAO-B inhibitors(Carotti et al.,

2007).Rasagiline [N-propargyl-l(R)-aminoindan], is a potent second generation irreversible MAO-B inhibitor and it has been found that the propargyl group present in the molecule plays a crucial role in the MAO-B inhibitory. Activity(J. J. Chen, Swope, & Dashtipour, 2007). In the structure-activity relationship studies, it has been established that the propargyl group promotes neuronal survival via neuroprotective/neurorescue pathways(Weinreb et al., 2009).

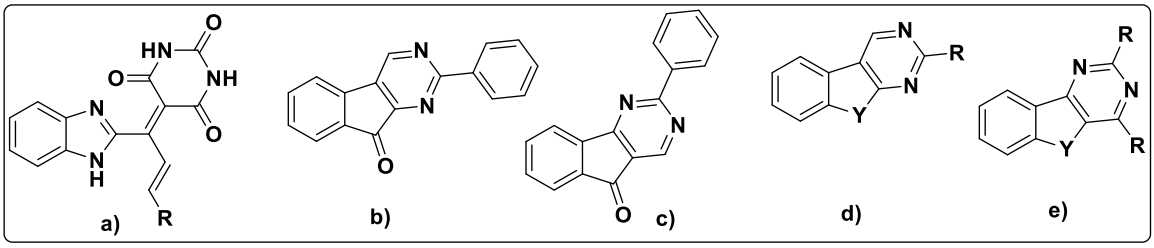

Fig. 2.4.8 Some earlier reported pyrimidine derivatives as MAO inhibitors

CHAPTER 3

RATIONALE

3. RATIONALE

MAO inhibitors can block the catalytic activities of the enzyme and terminate the catabolism process of monoamines. The concentration of the monoamine neurotransmitters such as dopamine, serotonin etc. which are stored in nerve terminals can be improved by inhibition of MAO enzyme. Thus MAO inhibitors can be developed as therapeutic agents in the disease state where MAO enzyme is overexpressed. MAO catalyzes the metabolism of monoamine neurotransmitters that generates hydrogen peroxide, toxic aldehydes and hydroxyl free radicals which causes neuronal damage and death. MAO inhibitors halt the production of these neurotoxic byproducts by halting monoamine oxidation process and thus stops the resulting damage to the neurons. So, MAO inhibitors are proposed as potential neuroprotecting agents.(Tripathi, Upadhyay, Paliwal, & Saraf, 2018). From study of the crystal structures of both MAO isoforms it has been established that pocket of MAO-A isoform interacts mainly with smaller and polar ligands while bulky and hydrophobic ligands show selectivity for MAO-B isoform. Recent literature studies showed that rasagiline is an effective drug that is in phase II clinical trial against MAO enzymes for the treatment of PD. The propargyl moiety of the drug binds with the receptor. Therefore, the aim of this project was to design and synthesize propargyl based compounds as potent MAO inhibitors acting against MAO enzyme. To achieve the goal of developing an effective drug candidate against PD we designed compounds by incorporating the propargyl moiety which serves as an essential group in MAO - inhibitors like selegiline and rasagiline, with the following considerations:

a) Addition of a propargyl moiety for escalating potency.

b) The aromatic ring for better interactions with the receptor improving affinity.

c) A pyrimidine linker serving as connecting link between actophoric propargyl moiety and haptophoric aromatic ring.

d) Substitutions of aromatic ring with various groups to generate the structure-activity relationship data of MAO inhibitors.

CHAPTER 4

AIM AND OBJECTIVES

4. AIM AND OBJECTIVES

- Synthesis of pyrimidine bridged biphenyls to target MAO enzyme
- in silico studies of the synthesized molecules with MAO-A (2BXR) and MAO-B (2V5Z) enzymes.
- in vitro screening of synthesized compounds as MAO inhibitors.

CHAPTER 5

MATERIAL AND METHODS

5. MATERIALS AND METHODS

5.1 General: Synthesis

All the reagents and solvents were purchased from Sigma-Aldrich, Spectrochem Pvt. Ltd., Avra Synthesis (AR/GR quality) and were used without further purification. Sartorius analytical balance (BSA224S - CW) was used for the weighing purposes. JSGW heating mantle for reflux reactions and ILMVAC rotary evaporator, were used for evaporating the organic solvents. The progress of the reactions was monitored by TLC, using either petroleum ether/ethyl acetate as the mobile phase on pre-coated Merck TLC plates or glass TLC plates in JSGW UV/fluorescent analysis cabinet and/or iodine chamber. Melting points were recorded on Stuart melting point apparatus (SMP-30) with open glass capillary tube and were uncorrected. Compounds were purified using flash chromatography (Biotage) / column chromatography (Unless otherwise stated, chromatography was conducted using high-purity grade, pore size 60 – 120 mesh particle size, 35 - 75 µm particle size, Silica, to obtain the pure desired product). Mass (EI) spectra were recorded on Shimazdu at Central University of Punjab. NMR of compounds were recorded on 400 MHz and 100 MHz NMRspectrometer at SAIF, IIT Ropar (Punjab, India).

5.1.1General procedure for synthesis of intermediates

To propargyl bromide (1.2 eq.) substituted acetophenone (2 g) was added in the presence of potassium carbonate as base (2.4 eq.) and potassium iodide as catalyst (0.5 eq.) and acetone (30 ml) as solvent. The reaction mixture was refluxed for 12 h at 60° C. The progress of reaction was monitored via TLC. After completion of reaction excess of solvent was evaporated from mixture, concentrated under vacuum using rotary evaporator, extracted with ethyl acetate (10 mL × 3), and washed with $Na_2S_2O_3$ in water, brine, dried over anhydrous Na_2SO_4 and obtained organic layer was then concentrated under vacuum using rotary evaporator. General reaction procedures for the synthesis of alkylated intermediates have been described in Figure: 5.1.1

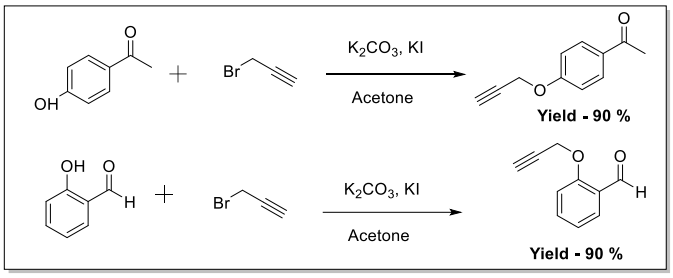

Fig 5.1.1 Synthesis of alkylated intermediates.

5.1.2 General procedure for the synthesis of chalcones

To substituted aldehyde (1 g) substituted ketone was added (1 g), along with the addition of sodium hydroxide (20 %) as base and methanol (10 mL) as solvent. The reaction mixture was stirred for 4 h at room temperature. The completion of reaction was monitored via TLC. After completion of reaction excess of solvent was evaporated from mixture, concentrated under vacuum using rotary evaporator. The chilled water was poured in reaction mixture and precipitates obtained were filtered and dried. The synthesized chalcones have been enlisted in Figure 5.1.2

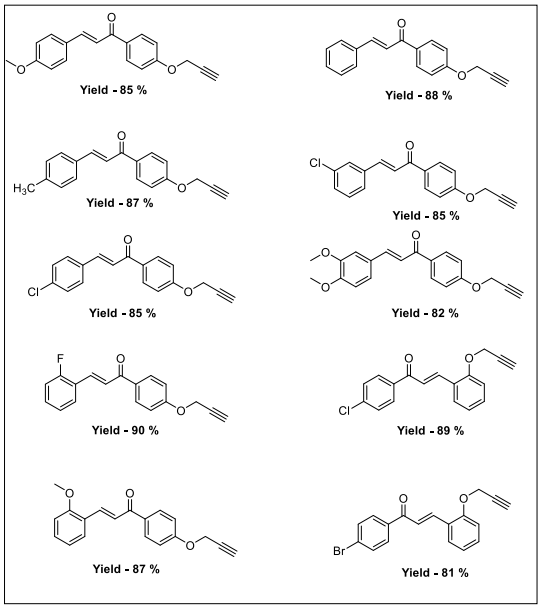

Fig 5.1.2: List of chalcones synthesized by Claisen-Schmidt condensation.

5.1.3 General procedure for the synthesis of proposed compounds

To chalcone (500 mg), benzamidine (1.2 eq.) was added along with the addition of anhydrous sodium carbonate (2.4 eq.) as base and acetonitrile (5 mL) as solvent. The reaction mixture was refluxed for 48 h at 85˚ C (Figure 5.1.3). The progress of reaction was monitored via TLC. After completion of reaction excess of solvent was evaporated from mixture, concentrated under vacuum using rotary evaporator, extracted with ethyl acetate (10 mL × 3), washed with water, brine, dried over anhydrous Na_2SO_4, obtained organic layer was then concentrated under vacuum using rotary evaporator and purified via column chromatography (EtOAc: Pet ether). The final compounds were further characterized by m.p., mass spectrometry and NMR spectroscopy.

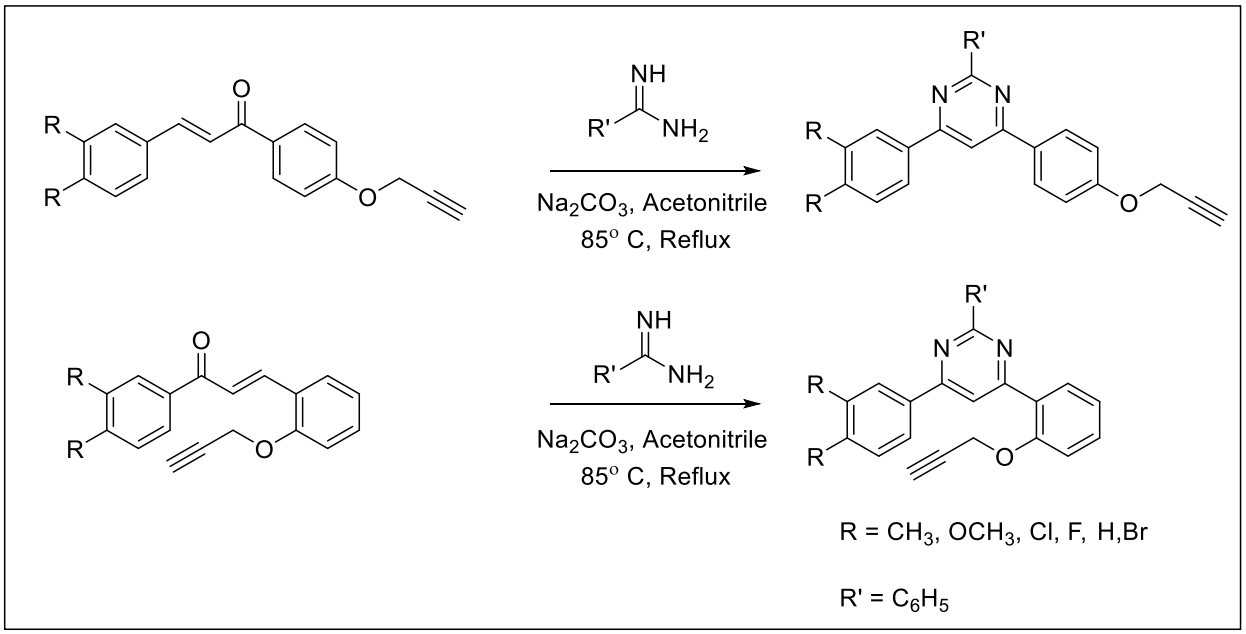

Fig 5.1.3: Synthesis of proposed compounds.

5.1.3.1) 2, 4-Diphenyl-6-(4-(prop-2-yn-1-yloxy) phenyl) pyrimidine (MV-1)

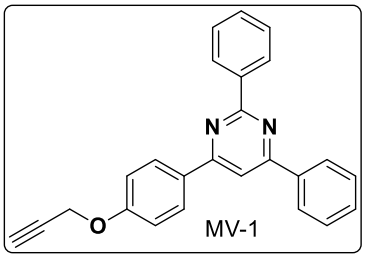

MV-1

Yield: 70%, Yellow solid, m.p. 118-120 °C;

^{1}H NMR ($CDCl_3$, 400 MHz, δ with TMS = 0): 8.73 - 8.71 (2H, m), 8.29 - 8.27 (4H, m), 7.94 (1H, s), 7.56 - 7.52 (6H, m), 7.15 - 7.13 (2H, m), 4.78 (2H, s), 2.58 (1H, s) 2.42 (3H, s); ^{13}C NMR ($CDCl_3$, 100 MHz, δ with TMS = 0) δ:164.57, 164.41, 164.09, 159.80, 138.30, 137.69, 130.70, 130.58, 128.80, 128.47, 128.44, 127.27, 115.21, 109.53, 78.20, 75.94, 55.93; **HRMS**: for $C_{25}H_{18}N_2O$, calculated $[M+H]^+$: 363.1497; observed $[M+H]^+$: 363.1476

5.1.3.2) 4-(3,4-Dimethoxyphenyl)-2-phenyl-6-(4-(prop-2-yn-1-yloxy)phenyl) pyrimidine (MV 2)

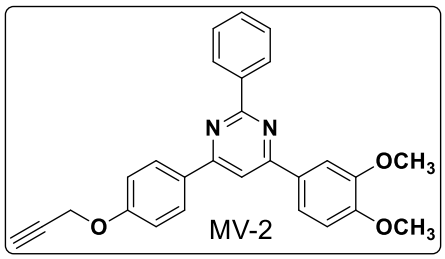

MV-2

Yield: 74%, Yellow solid, m.p. 140-142 °C;

^{1}H NMR ($CDCl_3$, 400 MHz, δ with TMS = 0): 8.70 - 8.68 (2H, m), 8.28 - 8.26 (2H, m), 7.92 (1H, d, J= 4 Hz), 7.87 (1H, s), 7.79 (1H, dd, J = 8 Hz: J= 4 Hz), 7.54 - 7.51 (3H, m) 7.15 - 7.13 (2H, m), 7.00 (1H, d, J= 4 Hz), 4.78 (2H, s), 4.06 (3H, s), 3.97 (3H, s) 2.57 (1H, s); ^{13}C NMR ($CDCl_3$, 100 MHz, δ with TMS = 0) δ:164.26, 164.11, 163.86, 159.75, 151.48, 149.39, 138.39, 131.01, 130.63, 130.44, 128.84, 128.53, 120.36, 115.21, 111.05, 110.10, 108.91, 78.26, 76.05, 56.18, 56.13, 55.96; **HRMS**: for $C_{27}H_{22}N_2O_3$, calculated $[M+H]^+$: 423.1709; observed $[M+H]^+$: 423.1696

5.1.3.3). **4-(4-Bromophenyl)-2-phenyl-6-(2-(prop-2-yn-1-yloxy) phenyl) pyrimidine (MV 3)**

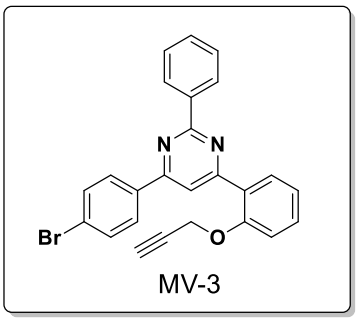

MV-3

Yield: 69%, Yellow solid, m.p. 131-133 °C

^{1}H NMR ($CDCl_3$, 400 MHz, δ with TMS = 0): 8.67 - 8.65 (2H, m), 8.33 (1H, s), 8.27 (1H, dd, J = 8 Hz; J= 4 Hz), 8.17 - 8.15 (2H, m), 7.67 - 7.65 (2H, m), 7.52 - 7.48 (4H, m), 7.24 - 7.19 (1H, m), 7.13 (1H, d, J = 8 Hz), 4.81 (2H, s), 2.57 (1H, s); ^{13}C NMR ($CDCl_3$, 100 MHz, δ with TMS = 0) δ:164.41, 163.28, 162.69, 156.29, 138.28, 136.84, 132.08, 131.61, 130.61, 129.01, 128.50, 128.43, 127.59, 125.22, 122.38, 115.23, 113.40, 78.38, 76.05, 56.80; **HRMS**: for $C_{25}H_{17}BrN_2O$, calculated $[M+H]^+$: 441.0603; observed $[M+H]^+$: 441.0590

5.1.3.4)4-(2-Methoxyphenyl)-2-phenyl-6-(4-(prop-2-yn-1-yloxy) phenyl) pyrimidine (MV 4)

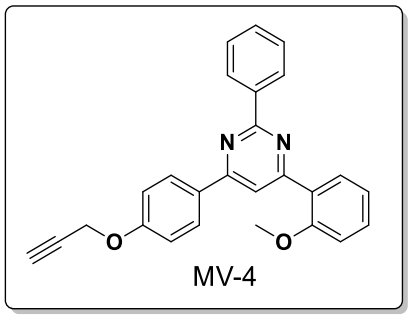

MV-4

Yield: 64%, Cream solid, m.p. 96-98 °C

^{1}H NMR ($CDCl_3$, 400 MHz, δ with TMS = 0): 8.68 - 8.66 (2H, m), 8.31 - 8.21 (4H, m), 7.51 - 7.46 (4H, m), 7.15 - 7.11 (3H, m), 7.05 (1H, d, J = 8 Hz), 4.77 (2H, s), 3.94 (3H, s), 2.54 (1H, s); ^{13}C NMR ($CDCl_3$, 100 MHz, δ with TMS = 0) δ:164.17, 163.27,

163.05, 159.61, 158.12, 138.55, 131.54, 131.32, 130.43, 128.92, 128.47, 124.40, 127.15, 121.27, 115.16, 114.76, 111.67, 78.84, 75.99, 55.95, 55.88; **HRMS**: for $C_{26}H_{20}N_2O_2$, calculated $[M+H]^+$: 393.1603; observed $[M+H]^+$: 393.1583

5.1.3.5). **4-(2-Fluorophenyl)-2-phenyl-6-(4-(prop-2-yn-1-yloxy) phenyl) pyrimidine (MV 5*)***

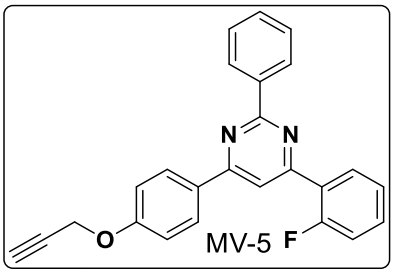

Yield: 62%, Yellow solid, m.p. 102-104 °C

^{1}H NMR ($CDCl_3$, 400 MHz, δ with TMS = 0): 8.69 - 8.66 (2H, m), 8.40 - 8.36 (1H, m), 8.27 - 8.25 (2H, m), 8.07 (1H, d, J = 8 Hz) 7.53 - 7.48 (4H, m), 7.36 - 7.32 (1H, m), 7.24 - 7.21 (1H, m), 7.14 - 7.11 (2H, m), 4.77 (2H, s), 2.56 (1H, s); ^{13}C NMR ($CDCl_3$, 100 MHz, δ with TMS = 0) δ:164.42, 164.04, 162.85, 160.74, 160.34, 159.91, 138.25, 132.07, 131.17, 130.58, 128.97, 128.46, 124.76, 116.61, 116.38, 115.27, 113.81, 78.26, 75.99, 55.97; **HRMS**: for $C_{25}H_{17}FN_2O$, calculated $[M+H]^+$: 381.1403; observed $[M+H]^+$: 381.1391

5.1.3.6)4-(4-Chlorophenyl)-2-phenyl-6-(2-(prop-2-yn-1-yloxy) phenyl) pyrimidine (MV 6)

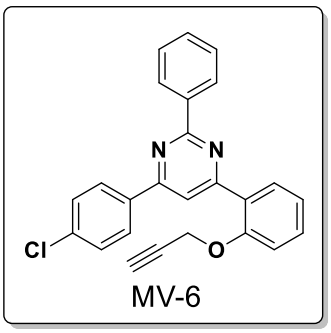

Yield: 74%, Cream solid, m.p. 124-126 °C

^{1}H NMR ($CDCl_3$, 400 MHz, δ with TMS = 0): 8.67 - 8.65 (2H, m), 8.32 (1H, s), 8.28 - 8.19 (3H, m), 7.52 - 7.39 (6H, m), 7.24 - 7.20 (1H, m), 7.13 (1H, d, J_{12} = 8 Hz), 4.81 (2H, s), 2.57 (1H, s); ^{13}C NMR ($CDCl_3$, 100 MHz, δ with TMS = 0) δ:164.35, 163.22, 162.59, 156.23, 138.25, 136.79, 136.33, 131.62, 130.65, 129.12, 128.77, 128.54, 127.42, 127.49, 122.37, 115.30, 113.30, 78.37, 76.10, 56.73; **HRMS**: for $C_{25}H_{17}ClN_2O$, calculated $[M+H]^+$: 397.1108; observed $[M+H]^+$: 397.1100

5.1.3.7) 4-(4-Chlorophenyl)-2-phenyl-6-(4-(prop-2-yn-1-yloxy) phenyl) pyrimidine (MV 7)

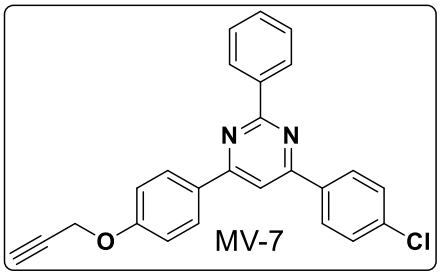

Yield: 72%, White solid, m.p. 136-138 °C

^{1}H NMR ($CDCl_3$, 400 MHz, δ with TMS = 0): 8.68 - 8.65 (2H, m), 8.26 - 8.18 (4H, m), 7.87 (1H, s), 7.52 - 7.49 (5H, m), 7.13 - 7.11 (2H, m), 4.76 (2H, s), 2.56 (1H, s); ^{13}C NMR ($CDCl_3$, 100 MHz, δ with TMS = 0) δ:164.49, 164.30, 163.34, 159.90, 138.10, 136.95, 136.09, 130.79, 129.19, 128.88, 128.60, 128.55, 115.24, 109.25, 78.19, 76.08, 55.95; **HRMS**: for $C_{25}H_{17}ClN_2O$, calculated $[M+H]^+$: 397.1108; observed $[M+H]^+$: 397.1095

5.1.3.8) 2-Phenyl-4-(4-(prop-2-yn-1-yloxy) phenyl)-6-(p-tolyl) pyrimidine (MV 8)

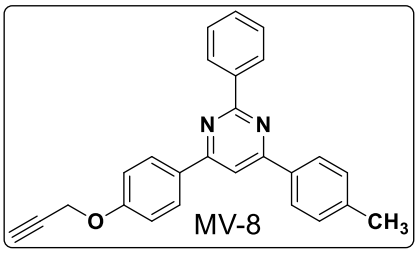

Yield: 64%, White solid, m.p. 130-132 °C

^{1}H NMR ($CDCl_3$, 400 MHz, δ with TMS = 0): 8.71 - 8.69 (2H, m), 8.27 - 8.25 (2H, m), 8.18 - 8.16 (2H, m), 7.90 (1H, s), 7.53 - 7.50 (3H, m), 7.34 (2H, d, J = 8 Hz), 7.13 - 7.20 (2H, m) 4.76 (2H, s), 2.56 (1Hs); ^{13}C NMR ($CDCl_3$, 100 MHz, δ with TMS = 0) δ:164.53, 164.35, 163.96, 159.75, 141.14, 138.40, 138.40, 134.87, 131.00, 130.60, 129.70, 128.84, 128.50, 127.23, 115.20, 109.24, 78.25, 76.03, 55.95; **HRMS**: for $C_{26}H_{20}N_2O$, calculated $[M+H]^+$: 377.1654; observed $[M+H]^+$: 377.1624

5.1.3.9)4-(3-Chlorophenyl)-2-phenyl-6-(4-(prop-2-yn-1-yloxy) phenyl) pyrimidine (MV 9)

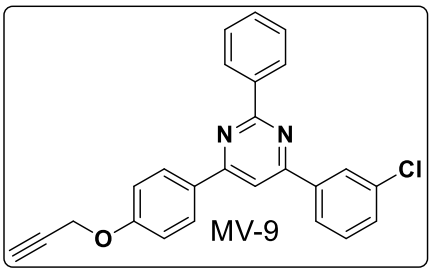

Yield: 78%, White solid, m.p. 116-118 °C

^{1}H NMR ($CDCl_3$, 400 MHz, δ with TMS = 0): 8.69 - 8.66 (2H, m), 8.27 - 8.24 (3H, m), 8.12 - 8.09 (1H, m), 7.87 (1H, s), 7.53 - 7.46 (5H, m), 7.14 - 7.10 (2H, m), 4.77 (2H, s), 2.57 (1H, s); ^{13}C NMR ($CDCl_3$, 100 MHz, δ with TMS = 0) δ:164.53, 164.37, 163.14, 159.95, 139.47, 136.54, 136.12, 130.84, 130.72, 128.90, 128.57, 128.53, 127.45, 125.39, 115.25, 114.71, 109.54, 78.21, 76.09, 55.95; **HRMS**: for $C_{25}H_{17}ClN_2O$, calculated $[M+H]^+$: 397.1108; observed $[M+H]^+$: 397.1100

5.1.3.10) 4-(4-Methoxyphenyl)-2-phenyl-6-(4-(prop-2-yn-1-yloxy) phenyl) pyrimidine (MV 10)

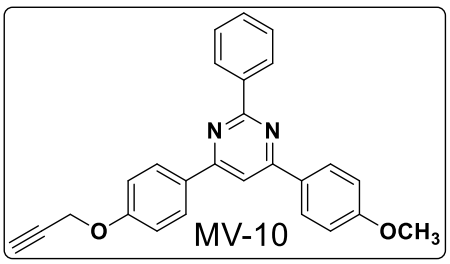

Yield: 82%, White solid, m.p. 119-121 °C

^{1}H NMR ($CDCl_3$, 400 MHz, δ with TMS = 0): 8.70 - 8.68 (2H, m), 8.26 - 8.23 (4H, m), 7.85 (1H, s), 7.54 - 7.49 (3H, m), 7.13 - 7.10 (2H, m), 7.05 - 7.02 (2H, m), 4.76 (2H, s), 3.88 (3H, s), 2.56 (1H, s); ^{13}C NMR ($CDCl_3$, 100 MHz, δ with TMS = 0) δ:164.06, 163.84, 161.92, 159.71, 138.44, 131.06, 130.56, 130.11, 128.82, 128.48, 115.18, 114.29, 108.71, 78.27, 76.03, 55.95, 55.53; **HRMS**: for $C_{26}H_{20}N_2O_2$, calculated $[M+H]^+$: 393.1603; observed $[M+H]^+$: 393.1586

5.2 In silico studies of synthesized compounds

To study the potential interactions between protein structure of MAO-A (2BXR) and MAO-B (2V5Z) with synthesized compounds, molecular modeling studies were performed on Maestro 16 software. Clorgyline and Rasagiline were taken as standard inhibitors. All synthesized compounds were docked with respect to the standard molecules for studying their binding mode with protein. The binding scores of the synthesized compounds were then compared with standard molecules (Clorgyline and rasagiline). Docking study was done by applying following steps in Maestro 16 software:

- Protein preparation
- Ligand preparation
- Grid generation
- Glide docking

5.3 Biological activity

5.3.1 Bioassay

The Amplex Red monoamine oxidase assay is beneficial for measuring both end-point and continuous amine oxidase activity. Clorgyline and pargyline, specific inhibitors of MAO-A and MAO-B activity respectively were used as standard. The potential applications of this kit comprise the measurement of amine oxidase activity in normal and diseased tissues, blood samples and other biological fluids, the

screening of drugs as possible MAO inhibitors or substrates and the generation of kinetic constants for different amine oxidase substrates.

5.3.2 Method

Fluorimetric method was used to evaluate the activity of test compounds against MAO-A and MAO-B enzyme isoforms using Amplex® Red assay kit.(Chimenti et al., 2010)

Briefly, 100 µL of sodium phosphate buffer (0.05 M, pH 7.4) containing the test drugs and reference inhibitors, in various concentrations along with adequate amounts of recombinant hMAO (hMAO-A: 1.1 µg protein; specific activity: 150 nmol of p-tyramine oxidized to p-hydroxyphenylacetaldehyde/min/mg protein; hMAO-B: 7.5 µg protein; specific activity: 22 nmol of p-tyramine transformed/min/mg protein) enzyme, were incubated for 15 min at 37 °C in a flat-black-bottom 96-well plate (Tarsons) in incubator. After this incubation period, the reaction was started by adding (final concentrations) 200 µM Amplex® Red reagent, 1 U/mL horseradish peroxidase and 1 mM p-tyramine. After 30 min incubation in dark, the production of H_2O_2 and was quantified at 37 °C in a multidetection microplate fluorescence reader (Synergy^{HI}, Bio-Tek® Instruments) based on the fluorescence generated at excitation wavelength 545 nm, and emission wavelength 590 nm. Control experiments were carried out simultaneously by replacing the test drugs with vehicle. No florescence could be observed in the absence of MAO enzyme thus eliminating the possibility of any false reading. The specific final fluorescence emission was calculated after subtraction of the background activity, determined from vials containing all components except the hMAO enzyme replaced by a sodium phosphate buffer solution.

CHAPTER 6

RESULTS AND DISCUSSION

6. RESULTS AND DISCUSSION

6.1.1 Synthesis

From exploration of crystal structures of both MAO isoforms it was recognized that pocket of MAO-A isoforms interacts mainly with smaller and polar ligands whereas bulkier and hydrophobic (lipophilic) ligands, display selectivity for MAO-B isoform. Recent literature studies indicated that rasagiline (targets MAO enzyme) is one of the effective drug approved by US FDA, for the treatment of PD. The propargyl moiety of the drug binds with the receptor. We followed scheme 6.1 to synthesize the compounds containing a propargyl moiety and proposed that propargyl based derivatives may target and inhibit MAO enzyme activity effectively and the resulting compounds would act as anti-PD agents.

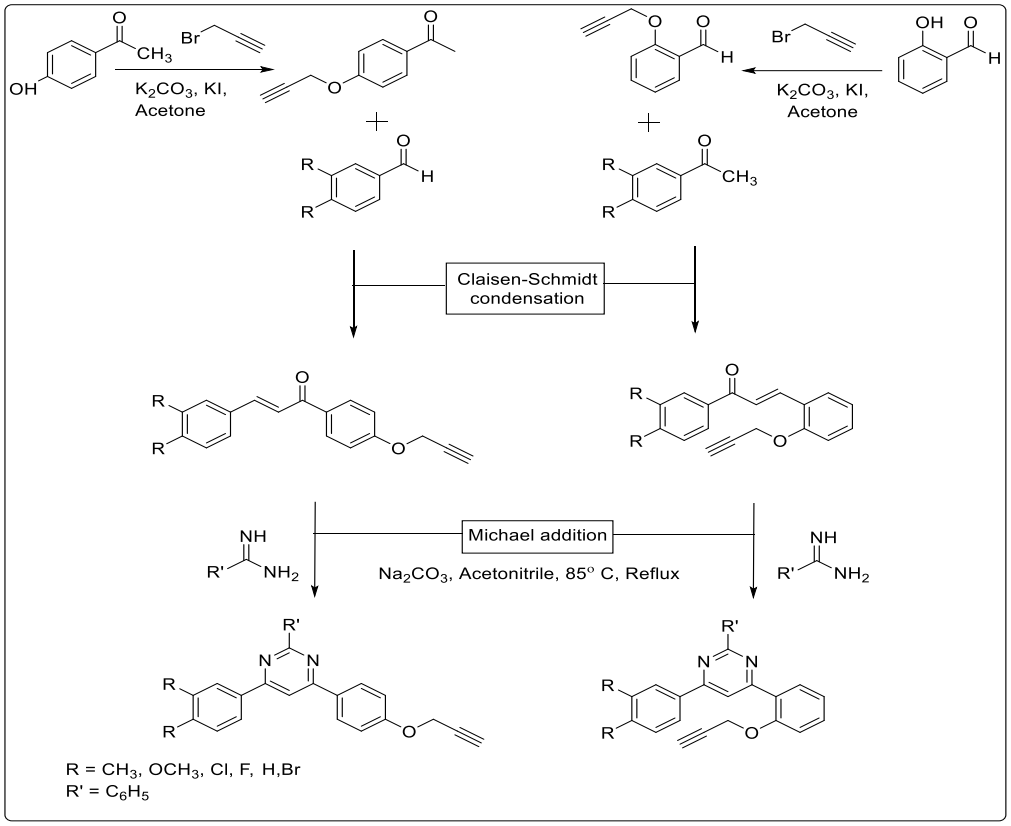

Scheme 6.1: Proposed route for the synthesis of target compounds

6.1.2 Synthesis of intermediates

The synthesis of intermediates was carried out through S_N2 reaction mechanism. Mechanistically, S_N2 is a nucleophilic substitution reaction mechanism in which one bond is broken and one bond is formed synchronously. It is one step reaction. O-alkylated benzaldehyde and acetophenone intermediates were prepared by this reaction mechanism.

6.1.3 Synthesis of chalcones

The synthesis of chalcone derivatives was carried out through base-catalyzed Claisen-Schmidt condensation. Mechanistically, in base-catalyzed reaction, the base abstracts proton from the α-carbon which leads to the formation of enolate ion. In next step the attack of nucleophile (carbanion) on the carbocationic center of aldehyde occurs, followed by the dehydration of water or an alcohol molecule (Figure 6.1.1)

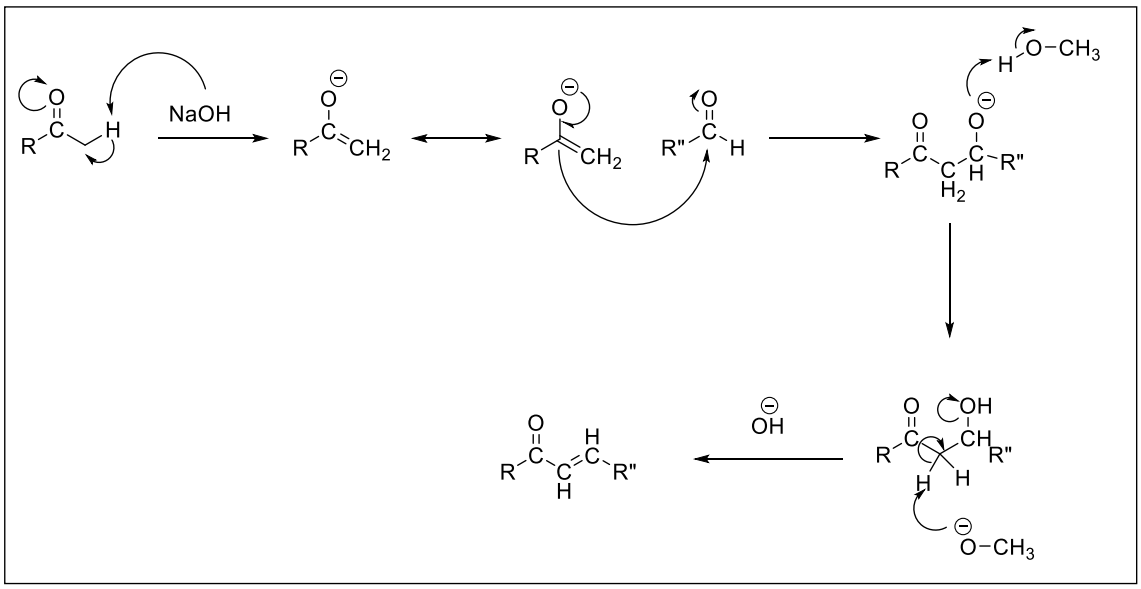

Fig: 6.1.1 General mechanism of Claisen-Schmidt condensation.

6.1.4 Synthesis of proposed molecules

The synthesis of proposed molecules was carried out through Michael addition reaction mechanism followed by ring cyclization for the formation of pyrimidine. Mechanistically, in Michael addition reaction,

protons are abstracted by suitable base for nucleophilic attack to perform 1,4-conjugation addition. The intermediates are unstable so, for attaining stability of molecule ring cyclization takes place in four steps as given in Figure 6.1.2.

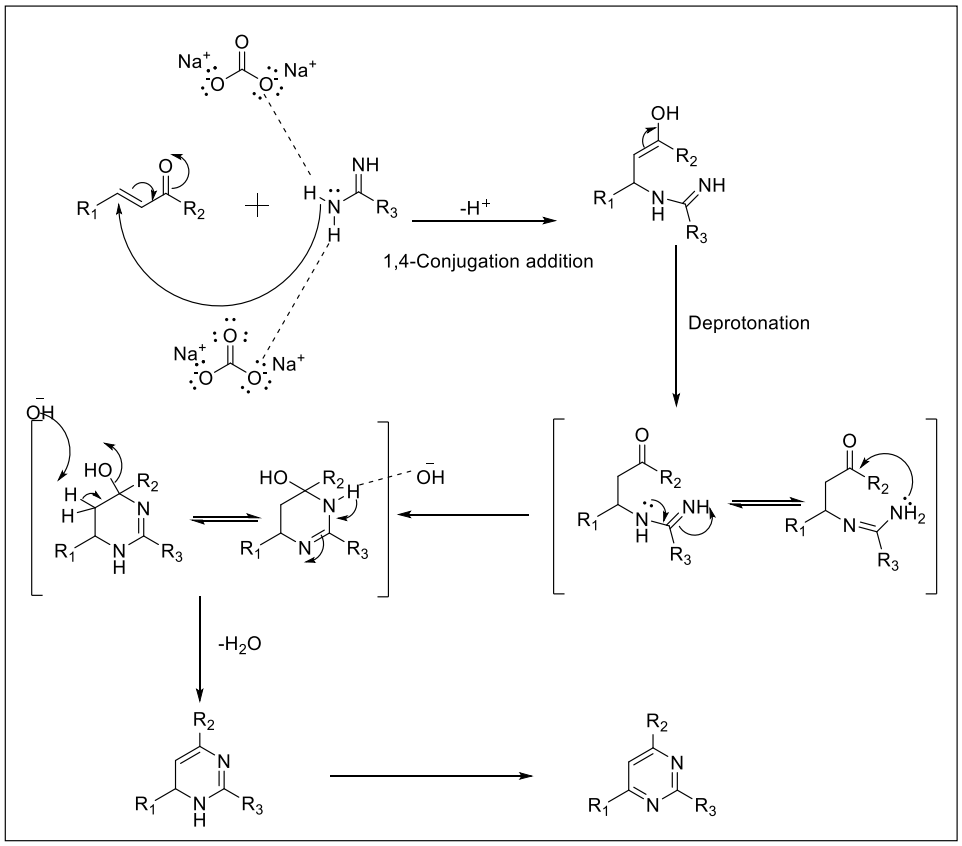

Fig:6.1.2 General mechanism of Michael addition followed by ring cyclization.

6.1.5 Proposed compounds

From the proposed scheme 6.1, ten propargyl pyrimidine derivatives were synthesized as shown in Figure 6.1.3.

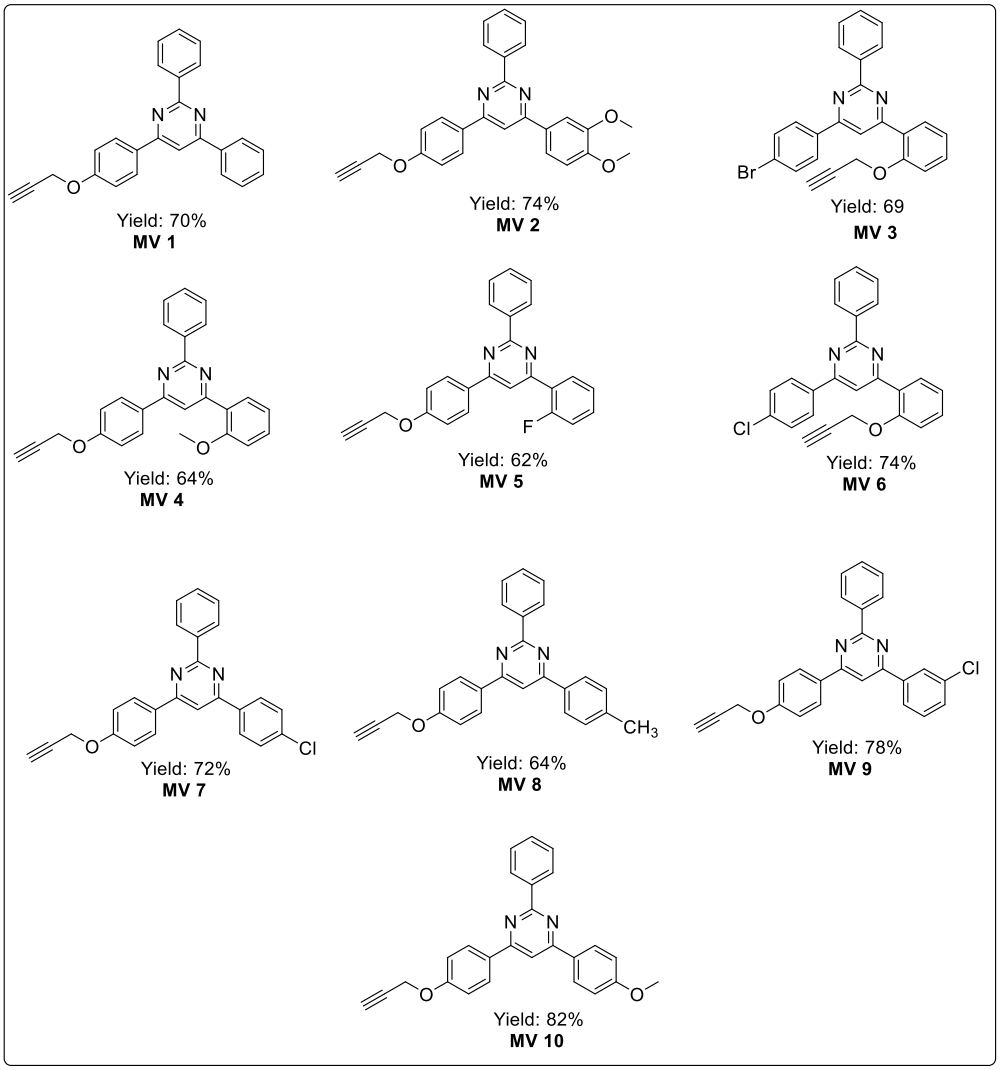

Fig 6.1.3: List of synthesized final compounds.

6.2 Docking results

The molecular docking studies of designed compounds were performed using Maestro 11.0. Clorgyline and rasagiline were taken as reference molecules for molecular docking studies of designed compounds on human MAO-A (2BXR) and MAO-B (2V5Z) proteins. The 2D interaction diagrams of clorgyline and rasagiline are shown below (Figure 6.2.1).

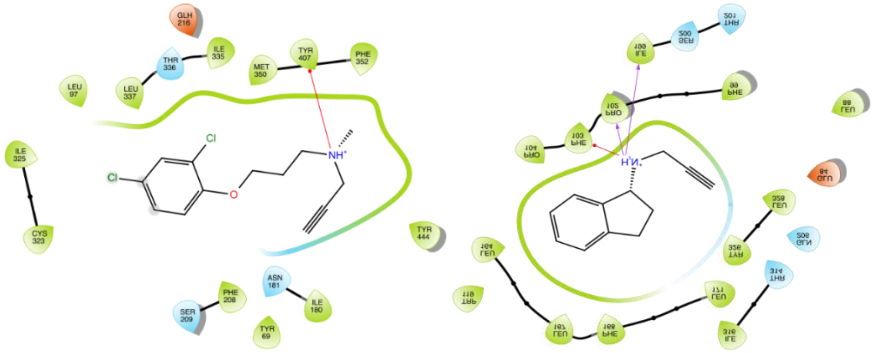

Fig 6.2.1: 2D interaction diagrams of clorgyline and rasagiline.

From 2D interaction diagrams it was found that standard inhibitor clorgyline binds to the target site and showed cation-π interactions with Tyr407. Rasagiline presented cation-π interactions with Phe103 and hydrogen bonding interactions with Pro102 and Ile199. Molecular docking studies of designed compounds demonstrated that the designed compounds have similar π – π interactions, cation-π interactions and hydrogen bonding interactions with several protein bases as of standard compounds. Table 6.2.1 and 6.2.2 shows interaction pattern of synthesized compounds with their respective MAO enzymes.

Table 6.2.1: Docking pose of the synthesized compounds and their dock score with human MAO-A protein (2BXR).

S. No.	Compound	Docking Pose	Dock Score
1.	**MV-3**	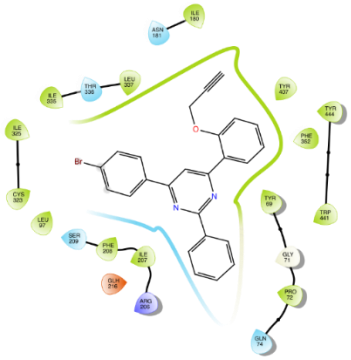	-8.13
2.	**MV-7**	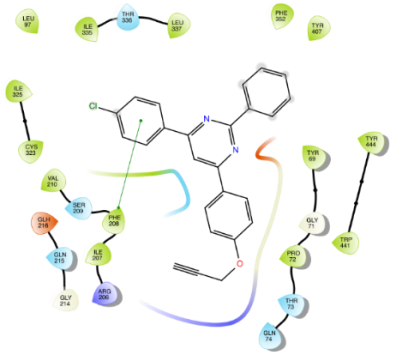	-8.04
3.	**MV-8**	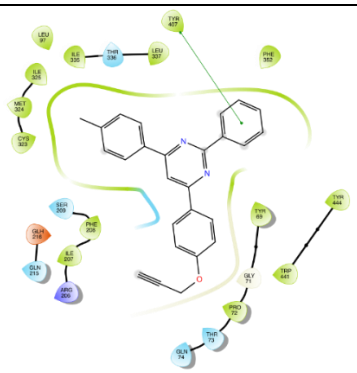	-7.86

4.	**MV-4**	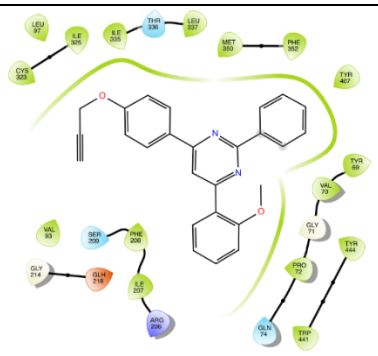	-7.75
5.	**MV-6**	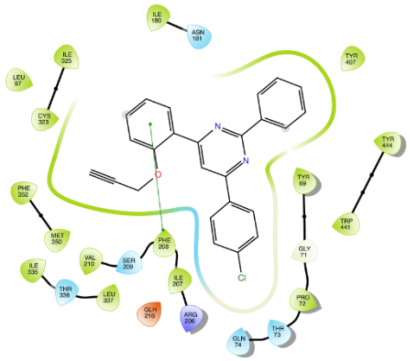	-5.66
6.	**MV-5**	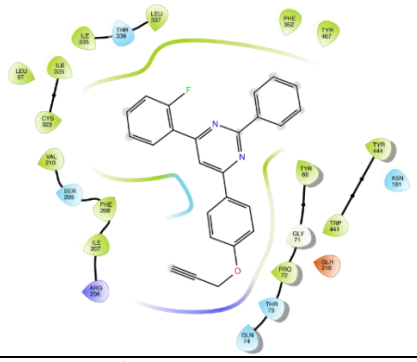	-5.41
7.	**MV-2**	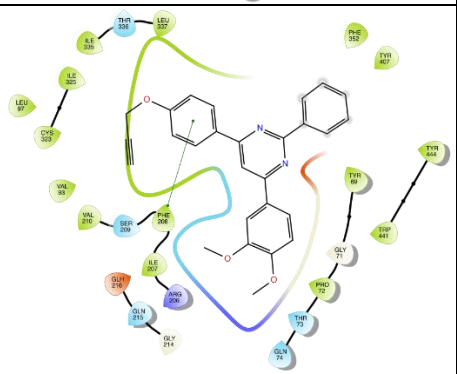	-5.24

8.	**MV-9**	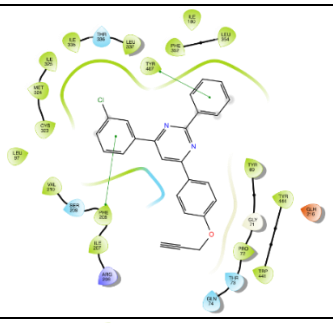	-5.09
9.	**MV-10**	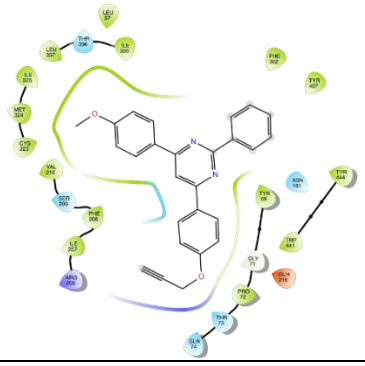	-5.01
10.	**MV-1**	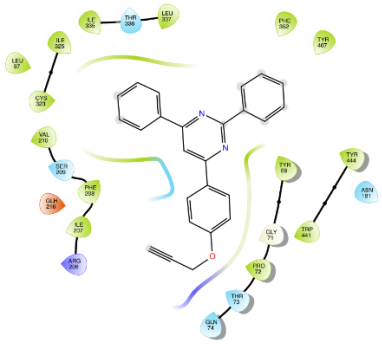	-4.99
11.	**CLORGYLINE**	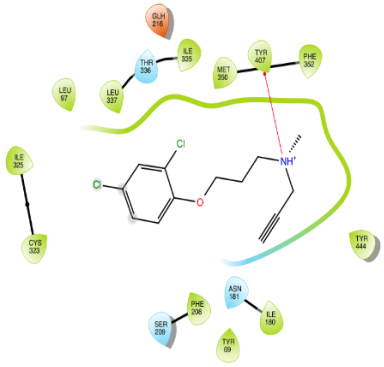	

Table 6.2.2: Docking pose of the synthesized compounds and their dock score with human MAO-B protein(2V5Z)

S. No.	Compound	Docking Pose	Dock Score
1.	**MV-8**	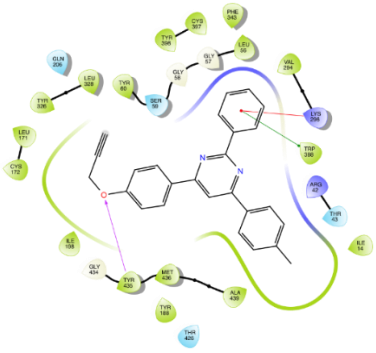	-10.86
2.	**MV-3**	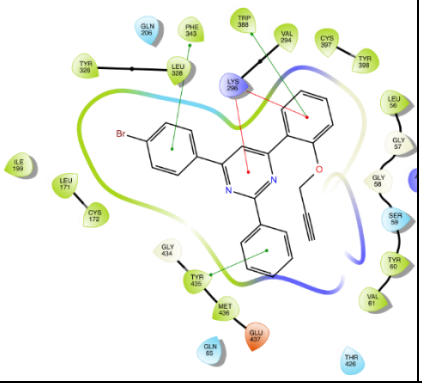	-8.91
3.	**MV-6**	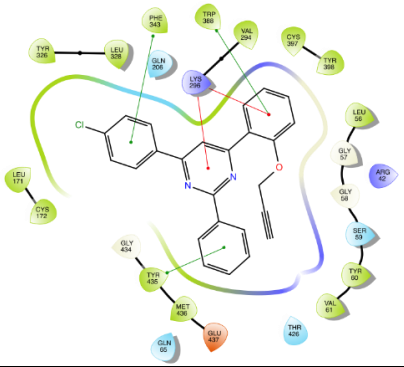	-8.89
4.	**MV-10**	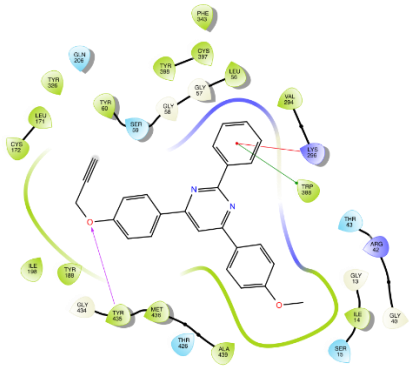	-7.74

6.	**MV-4**	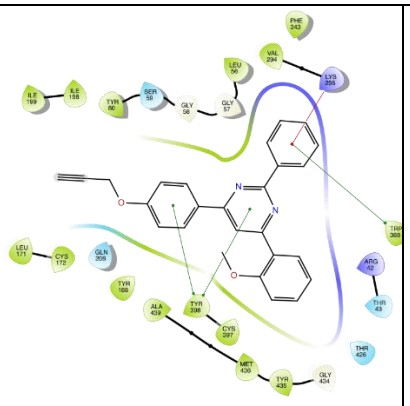	-7.07
7.	**MV-9**	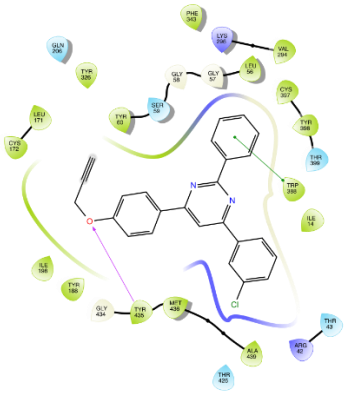	-6.5
8.	**RASAGILINE**	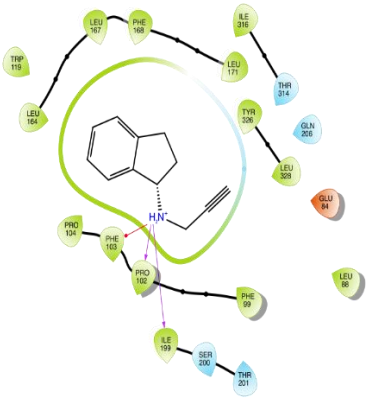	-4.51

6.3 Biological studies

The MAO inhibition potential of the pyrimidine derivatives (MVB1-10) was evaluated on recombinant human MAO-B enzymes (purchased from Sigma Aldrich) using Amplex® Red assay kit(De Colibus et al., 2005). The MAO-B inhibition data of the compounds and standard inhibitors (pargyline) are reported in Table 6.3.1 All the

synthesized compounds showed low micromolar inhibition activities for the MAO-B isoform and their IC_{50} values against MAO-B isoform are given in the Table 6.3.1. From all the synthesized compound Compound MV-7, MV-6 and MV-4 shows very good inhibitory activity as compare to other synthesized derivative. From IC50 values it is clear that molecule having electron withdrawing group at para position are more active towards MAO enzymes such as MV-7and MV-6. From all the synthesized compounds, compounds having electron withdrawing group on R_2positionshows very prominent MAO-B inhibitory activity such as MV-5, MV-6.

Table 6.3.1 Results of MAO inhibition studies of the synthesized compounds. All the compounds were evaluated against MAO-B isoforms

Entry name	**R1**	**R2**	**Propargyl group position**	**IC_{50}(mean±SEM μM)**
MV-1	$-C_6H_5$	-H	C_4	0.69± 0.16
MV-2	$-C_6H_5$	3,4-$DiOCH_3$	C_4	0.60± 0.02
MV-3	$-C_6H_5$	4-Br	C_2	0.56± 0.06
MV-4	$-C_6H_5$	2-OCH_3	C_4	0.55± 0.05
MV-5	$-C_6H_5$	2-F	C_4	0.87± 0.18
MV-6	$-C_6H_5$	4-Cl	C_2	0.48± 0.06
MV-7	$-C_6H_5$	4-Cl	C_4	0.44± 0.14
MV-8	$-C_6H_5$	4-CH_3	C_4	0.66± 0.18
MV-9	$-C_6H_5$	3-Cl	C_4	0.56± 0.27
MV-10	$-C_6H_5$	4-OCH_3	C_4	0.55± 0.08
11	Pargyline	------	------	0.15± 0.02

CHAPTER 7

CONCLUSION

7. CONCLUSION

MAO-B inhibitors have been explored as therapeutic agents for the treatment or management of PD. A series of new propargyl containing 2,4,6-trisubstituted pyrimidine derivatives incorporating a propargyl moiety were synthesized, docked over MAO-A and MAO-B protein and screened for their MAO inhibition potential using Amplex® Red assay. From docking score, it is clear that all the compounds showed good binding affinity towards MAO-A as well as MAO-B, they properly fit in to the cavity of MAO enzymes. Inhibitory activities of synthesized compounds were assayed for MAO-B iso-form, and most of the compounds showed good inhibitory potential at sub-micro molar concentrations. The structure-activity relationship profile has been developed with number of electron releasing and electron withdrawing substituents attached to the pyrimidine nucleus. **MV7** was found to be the most potent MAO-B inhibitor with IC_{50} value of 0.44 ± 0.02 μM, while **MV6** with IC_{50} value of 0.48 ± 0.04 μM and **MV4** with IC_{50} value of 0.55 ± 0.06 μM have also showed comparable inhibitory activity. From molecular docking studies and biological activity, it was found that compounds such as **MV7** and **MV6** obtained in this series can act as promising leads for the development of pyrimidine based effective and potent MAO-B inhibitors for the treatment of Parkinson's disease.

REFERENCES

8. References

Altomare, C., Cellamare, S., Summo, L., Catto, M., Carotti, A., Thull, U.,Stoeckli-Evans, H. (1998). Inhibition of monoamine oxidase-B by condensed pyridazines and pyrimidines: Effects of lipophilicity and structure− activity relationships. Journal of Medicinal Chemistry, ***41***(20), 3812-3820.

Betarbet, R., Sherer, T. B., MacKenzie, G., Garcia-Osuna, M., Panov, A. V., & Greenamyre, J. T. (2000). Chronic systemic pesticide exposure reproduces features of Parkinson's disease. Nature Neuroscience, ***3***(12), 1301-1306.

Carotti, A., Catto, M., Leonetti, F., Campagna, F., Soto-Otero, R., Méndez-Álvarez, E Altomare, C. (2007). Synthesis and monoamine oxidase inhibitory activity of new pyridazine-, pyrimidine-and 1, 2, 4-triazine-containing tricyclic derivatives. Journal of Medicinal Chemistry, ***50***(22), 5364-5371.

Cerqueira, E. C., Netz, P. A., Diniz, C., do Canto, V. P., & Follmer, C. (2011). Molecular insights into human monoamine oxidase (MAO) inhibition by 1, 4-naphthoquinone: Evidences for menadione (vitamin K3) acting as a competitive and reversible inhibitor of MAO. Bioorganic & Medicinal Chemistry, ***19***(24), 7416-7424.

Chaudhuri, K. R., & Schapira, A. H. (2009). Non-motor symptoms of Parkinson's disease: dopaminergic pathophysiology and treatment. The Lancet Neurology, ***8***(5), 464-474.

Chen, J. J., Swope, D. M., & Dashtipour, K. (2007). Comprehensive review of rasagiline, a second-generation monoamine oxidase inhibitor, for the treatment of Parkinson's disease. Clinical Therapeutics, ***29***(9), 1825-1849.

Chen, R., Xiao, J., Ni, Y., Xu, H.-F., Zheng, M., Tong, X.Tang, W.-J. (2016). Novel tricyclic pyrazolo [1, 5-d][1, 4] benzoxazepin-5 (6H)-one: Design, synthesis, model and use as hMAO-B inhibitors. Bioorganic & Medicinal Chemistry, ***24***(8), 1741-1748.

Chimenti, F., Carradori, S., Secci, D., Bolasco, A., Bizzarri, B., Chimenti, P., Orallo, F. (2010). Synthesis and inhibitory activity against human monoamine oxidase of N1-thiocarbamoyl-3, 5-di (hetero) aryl-4, 5-dihydro-(1H)-pyrazole derivatives. European Journal of Medicinal. Chemistry, ***45***(2), 800-804.

Chinta, S. J., & Andersen, J. K. (2006). Reversible inhibition of mitochondrial complex I activity following chronic dopaminergic glutathione depletion in vitro: implications for Parkinson's disease. Free Radical Biology and Medicine, ***41***(9), 1442-1448.

Chirkova, Z. V., Kabanova, M. V., Filimonov, S. I., Abramov, I. G., Petzer, A., Petzer, J. P., & Suponitsky, K. Y. (2016). An evaluation of synthetic indole derivatives as inhibitors of monoamine oxidase. Bioorganic & Medicinal Chemistry Letters, ***26***(9), 2214-2219.

Choi, J. W., Jang, B. K., Cho, N.-c., Park, J.-H., Yeon, S. K., Ju, E. J.,Kim, D. J. (2015). Synthesis of a series of unsaturated ketone derivatives as selective and reversible monoamine oxidase inhibitors. Bioorganic & Medicinal Chemistry, ***23***(19), 6486-6496.

Conway, K. A., Rochet, J.-C., Bieganski, R. M., & Lansbury, P. T. (2001). Kinetic stabilization of the α-synuclein protofibril by a dopamine-α-synuclein adduct. Science, ***294***(5545), 1346-1349.

Costas-Lago, M. C., Besada, P., Rodríguez-Enríquez, F., Viña, D., Vilar, S., Uriarte, E., Terán, C. (2017). Synthesis and structure-activity relationship study of novel 3-heteroarylcoumarins based on pyridazine scaffold as selective MAO-B inhibitors. European Journal of Medicinal Chemistry, 139, 1-11.

Crosby, N. J., Deane, K., & Clarke, C. E. (2003). Amantadine in Parkinson's disease. The Cochrane Library.

Dauer, W., & Przedborski, S. (2003). Parkinson's disease: mechanisms and models. Neuron, ***39***(6), 889-909.

De Colibus, L., Li, M., Binda, C., Lustig, A., Edmondson, D. E., & Mattevi, A. (2005). Three-dimensional structure of human monoamine oxidase A (MAO A): relation to the structures of rat MAO A and human MAO B. Proceedings of The National Academy of Sciences of The United States of America, ***102***(36), 12684-12689.

Delamarre, A., & Meissner, W. G. (2017). Epidemiology, environmental risk factors and genetics of Parkinson's disease. La Presse Médicale, ***46(***2), 175-181.

Deshwal, S., Di Sante, M., Di Lisa, F., & Kaludercic, N. (2017). Emerging role of monoamine oxidase as a therapeutic target for cardiovascular disease. Current Opinion in Pharmacology, 33, 64-69.

Dexter, D., Sian, J., Rose, S., Hindmarsh, J., Mann, V., Cooper, J., .Schapira, A. (1994). Indices of oxidative stress and mitochondrial function in individuals with incidental Lewy body disease. Annals of Neurology, ***35***(1), 38-44.

Dickson, D. W. (2017). Neuropathology of Parkinson disease. Parkinsonism & Related Disorders.

Ellis, J. M., & Fell, M. J. (2017). Current Approaches to the Treatment of Parkinson's Disease. Bioorganic & Medicinal Chemistry Letters.

Encarnacion, E. V., & Hauser, R. A. (2010). COMT Inhibitors in the Treatment of Parkinson's Disease Encyclopedia of Movement Disorders (pp. 246-249). Oxford: Academic Press.

Feng, J. (2003). Genetic factors in Parkinson's disease and potential therapeutic targets. Current Neuropharmacology, ***1***(4), 301-313.

Fioravanti, R., Desideri, N., Biava, M., Monaco, L. P., Grammatica, L., & Yáñez, M. (2013). Design, synthesis, and in vitro hMAO-B inhibitory evaluation of some 1-methyl-3, 5-diphenyl-4, 5-dihydro-1H-pyrazoles. Bioorganic & Medicinal Chemistry Letters, ***23***(18), 5128-5130.

Fumagalli, M., Lecca, D., Abbracchio, M. P., & Ceruti, S. (2017). Pathophysiological role of purines and pyrimidines in neurodevelopment: unveiling new pharmacological approaches to congenital brain diseases. Frontiers in Pharmacology, 8, 941.

Gogvadze, V., Orrenius, S., & Zhivotovsky, B. (2006). Multiple pathways of cytochrome c release from mitochondria in apoptosis. Biochimica et Biophysica Acta (BBA)-Bioenergetics, ***1757***(5), 639-647.

Goswami, P., Joshi, N., & Singh, S. (2017). Neurodegenerative signaling factors and mechanisms in Parkinson's pathology. Toxicology in Vitro.

Hatano, T., & Hattori, N. (2011). Etiology and Pathogenesis of Parkinson's Disease: INTECH Open Access Publisher.

Herrera, A., Muñoz, P., Steinbusch, H. W., & Segura-Aguilar, J. (2017). Are dopamine oxidation metabolites involved in the loss of dopaminergic neurons in the nigrostriatal system in Parkinson's disease? ACS Chemical Neuroscience, 8(4), 702-711.

Hu, Q., & Wang, G. (2016). Mitochondrial dysfunction in Parkinson's disease. Translational neurodegeneration, ***5***(1), 14.

Jain, K., Arya, N., Inamdar, N., Auti, P., Unawane, S., Puranik, H., Prajapati, C. (2016). The chemistry and bio-medicinal significance of pyrimidines & condensed pyrimidines. Current Topics in Medicinal Chemistry, ***16***(28), 3133-3174.

Jenner, P. (2007). Oxidative stress and Parkinson's disease. Handbook of Clinical Neurology, 83, 507-520.

Jones, D. R., Delenclos, M., Baine, A. T., DeTure, M., Murray, M. E., Dickson, D. W., & McLean, P. J. (2015). Transmission of soluble and insoluble α-Synuclein to mice. Journal of Neuropathology and Experimental Neurology, ***74***(12), 1158-1169.

Juárez-Jiménez, J., Mendes, E., Galdeano, C., Martins, C., Silva, D. B., Marco-Contelles, J. Ramsay, R. R. (2014). Exploring the structural basis of the selective inhibition of monoamine oxidase A by dicarbonitrile aminoheterocycles: Role of Asn181 and Ile335 validated by spectroscopic and computational studies. Biochimica et Biophysica Acta (BBA)-Proteins and Proteomics, ***1844***(2), 389-397.

Kim, J., Fiesel, F. C., Belmonte, K. C., Hudec, R., Wang, W.-X., Kim, C.,Kim, J. (2016). miR-27a and miR-27b regulate autophagic clearance of damaged mitochondria by targeting PTEN-induced putative kinase 1 (PINK1). Molecular Neurodegeneration, ***11***(1), 55.

Kones, R. (2010). Mitochondrial therapy for Parkinson's disease: Neuroprotective pharmaconutrition may be disease-modifying. Clinical Pharmacology: Advances and Applications, 2, 185.

Kraytsberg, Y., Kudryavtseva, E., McKee, A. C., Geula, C., Kowall, N. W., & Khrapko, K. (2006). Mitochondrial DNA deletions are abundant and cause functional impairment in aged human substantia nigra neurons. Nature Genetics, ***38***(5), 518.

Kumar, B., Prakash Gupta, V., & Kumar, V. (2017). A Perspective on Monoamine Oxidase Enzyme as Drug Target: Challenges and Opportunities. Current Drug Targets, ***18***(1), 87-97.

Legoabe, L. J., Petzer, A., & Petzer, J. P. (2012). Inhibition of monoamine oxidase by selected C6-substituted chromone derivatives. European Journal of Medicinal Chemistry, ***49***, 343-353.

Lichtenberg, M., Mansilla, A., Zecchini, V., Fleming, A., & Rubinsztein, D. (2011). The Parkinson's disease protein LRRK2 impairs proteasome substrate clearance without affecting proteasome catalytic activity. Cell Death & Disease, ***2***(8), e196.

Liu, Z., Cai, W., Lang, M., Yan, R., Li, Z., Zhang, G., Zhang, Z. (2017). Neuroprotective Effects and Mechanisms of Action of Multifunctional Agents Targeting Free Radicals, Monoamine Oxidase B and Cholinesterase in Parkinson's Disease Model. Journal of Molecular Neuroscience, ***61***(4), 498-510.

Mann, V., Cooper, J., Daniel, S., Srai, K., Jenner, P., Marsden, C., & Schapira, A. (1994). Complex I, iron, and ferritin in Parkinson's disease substantia nigra. Annals of Neurology, ***36***(6), 876-881.

Marambaud, P., Dreses-Werringloer, U., & Vingtdeux, V. (2009). Calcium signaling in neurodegeneration. Molecular Neurodegeneration, ***4***(1), 20.

Martin, L. J., Pan, Y., Price, A. C., Sterling, W., Copeland, N. G., Jenkins, N. A., Lee, M. K. (2006). Parkinson's disease α-synuclein transgenic mice develop neuronal mitochondrial degeneration and cell death. Journal of Neuroscience, ***26***(1), 41-50.

Mathew, B., Suresh, J., & Anbazhagan, S. (2016). Development of novel (1-H) benzimidazole bearing pyrimidine-trione based MAO-A inhibitors: Synthesis, docking studies and antidepressant activity. Journal of Saudi Chemical Society, ***20***, S132-S139.

Mostert, S., Petzer, A., & Petzer, J. P. (2016). Inhibition of monoamine oxidase by benzoxathiolone analogues. Bioorganic & Medicinal Chemistry Letters, ***26***(4), 1200-1204.

Nel, M. S., Petzer, A., Petzer, J. P., & Legoabe, L. J. (2016). 2-Heteroarylidene-1-indanone derivatives as inhibitors of monoamine oxidase. Bioorganic Chemistry, ***69***, 20-28.

Norberg, E., Orrenius, S., & Zhivotovsky, B. (2010). Mitochondrial regulation of cell death: processing of apoptosis-inducing factor (AIF). Biochemical and Biophysical Research Communications, ***396***(1), 95-100.

Olanow, C., & Tatton, W. (1999). Etiology and pathogenesis of Parkinson's disease. Annual Review of Neuroscience, ***22***(1), 123-144.

Pandey, S. (2012). Parkinson's disease: recent advances. J Assoc Physicians India, 60, 30-32.

Parkinson, J. (2002). An essay on the shaking palsy. The Journal of Neuropsychiatry and Clinical Neurosciences, ***14***(2), 223-236.

Petrucelli, L., O'Farrell, C., Lockhart, P. J., Baptista, M., Kehoe, K., Vink, L.,. Hardy, J. (2002). Parkin protects against the toxicity associated with mutant α-synuclein: proteasome dysfunction selectively affects catecholaminergic neurons. Neuron, ***36***(6), 1007-1019.

Pienaar, I. S., Dexter, D. T., & Burkhard, P. R. (2010). Mitochondrial proteomics as a selective tool for unraveling Parkinson's disease pathogenesis. Expert Review of Proteomics, ***7***(2), 205-226.

Poewe, W., Seppi, K., Tanner, C. M., Halliday, G. M., Brundin, P., Volkmann, J., Lang, A. E. (2017). Parkinson disease. Nature Reviews Disease Primers, 3, 17013.

Przedborski, S., & Vila, M. (2003). The 1-Methyl-4-Phenyl-1, 2, 3, 6-Tetrahydropyridine Mouse Model. Annals of the New York Academy of Sciences, ***991***(1), 189-198.

Radad, K., Gille, G., & Rausch, W.-D. (2005). Short review on dopamine agonists: insight into clinical and research studies relevant to Parkinson's disease. Pharmacol Rep, ***57***(6), 701-712.

Rcom-H'cheo-Gauthier, A., Goodwin, J., & Pountney, D. L. (2014). Interactions between calcium and alpha-synuclein in neurodegeneration. Biomolecules, ***4***(3), 795-811.

Sachs, J. N., & Engelman, D. M. (2006). Introduction to the membrane protein reviews: the interplay of structure, dynamics, and environment in membrane protein function. Annual Review of Biochemistry., ***75***, 707-712.

Santana, L., Uriarte, E., González-Díaz, H., Zagotto, G., Soto-Otero, R., & Méndez-Álvarez, E. (2006). A QSAR model for in silico screening of MAO-A inhibitors. Prediction, synthesis, and biological assay of novel coumarins. Journal of Medicinal Chemistry, ***49***(3), 1149-1156.

Sassi, C. (2011). Genetics of parkinson disease Etiology and Pathophysiology of Parkinson's Disease: InTech.

Schapira, A. H., & Jenner, P. (2011). Etiology and pathogenesis of Parkinson's disease. Movement Disorders, ***26***(6), 1049-1055.

Singh, S., & Dikshit, M. (2007). Apoptotic neuronal death in Parkinson's disease: involvement of nitric oxide. Brain Research Reviews, ***54***(2), 233-250.

Smeyne, R. J., & Jackson-Lewis, V. (2005). The MPTP model of Parkinson's disease. Molecular Brain Research, ***134***(1), 57-66.

Thal, D. R. (2015). Clearance of Amyloid β-Protein and its role in the Spreading of Alzheimer's disease Pathology. Frontiers in Aging Neuroscience, 7, 25.

Thomas, B., & Beal, M. (2007). Parkinson's disease. Hum Mol Genet 16 Spec No.

Tolosa, E., Martí, M. J., Valldeoriola, F., & Molinuevo, J. L. (1998). History of levodopa and dopamine agonists in Parkinson's disease treatment. Neurology, ***50***(6 Suppl 6), S2-S10.

Tripathi, A. C., Upadhyay, S., Paliwal, S., & Saraf, S. K. (2018). Privileged scaffolds as MAO inhibitors: Retrospect and prospects. European Journal of Medicinal Chemistry.

Tsang, A. H., & Chung, K. K. (2009). Oxidative and nitrosative stress in Parkinson's disease. Biochimica et Biophysica Acta (BBA)-Molecular Basis of Disease, ***1792***(7), 643-650.

Turnbull, S., Tabner, B. J., El-Agnaf, O. M., Moore, S., Davies, Y., & Allsop, D. (2001). α-Synuclein implicated in Parkinson's disease catalyses the formation of hydrogen peroxide in vitro. Free Radical Biology and Medicine, ***30***(10), 1163-1170.

Van der Walt, M. M., Terre'Blanche, G., Petzer, J. P., & Petzer, A. (2017). Benzyloxynitrostyrene analogues–A novel class of selective and highly potent inhibitors of monoamine oxidase B. European Journal of Medicinal Chemistry, 125, 1193-1199.

Wang, Z., Wu, J., Yang, X., Cai, P., Liu, Q., Wang, K. D.,Wang, X. (2016). Neuroprotective effects of benzyloxy substituted small molecule monoamine oxidase B inhibitors in Parkinson's disease. Bioorganic & Medicinal Chemistry, ***24***(22), 5929-5940.

Weinreb, O., Mandel, S., Bar-Am, O., Yogev-Falach, M., Avramovich-Tirosh, Y., Amit, T., & Youdim, M. B. (2009). Multifunctional neuroprotective derivatives of rasagiline as anti-Alzheimer's disease drugs. Neurotherapeutics, ***6***(1), 163-174.

Winklhofer, K. F., & Haass, C. (2010). Mitochondrial dysfunction in Parkinson's disease. Biochimica et Biophysica Acta (BBA)-Molecular Basis of Disease, ***1802***(1), 29-44.

Yacoubian, T. A., & Standaert, D. G. (2009). Targets for neuroprotection in Parkinson's disease. Biochimica et Biophysica Acta (BBA)-Molecular Basis of Disease, ***1792***(7), 676-687.

Zaib, S., Umar Farooq Rizvi, S., Aslam, S., Ahmad, M., al-Rashida, M., & Iqbal, J. (2015). Monoamine oxidase inhibition and molecular modeling studies of piperidyl-thienyl and 2-pyrazoline derivatives of chalcones. Medicinal Chemistry, ***11***(5), 497-505.

Zecca, L., Youdim, M. B., Riederer, P., Connor, J. R., & Crichton, R. R. (2004). Iron, brain ageing and neurodegenerative disorders. Nature Reviews. Neuroscience, ***5***(11), 863.

APPENDIX

Spectral data of synthesized compounds

Spectral data of synthesized compounds

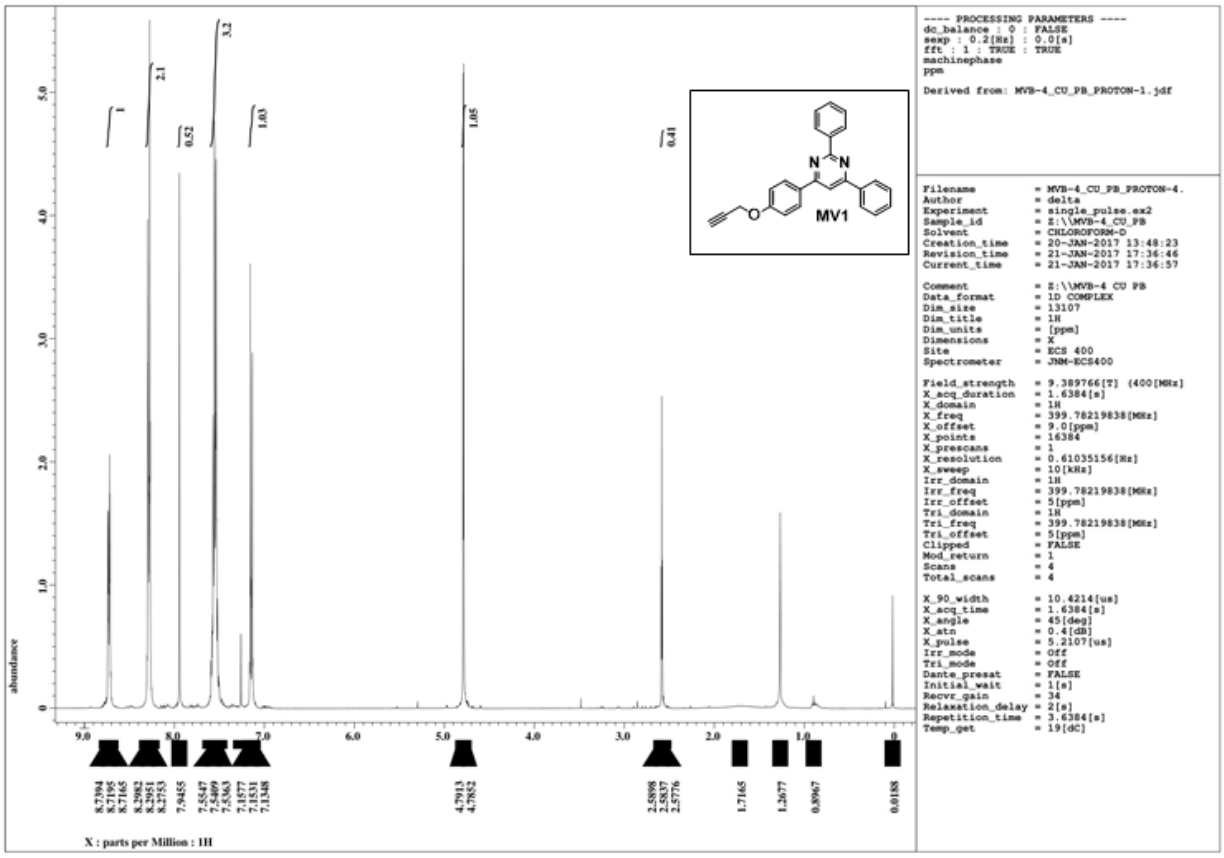

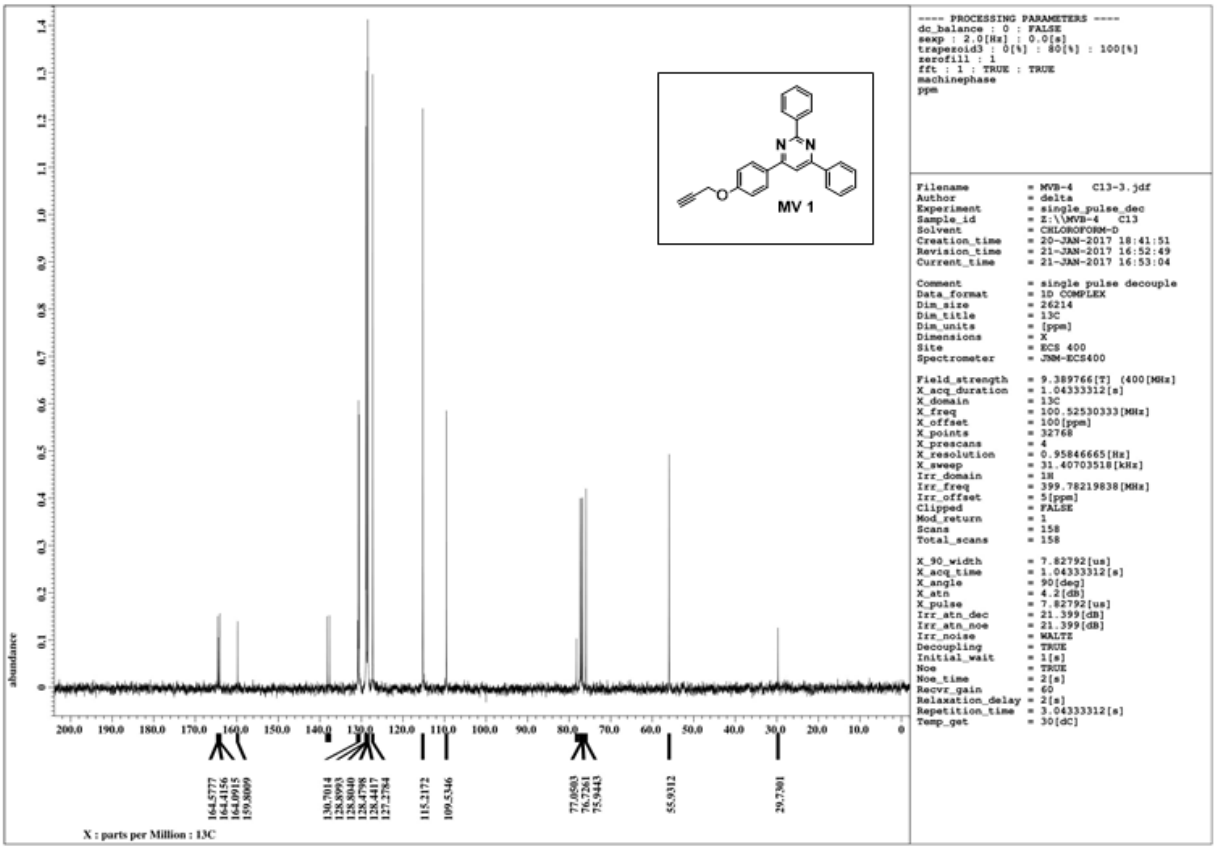
MV 1
abundance
X : parts per Million : 13C
164.5777
164.4156
164.0915
159.8099
130.7014
128.8993
128.8040
128.4798
128.4417
127.2784
115.2172
109.5346
77.0583
76.7261
75.9443
55.9312
29.7301
---- PROCESSING PARAMETERS ----
dc_balance : 0 : FALSE
sexp : 2.0[Hz] : 0.0[s]
trapezoid3 : 0[%] : 80[%] : 100[%]
zerofill : 1
fft : 1 : TRUE : TRUE
machinephase
ppm
Filename = MVB-4 C13-3.jdf
Author = delta
Experiment = single_pulse_dec
Sample_id = Z:\\MVB-4 C13
Solvent = CHLOROFORM-D
Creation_time = 20-JAN-2017 18:41:51
Revision_time = 21-JAN-2017 16:52:49
Current_time = 21-JAN-2017 16:53:04
Comment = single pulse decouple
Data_format = 1D COMPLEX
Dim_size = 26214
Dim_title = 13C
Dim_units = [ppm]
Dimensions = X
Site = ECS 400
Spectrometer = JNM-ECS400
Field_strength = 9.389766[T] (400[MHz]
X_acq_duration = 1.04333312[s]
X_domain = 13C
X_freq = 100.52530333[MHz]
X_offset = 100[ppm]
X_points = 32768
X_prescans = 4
X_resolution = 0.95846665[Hz]
X_sweep = 31.40703518[kHz]
Irr_domain = 1H
Irr_freq = 399.78219838[MHz]
Irr_offset = 5[ppm]
Clipped = FALSE
Mod_return = 1
Scans = 158
Total_scans = 158
X_90_width = 7.82792[us]
X_acq_time = 1.04333312[s]
X_angle = 90[deg]
X_atn = 4.2[dB]
X_pulse = 7.82792[us]
Irr_atn_dec = 21.399[dB]
Irr_atn_noe = 21.399[dB]
Irr_noise = WALTZ
Decoupling = TRUE
Initial_wait = 1[s]
Noe = TRUE
Noe_time = 2[s]
Recvr_gain = 60
Relaxation_delay = 2[s]
Repetition_time = 3.04333312[s]
Temp_get = 30[dC]

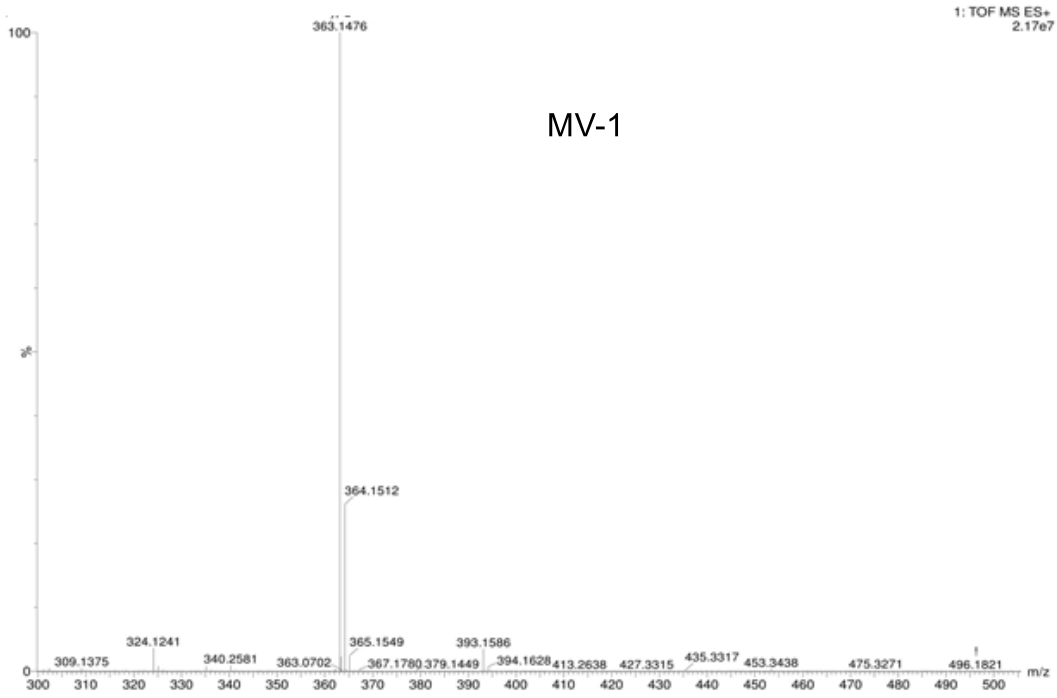
1: TOF MS ES+
2.17e7
100
%
0
363.1476
364.1512
324.1241
309.1375
340.2581
363.0702
365.1549
367.1780
379.1449
393.1586
394.1628
413.2638
427.3315
435.3317
453.3438
475.3271
496.1821
m/z
300 310 320 330 340 350 360 370 380 390 400 410 420 430 440 450 460 470 480 490 500

MV-1

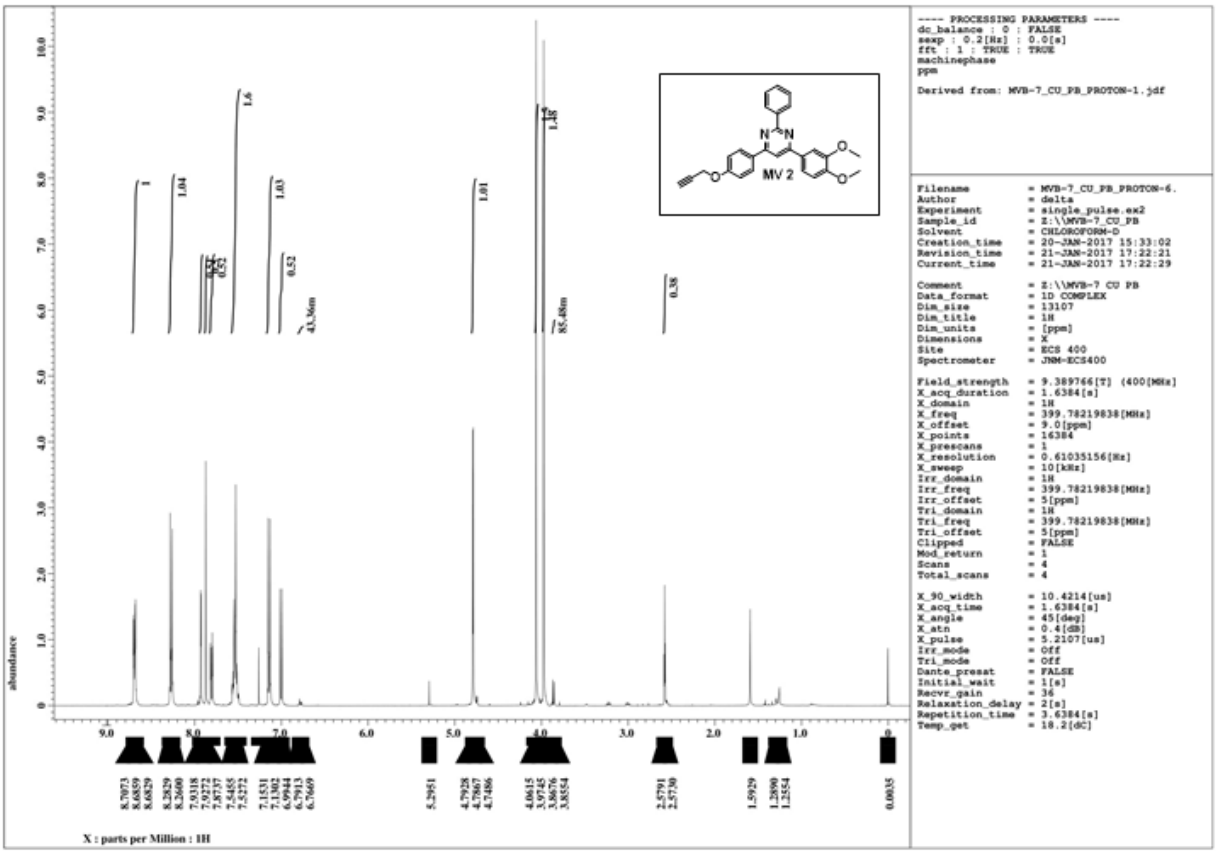
MV 2
abundance
X : parts per Million : 1H
---- PROCESSING PARAMETERS ----
dc_balance : 0 : FALSE
sexp : 0.2[Hz] : 0.0[s]
fft : 1 : TRUE : TRUE
machinephase
ppm
Derived from: MVB-7_CU_PB_PROTON-1.jdf
Filename = MVB-7_CU_PB_PROTON-6.
Author = delta
Experiment = single_pulse.ex2
Sample_id = I:\\MVB-7_CU_PB
Solvent = CHLOROFORM-D
Creation_time = 20-JAN-2017 15:33:02
Revision_time = 21-JAN-2017 17:22:21
Current_time = 21-JAN-2017 17:22:29
Comment = I:\\MVB-7 CU PB
Data_format = 1D COMPLEX
Dim_size = 13107
Dim_title = 1H
Dim_units = [ppm]
Dimensions = X
Site = ECS 400
Spectrometer = JNM-ECS400
Field_strength = 9.389766[T] (400[MHz]
X_acq_duration = 1.6384[s]
X_domain = 1H
X_freq = 399.78219838[MHz]
X_offset = 9.0[ppm]
X_points = 16384
X_prescans = 1
X_resolution = 0.61035156[Hz]
X_sweep = 10[kHz]
Irr_domain = 1H
Irr_freq = 399.78219838[MHz]
Irr_offset = 5[ppm]
Tri_domain = 1H
Tri_freq = 399.78219838[MHz]
Tri_offset = 5[ppm]
Clipped = FALSE
Mod_return = 1
Scans = 4
Total_scans = 4
X_90_width = 10.4214[us]
X_acq_time = 1.6384[s]
X_angle = 45[deg]
X_atn = 0.4[dB]
X_pulse = 5.2107[us]
Irr_mode = Off
Tri_mode = Off
Dante_presat = FALSE
Initial_wait = 1[s]
Recvr_gain = 36
Relaxation_delay = 2[s]
Repetition_time = 3.6384[s]
Temp_get = 18.2[dC]

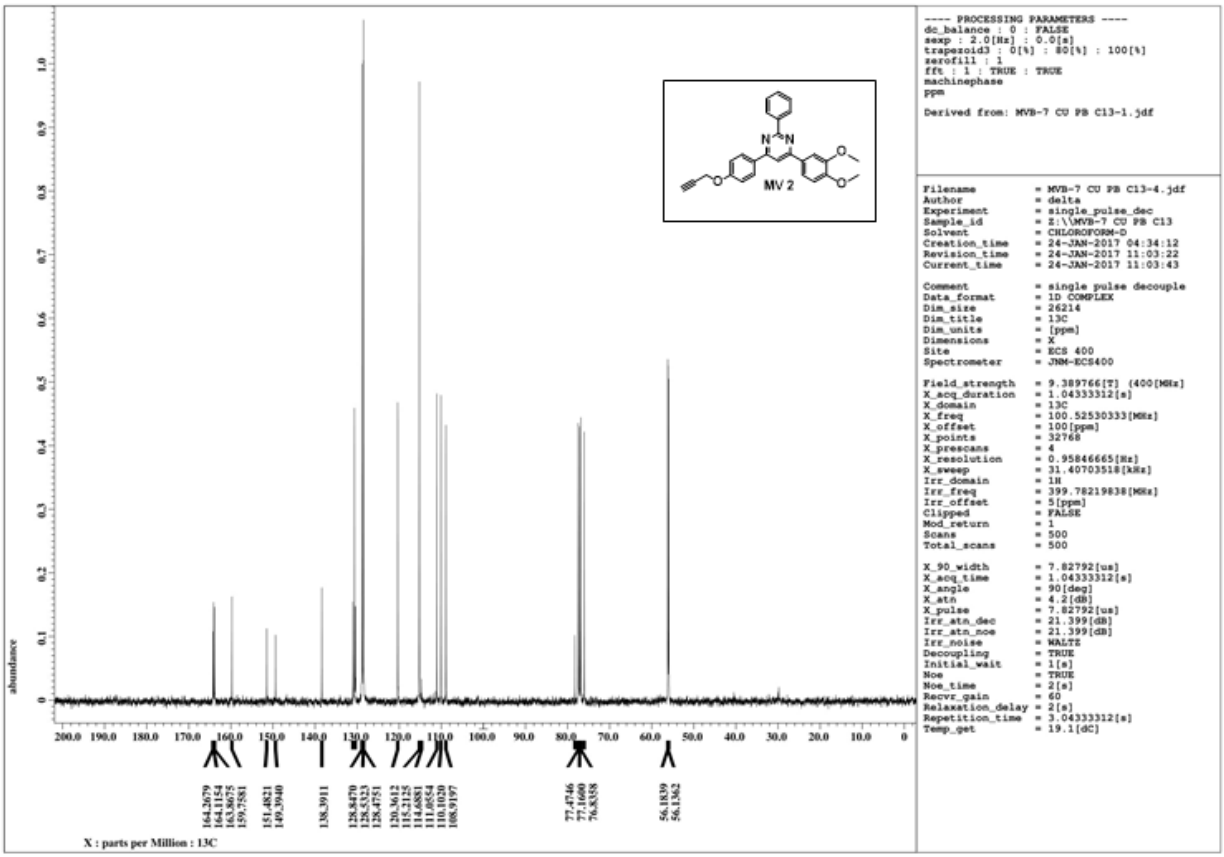


```
---- PROCESSING PARAMETERS ----
dc_balance : 0 : FALSE
sexp : 2.0[Hz] : 0.0[s]
trapezoid3 : 0[%] : 80[%] : 100[%]
zerofill : 1
fft : 1 : TRUE : TRUE
machinephase
ppm

Derived from: MVB-7 CU PB C13-1.jdf
```

```
Filename            = MVB-7 CU PB C13-4.jdf
Author              = delta
Experiment          = single_pulse_dec
Sample_id           = Z:\\MVB-7 CU PB C13
Solvent             = CHLOROFORM-D
Creation_time       = 24-JAN-2017 04:34:12
Revision_time       = 24-JAN-2017 11:03:22
Current_time        = 24-JAN-2017 11:03:43

Comment             = single pulse decouple
Data_format         = 1D COMPLEX
Dim_size            = 26214
Dim_title           = 13C
Dim_units           = [ppm]
Dimensions          = X
Site                = ECS 400
Spectrometer        = JNM-ECS400

Field_strength      = 9.389766[T] (400[MHz]
X_acq_duration      = 1.04333312[s]
X_domain            = 13C
X_freq              = 100.52530333[MHz]
X_offset            = 100[ppm]
X_points            = 32768
X_prescans          = 4
X_resolution        = 0.95846665[Hz]
X_sweep             = 31.40703518[kHz]
Irr_domain          = 1H
Irr_freq            = 399.78219838[MHz]
Irr_offset          = 5[ppm]
Clipped             = FALSE
Mod_return          = 1
Scans               = 500
Total_scans         = 500

X_90_width          = 7.82792[us]
X_acq_time          = 1.04333312[s]
X_angle             = 90[deg]
X_atn               = 4.2[dB]
X_pulse             = 7.82792[us]
Irr_atn_dec         = 21.399[dB]
Irr_atn_noe         = 21.399[dB]
Irr_noise           = WALTZ
Decoupling          = TRUE
Initial_wait        = 1[s]
Noe                 = TRUE
Noe_time            = 2[s]
Recvr_gain          = 60
Relaxation_delay    = 2[s]
Repetition_time     = 3.04333312[s]
Temp_get            = 19.1[dC]
```

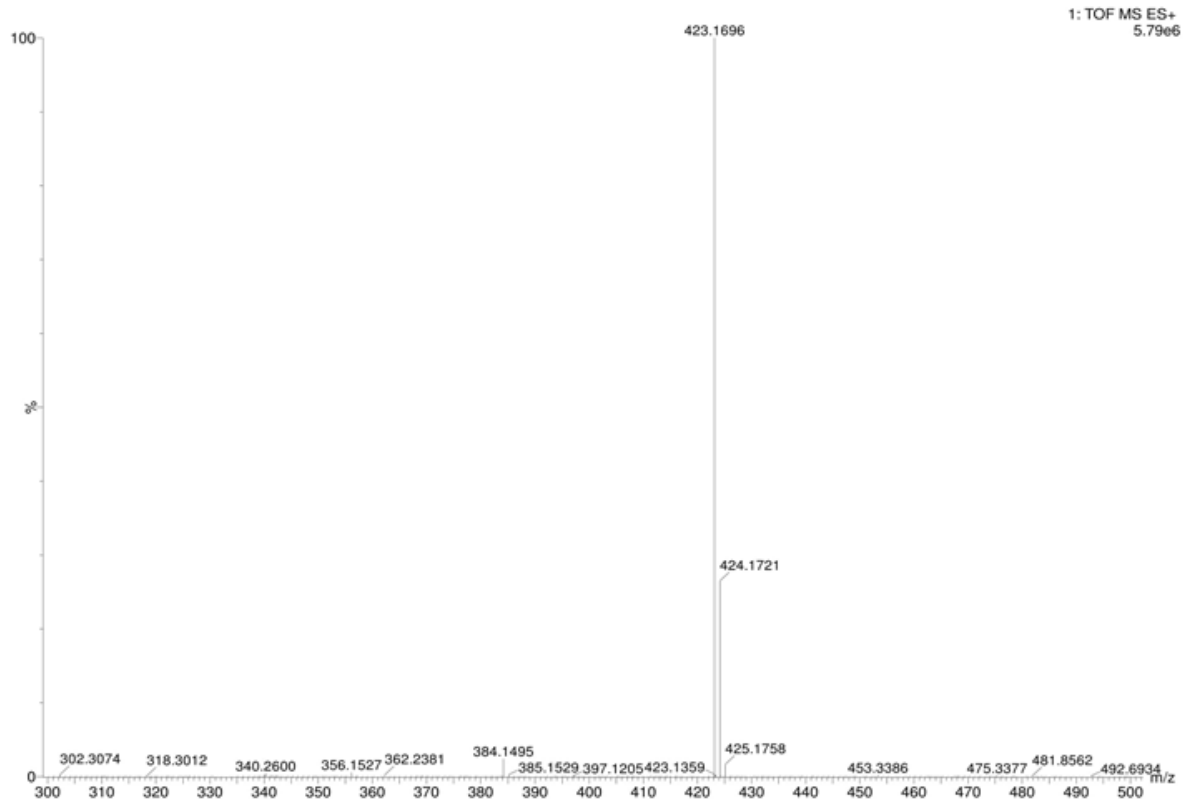
1: TOF MS ES+
5.79e6
100
%
0
423.1696
424.1721
425.1758
302.3074
318.3012
340.2600
356.1527
362.2381
384.1495
385.1529
397.1205
423.1359
453.3386
475.3377
481.8562
492.6934
300 310 320 330 340 350 360 370 380 390 400 410 420 430 440 450 460 470 480 490 500
m/z

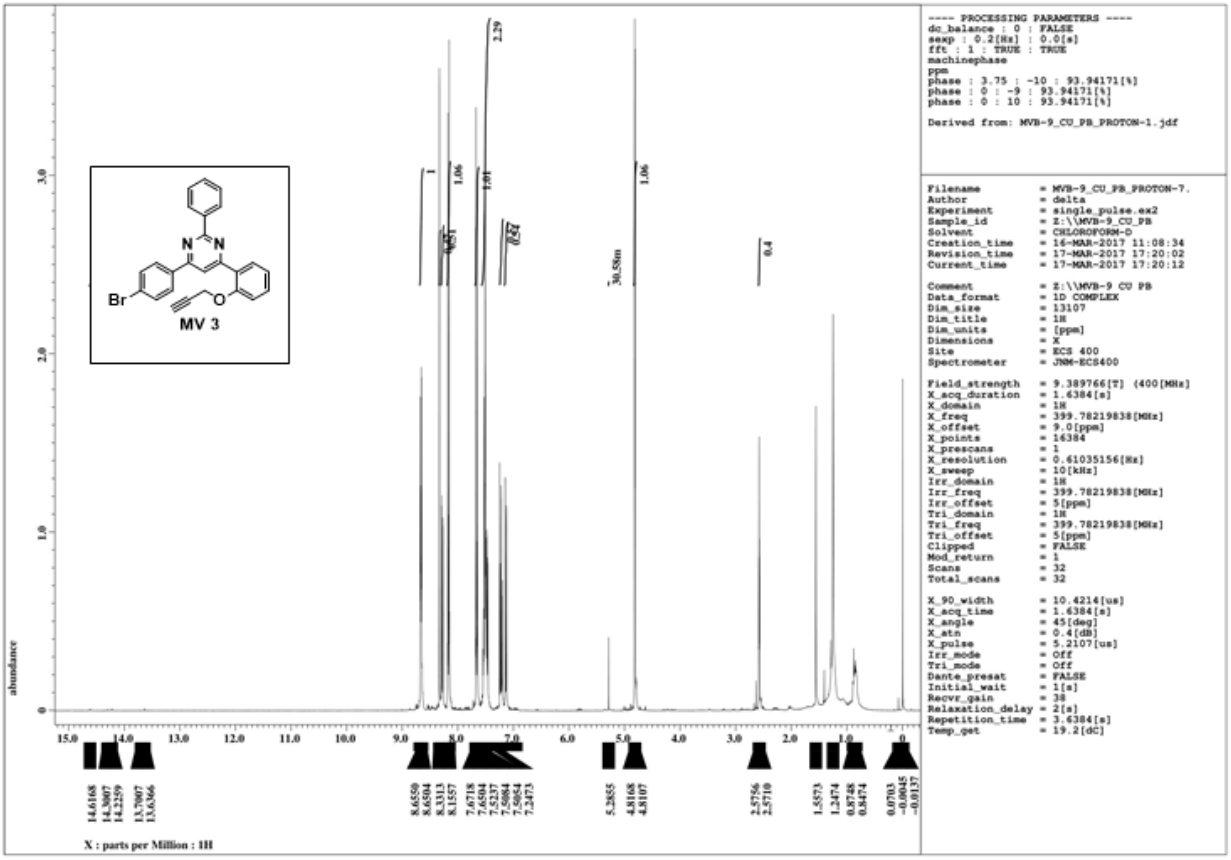
MV 3
Br
N
N
O
abundance
X : parts per Million : 1H
---- PROCESSING PARAMETERS ----
dc_balance : 0 : FALSE
sexp : 0.2[Hz] : 0.0[s]
fft : 1 : TRUE : TRUE
machinephase
ppm
phase : 3.75 : -10 : 93.94171[%]
phase : 0 : -9 : 93.94171[%]
phase : 0 : 10 : 93.94171[%]
Derived from: MVB-9_CU_PB_PROTON-1.jdf
Filename = MVB-9_CU_PB_PROTON-7.
Author = delta
Experiment = single_pulse.ex2
Sample_id = Z:\\MVB-9_CU_PB
Solvent = CHLOROFORM-D
Creation_time = 16-MAR-2017 11:08:34
Revision_time = 17-MAR-2017 17:20:02
Current_time = 17-MAR-2017 17:20:12
Comment = Z:\\MVB-9 CU PB
Data_format = 1D COMPLEX
Dim_size = 13107
Dim_title = 1H
Dim_units = [ppm]
Dimensions = X
Site = ECS 400
Spectrometer = JNM-ECS400
Field_strength = 9.389766[T] (400[MHz]
X_acq_duration = 1.6384[s]
X_domain = 1H
X_freq = 399.78219838[MHz]
X_offset = 9.0[ppm]
X_points = 16384
X_prescans = 1
X_resolution = 0.61035156[Hz]
X_sweep = 10[kHz]
Irr_domain = 1H
Irr_freq = 399.78219838[MHz]
Irr_offset = 5[ppm]
Tri_domain = 1H
Tri_freq = 399.78219838[MHz]
Tri_offset = 5[ppm]
Clipped = FALSE
Mod_return = 1
Scans = 32
Total_scans = 32
X_90_width = 10.4214[us]
X_acq_time = 1.6384[s]
X_angle = 45[deg]
X_atn = 0.4[dB]
X_pulse = 5.2107[us]
Irr_mode = Off
Tri_mode = Off
Dante_presat = FALSE
Initial_wait = 1[s]
Recvr_gain = 38
Relaxation_delay = 2[s]
Repetition_time = 3.6384[s]
Temp_get = 19.2[dC]

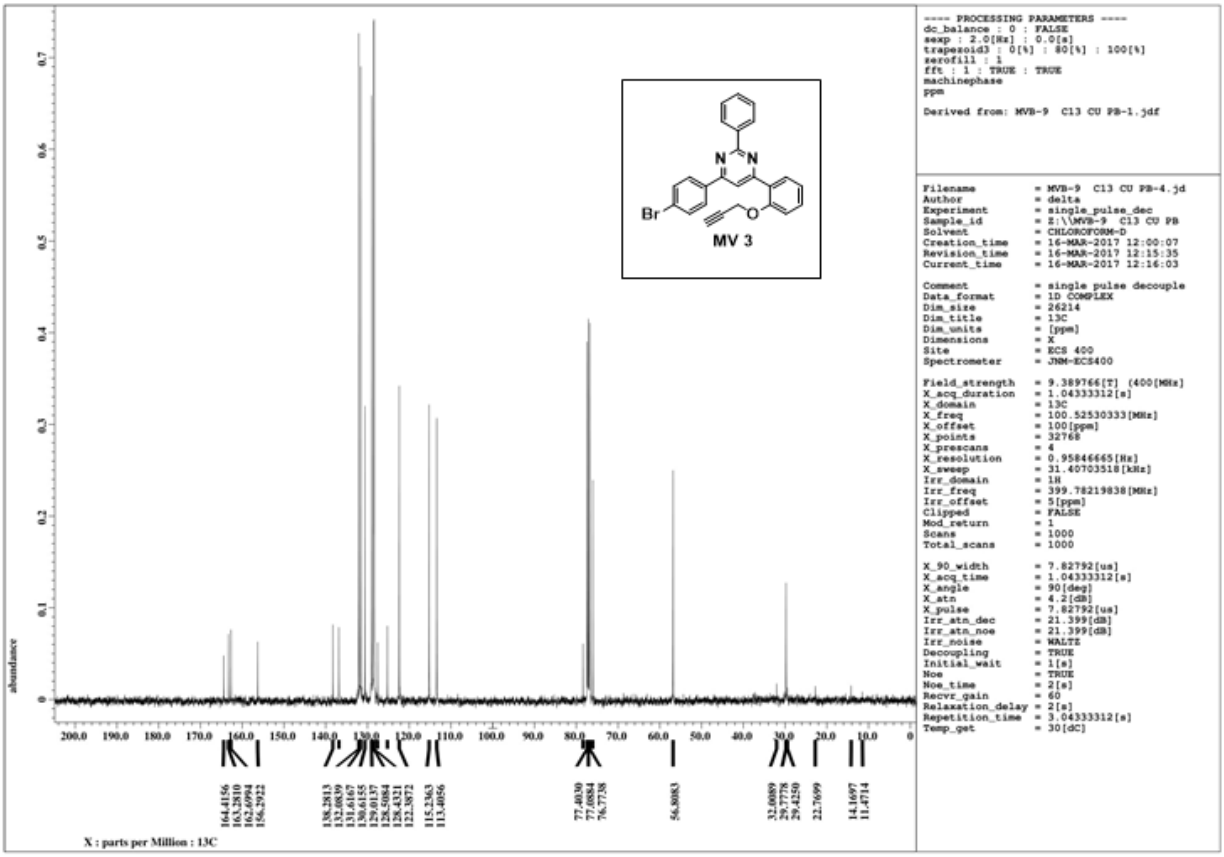
MV 3
Br
N
N
O
abundance
X : parts per Million : 13C
164.4156
163.2810
162.6994
156.2922
138.2813
132.6839
131.1457
130.6155
129.0137
128.5084
128.4321
122.3872
115.2363
113.4056
77.4030
77.0884
76.7738
56.6083
32.6089
29.7778
29.4250
22.7699
14.1697
11.4714
==== PROCESSING PARAMETERS ====
dc_balance : 0 : FALSE
sexp : 2.0[Hz] : 0.0[s]
trapezoid3 : 0[%] : 80[%] : 100[%]
zerofill : 1
fft : 1 : TRUE : TRUE
machinephase
ppm
Derived from: MVB-9 C13 CU PB-1.jdf
Filename = MVB-9 C13 CU PB-4.jd
Author = delta
Experiment = single_pulse_dec
Sample_id = Z:\\MVB-9 C13 CU PB
Solvent = CHLOROFORM-D
Creation_time = 16-MAR-2017 12:00:07
Revision_time = 16-MAR-2017 12:15:35
Current_time = 16-MAR-2017 12:16:03
Comment = single pulse decouple
Data_format = 1D COMPLEX
Dim_size = 26214
Dim_title = 13C
Dim_units = [ppm]
Dimensions = X
Site = ECS 400
Spectrometer = JNM-ECS400
Field_strength = 9.389766[T] (400[MHz]
X_acq_duration = 1.04333312[s]
X_domain = 13C
X_freq = 100.52530333[MHz]
X_offset = 100[ppm]
X_points = 32768
X_prescans = 4
X_resolution = 0.95846665[Hz]
X_sweep = 31.40703518[kHz]
Irr_domain = 1H
Irr_freq = 399.78219838[MHz]
Irr_offset = 5[ppm]
Clipped = FALSE
Mod_return = 1
Scans = 1000
Total_scans = 1000
X_90_width = 7.82792[us]
X_acq_time = 1.04333312[s]
X_angle = 90[deg]
X_atn = 4.2[dB]
X_pulse = 7.82792[us]
Irr_atn_dec = 21.399[dB]
Irr_atn_noe = 21.399[dB]
Irr_noise = WALTZ
Decoupling = TRUE
Initial_wait = 1[s]
Noe = TRUE
Noe_time = 2[s]
Recvr_gain = 60
Relaxation_delay = 2[s]
Repetition_time = 3.04333312[s]
Temp_get = 30[dC]

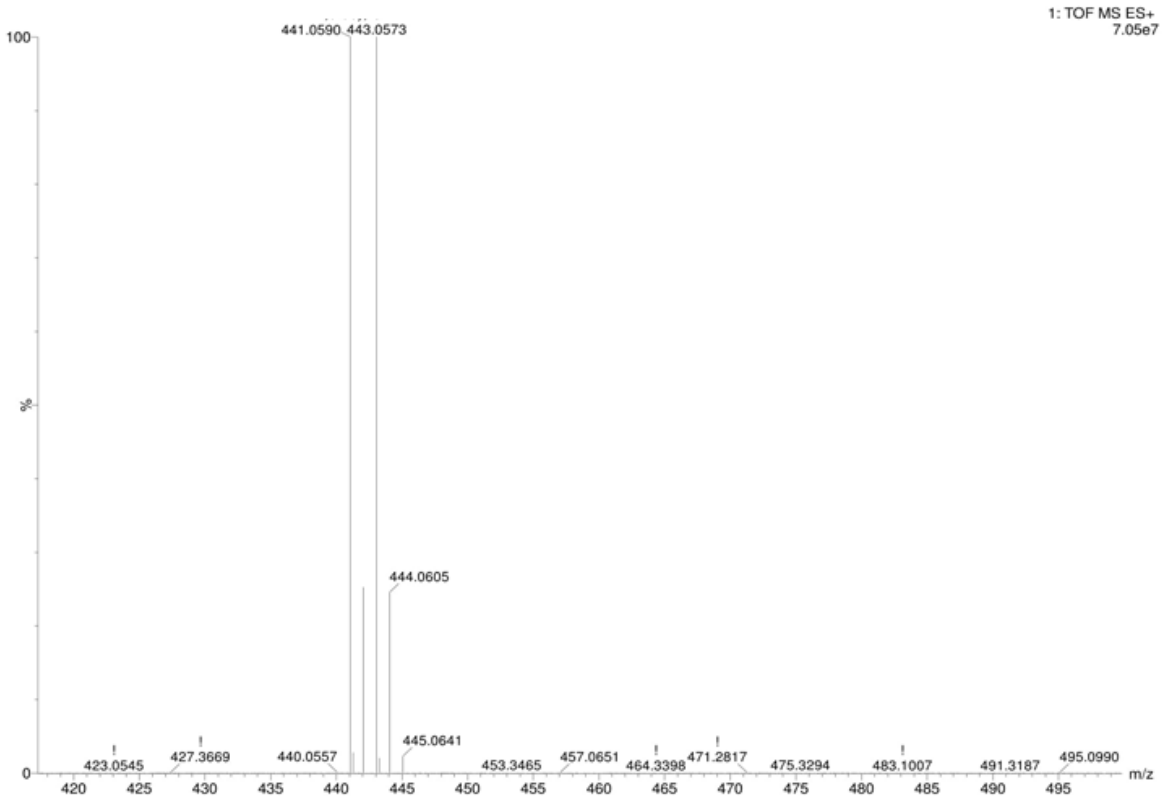
1: TOF MS ES+
7.05e7
100
%
0
441.0590
443.0573
444.0605
445.0641
423.0545
427.3669
440.0557
453.3465
457.0651
464.3398
471.2817
475.3294
483.1007
491.3187
495.0990
420
425
430
435
440
445
450
455
460
465
470
475
480
485
490
495
m/z

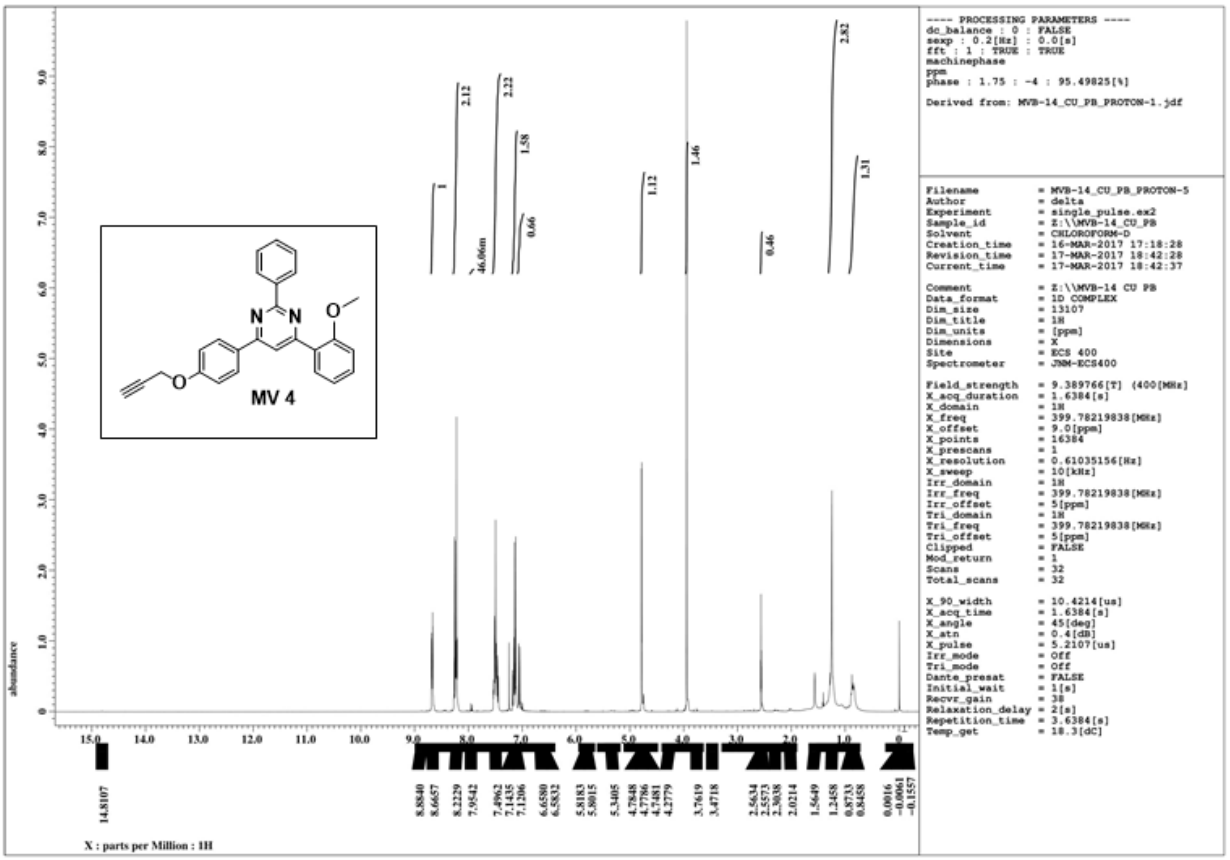
MV 4
abundance
X : parts per Million : 1H
---- PROCESSING PARAMETERS ----
dc_balance : 0 : FALSE
sexp : 0.2[Hz] : 0.0[s]
fft : 1 : TRUE : TRUE
machinephase
ppm
phase : 1.75 : -4 : 95.49825[%]
Derived from: MVB-14_CU_PB_PROTON-1.jdf
Filename = MVB-14_CU_PB_PROTON-5
Author = delta
Experiment = single_pulse.ex2
Sample_id = Z:\\MVB-14_CU_PB
Solvent = CHLOROFORM-D
Creation_time = 16-MAR-2017 17:18:28
Revision_time = 17-MAR-2017 18:42:28
Current_time = 17-MAR-2017 18:42:37
Comment = Z:\\MVB-14 CU PB
Data_format = 1D COMPLEX
Dim_size = 13107
Dim_title = 1H
Dim_units = [ppm]
Dimensions = X
Site = ECS 400
Spectrometer = JNM-ECS400
Field_strength = 9.389766[T] (400[MHz]
X_acq_duration = 1.6384[s]
X_domain = 1H
X_freq = 399.78219838[MHz]
X_offset = 9.0[ppm]
X_points = 16384
X_prescans = 1
X_resolution = 0.61035156[Hz]
X_sweep = 10[kHz]
Irr_domain = 1H
Irr_freq = 399.78219838[MHz]
Irr_offset = 5[ppm]
Tri_domain = 1H
Tri_freq = 399.78219838[MHz]
Tri_offset = 5[ppm]
Clipped = FALSE
Mod_return = 1
Scans = 32
Total_scans = 32
X_90_width = 10.4214[us]
X_acq_time = 1.6384[s]
X_angle = 45[deg]
X_atn = 0.4[dB]
X_pulse = 5.2107[us]
Irr_mode = Off
Tri_mode = Off
Dante_presat = FALSE
Initial_wait = 1[s]
Recvr_gain = 38
Relaxation_delay = 2[s]
Repetition_time = 3.6384[s]
Temp_get = 18.3[dC]

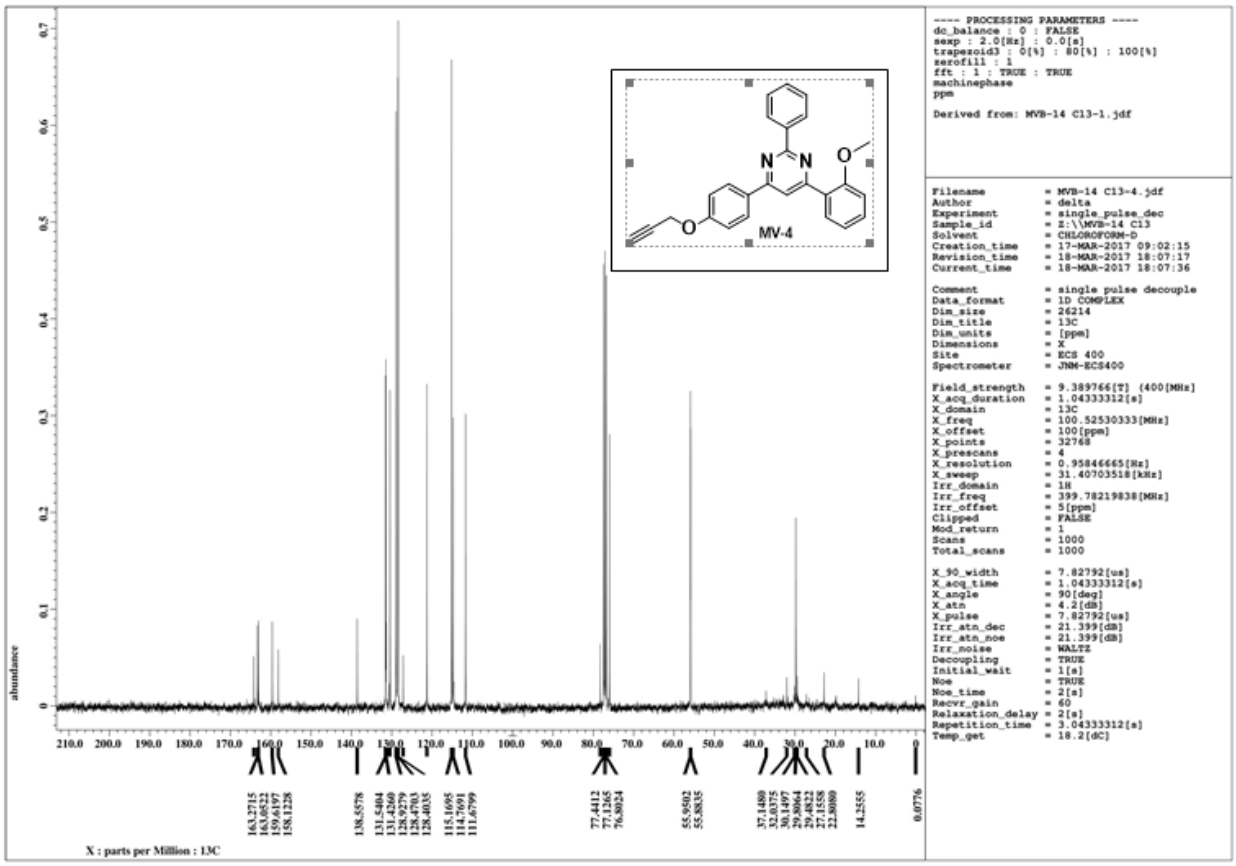


```
----- PROCESSING PARAMETERS -----
dc_balance : 0 : FALSE
sexp : 2.0[Hz] : 0.0[s]
trapezoid3 : 0[%] : 80[%] : 100[%]
zerofill : 1
fft : 1 : TRUE : TRUE
machinephase
ppm

Derived from: MVB-14 C13-1.jdf
```

```
Filename          = MVB-14 C13-4.jdf
Author            = delta
Experiment        = single_pulse_dec
Sample_id         = Z:\\MVB-14 C13
Solvent           = CHLOROFORM-D
Creation_time     = 17-MAR-2017 09:02:15
Revision_time     = 18-MAR-2017 18:07:17
Current_time      = 18-MAR-2017 18:07:36

Comment           = single pulse decouple
Data_format       = 1D COMPLEX
Dim_size          = 26214
Dim_title         = 13C
Dim_units         = [ppm]
Dimensions        = X
Site              = ECS 400
Spectrometer      = JNM-ECS400

Field_strength    = 9.389766[T] (400[MHz]
X_acq_duration    = 1.04333312[s]
X_domain          = 13C
X_freq            = 100.52530333[MHz]
X_offset          = 100[ppm]
X_points          = 32768
X_prescans        = 4
X_resolution      = 0.95846665[Hz]
X_sweep           = 31.40703518[kHz]
Irr_domain        = 1H
Irr_freq          = 399.78219838[MHz]
Irr_offset        = 5[ppm]
Clipped           = FALSE
Mod_return        = 1
Scans             = 1000
Total_scans       = 1000

X_90_width        = 7.82792[us]
X_acq_time        = 1.04333312[s]
X_angle           = 90[deg]
X_atn             = 4.2[dB]
X_pulse           = 7.82792[us]
Irr_atn_dec       = 21.399[dB]
Irr_atn_noe       = 21.399[dB]
Irr_noise         = WALTZ
Decoupling        = TRUE
Initial_wait      = 1[s]
Noe               = TRUE
Noe_time          = 2[s]
Recvr_gain        = 60
Relaxation_delay  = 2[s]
Repetition_time   = 3.04333312[s]
Temp_get          = 18.2[dC]
```

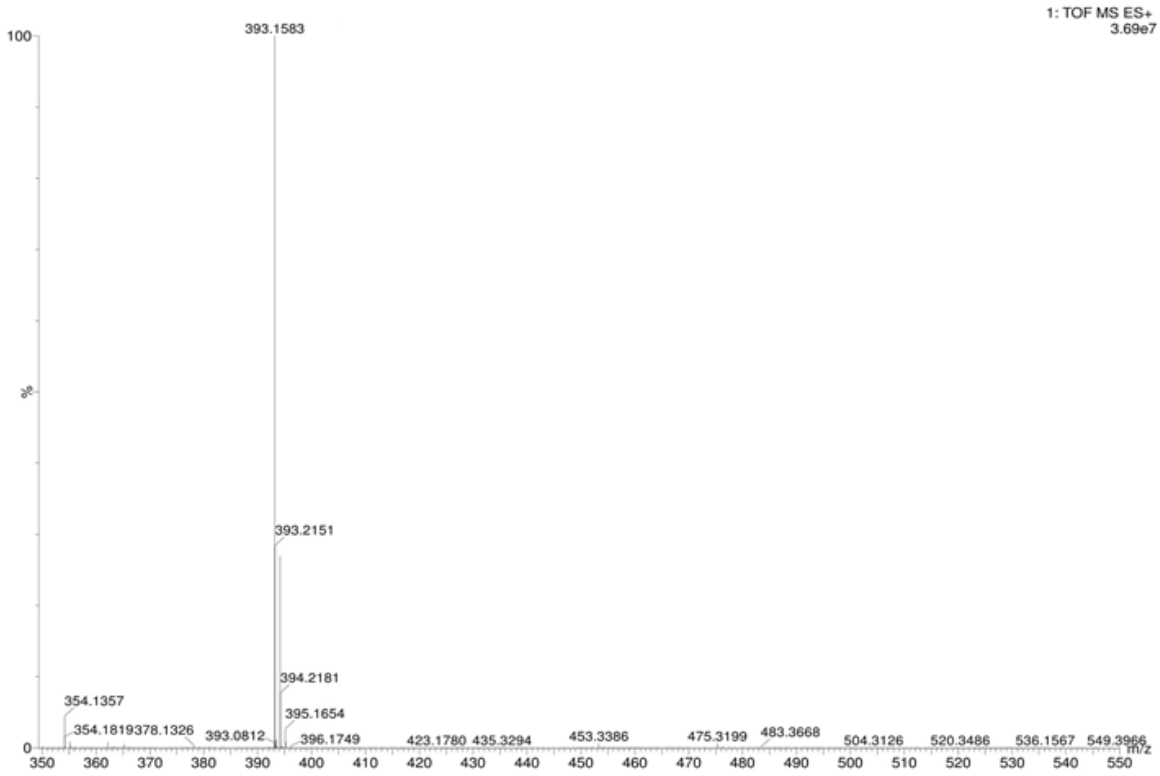
1: TOF MS ES+
3.69e7
100
%
0
393.1583
393.2151
394.2181
354.1357
395.1654
354.1819
378.1326
393.0812
396.1749
423.1780
435.3294
453.3386
475.3199
483.3668
504.3126
520.3486
536.1567
549.3966
m/z
350
360
370
380
390
400
410
420
430
440
450
460
470
480
490
500
510
520
530
540
550

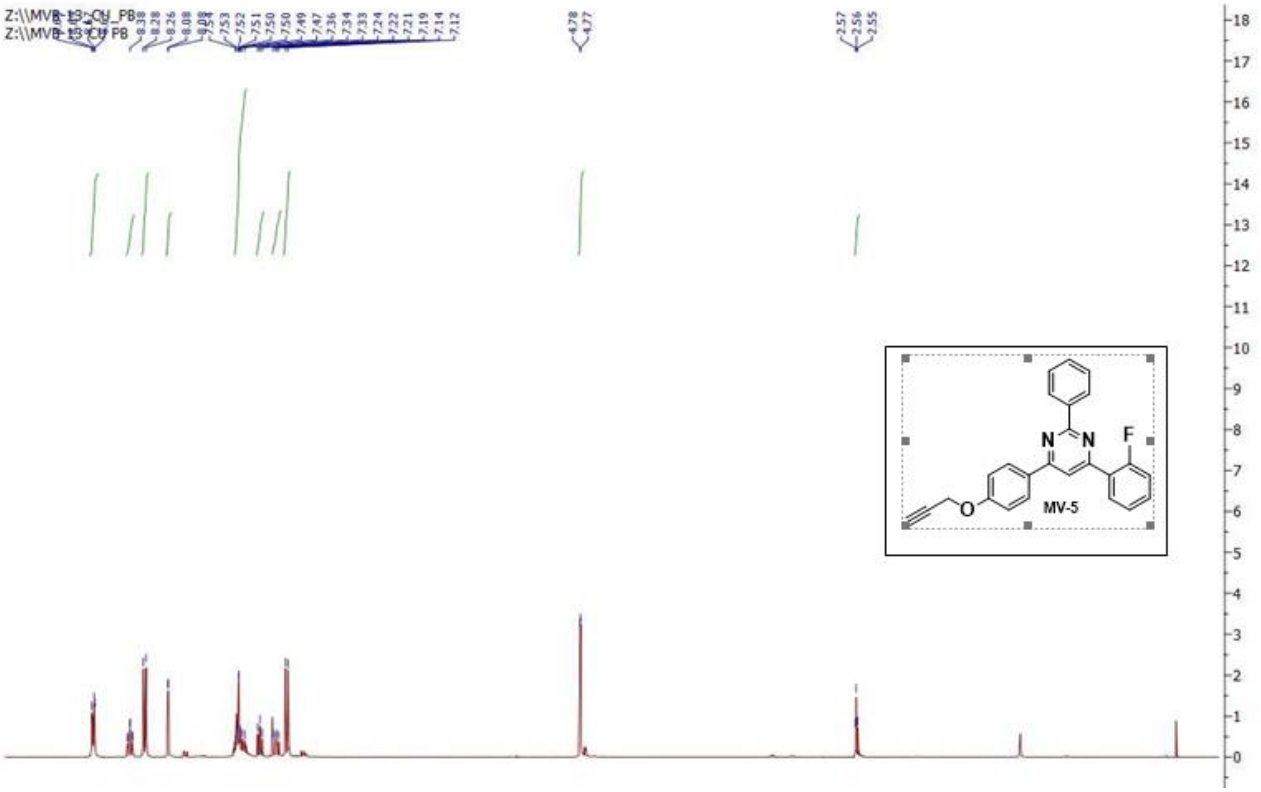
MV-5
N
N
F
O

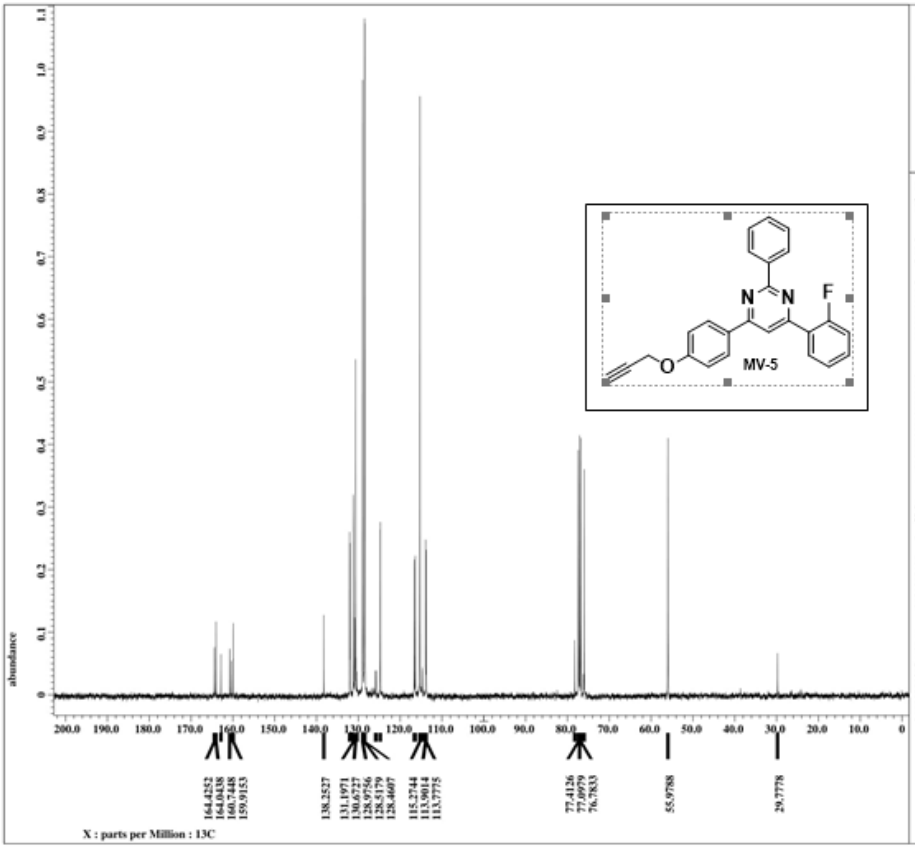


```
---- PROCESSING PARAMETERS ----
dc_balance : 0 : FALSE
seap : 2.0[Hz] : 0.0[s]
trapezoid3 : 0[%] : 80[%] : 100[%]
zerofill : 1
fft : 1 : TRUE : TRUE
machinephase
ppm

Derived from: MVB-13  C13 CU PB-1.jdf
```

Filename	= MVB-13 C13 CU PB-4.j
Author	= delta
Experiment	= single_pulse_dec
Sample_id	= I:\\MVB-13 C13 CU PB
Solvent	= CHLOROFORM-D
Creation_time	= 16-MAR-2017 10:58:09
Revision_time	= 16-MAR-2017 12:11:51
Current_time	= 16-MAR-2017 12:12:24
Comment	= single pulse decouple
Data_format	= 1D COMPLEX
Dim_size	= 26214
Dim_title	= 13C
Dim_units	= [ppm]
Dimensions	= X
Site	= ECS 400
Spectrometer	= JNM-ECS400
Field_strength	= 9.389766[T] (400[MHz]
X_acq_duration	= 1.04333312[s]
X_domain	= 13C
X_freq	= 100.52530333[MHz]
X_offset	= 100[ppm]
X_points	= 32768
X_prescans	= 4
X_resolution	= 0.95846665[Hz]
X_sweep	= 31.40703518[kHz]
Irr_domain	= 1H
Irr_freq	= 399.78219838[MHz]
Irr_offset	= 5[ppm]
Clipped	= FALSE
Mod_return	= 1
Scans	= 1000
Total_scans	= 1000
X_90_width	= 7.82792[us]
X_acq_time	= 1.04333312[s]
X_angle	= 90[deg]
X_atn	= 4.2[dB]
X_pulse	= 7.82792[us]
Irr_atn_dec	= 21.399[dB]
Irr_atn_noe	= 21.399[dB]
Irr_noise	= WALTZ
Decoupling	= TRUE
Initial_wait	= 1[s]
Noe	= TRUE
Noe_time	= 2[s]
Recvr_gain	= 60
Relaxation_delay	= 2[s]
Repetition_time	= 3.04333312[s]
Temp_get	= 30[dC]

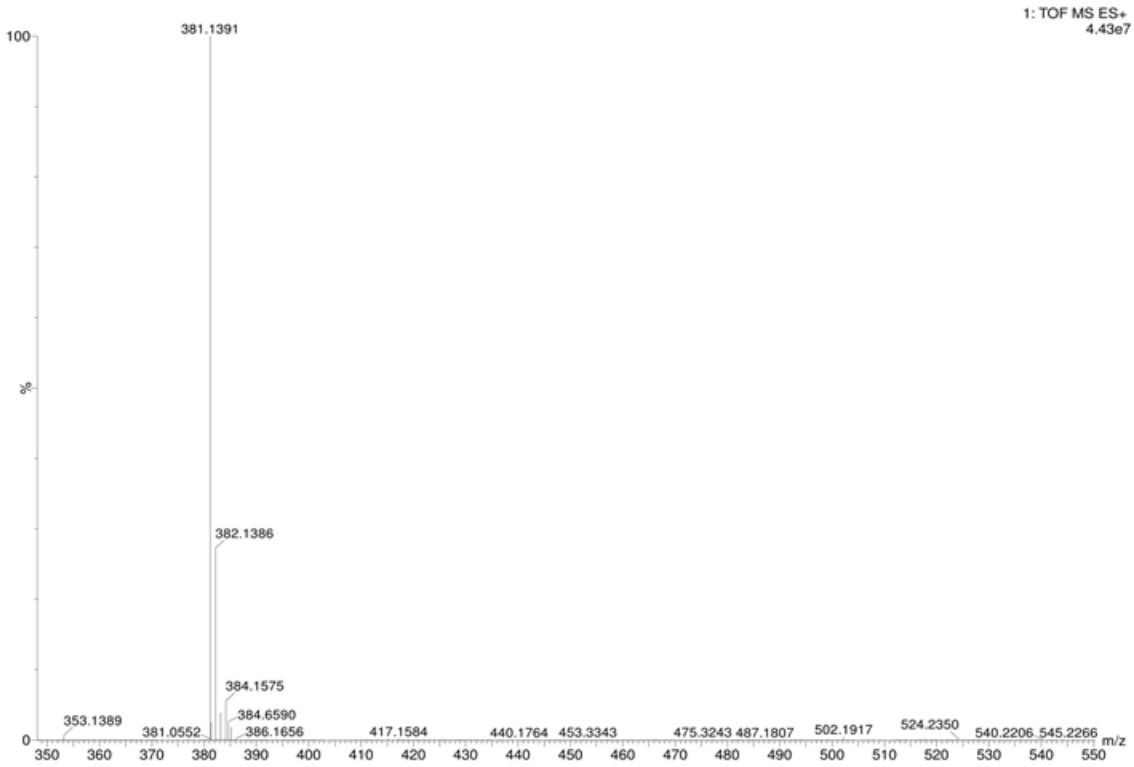
1: TOF MS ES+
4.43e7
100
%
0
381.1391
382.1386
384.1575
384.6590
353.1389
381.0552
386.1656
417.1584
440.1764
453.3343
475.3243
487.1807
502.1917
524.2350
540.2206
545.2266
350
360
370
380
390
400
410
420
430
440
450
460
470
480
490
500
510
520
530
540
550
m/z

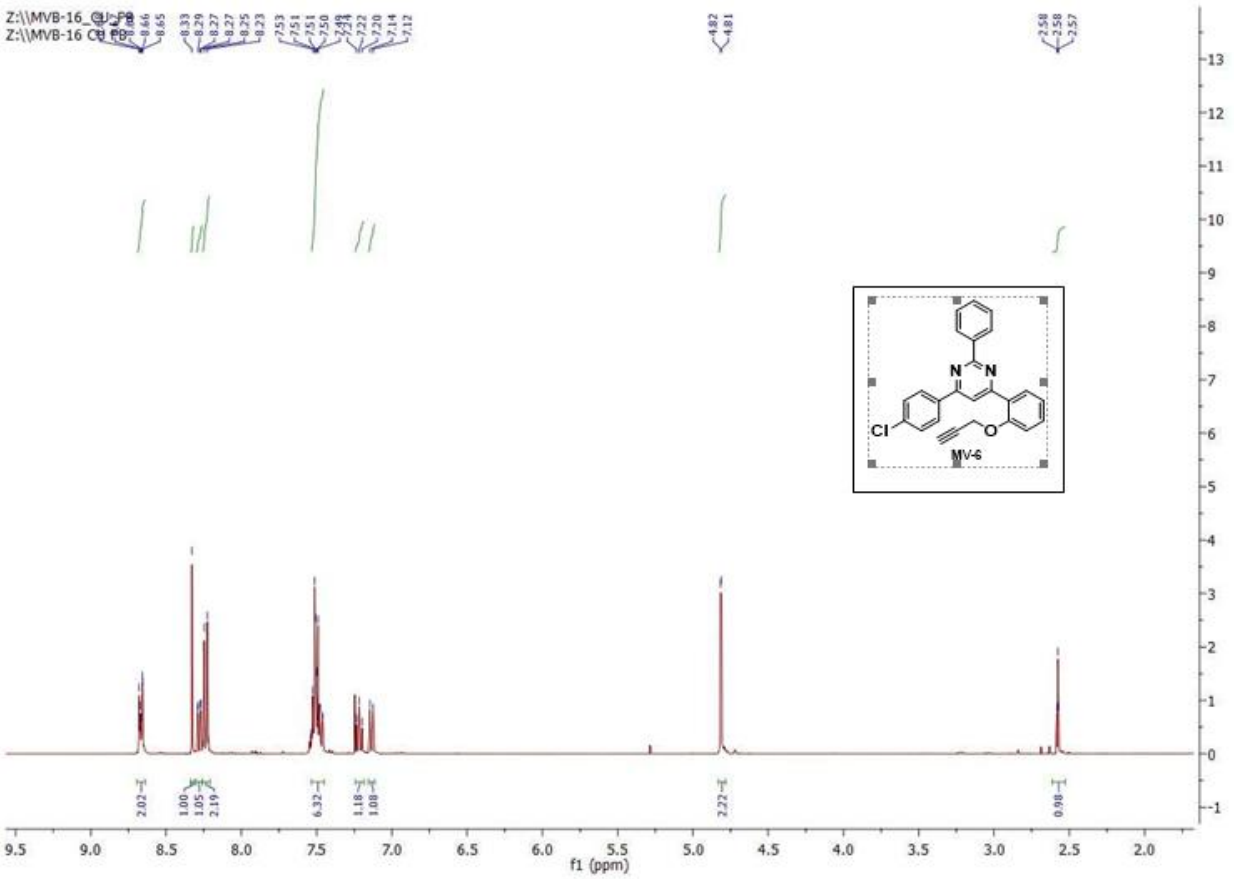
Z:\\MVB-16_01_FID
Z:\\MVB-16 C1 FID
8.66
8.65
8.33
8.29
8.27
8.27
8.25
8.23
7.53
7.51
7.51
7.50
7.24
7.22
7.20
7.14
7.12
4.82
4.81
2.58
2.58
2.57
Cl
N
N
O
MV-6
2.02
1.00
1.05
2.19
6.32
1.18
1.08
2.22
0.98
9.5
9.0
8.5
8.0
7.5
7.0
6.5
6.0
5.5
5.0
4.5
4.0
3.5
3.0
2.5
2.0
f1 (ppm)

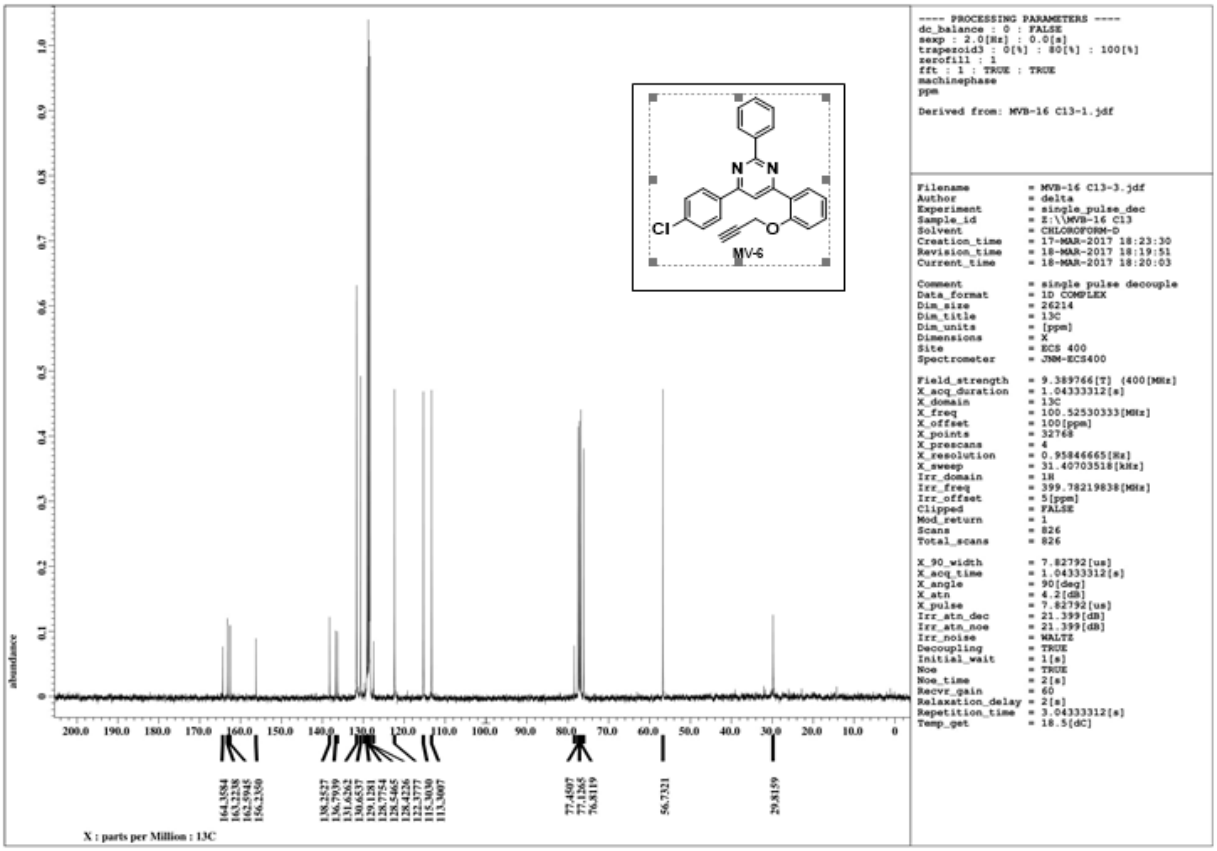


```
---- PROCESSING PARAMETERS ----
dc_balance : 0 : FALSE
sexp : 2.0[Hz] : 0.0[s]
trapezoid3 : 0[%] : 80[%] : 100[%]
zerofill : 1
fft : 1 : TRUE : TRUE
machinephase
ppm

Derived from: MVB-16 C13-1.jdf
```

```
Filename          = MVB-16 C13-3.jdf
Author            = delta
Experiment        = single_pulse_dec
Sample_id         = E:\\MVB-16 C13
Solvent           = CHLOROFORM-D
Creation_time     = 17-MAR-2017 18:23:30
Revision_time     = 18-MAR-2017 18:19:51
Current_time      = 18-MAR-2017 18:20:03

Comment           = single pulse decouple
Data_format       = 1D COMPLEX
Dim_size          = 26214
Dim_title         = 13C
Dim_units         = [ppm]
Dimensions        = X
Site              = ECS 400
Spectrometer      = JNM-ECS400

Field_strength    = 9.389766[T] (400[MHz]
X_acq_duration    = 1.04333312[s]
X_domain          = 13C
X_freq            = 100.52530333[MHz]
X_offset          = 100[ppm]
X_points          = 32768
X_prescans        = 4
X_resolution      = 0.95846665[Hz]
X_sweep           = 31.40703518[kHz]
Irr_domain        = 1H
Irr_freq          = 399.78219838[MHz]
Irr_offset        = 5[ppm]
Clipped           = FALSE
Mod_return        = 1
Scans             = 826
Total_scans       = 826

X_90_width        = 7.82792[us]
X_acq_time        = 1.04333312[s]
X_angle           = 90[deg]
X_atn             = 4.2[dB]
X_pulse           = 7.82792[us]
Irr_atn_dec       = 21.399[dB]
Irr_atn_noe       = 21.399[dB]
Irr_noise         = WALTZ
Decoupling        = TRUE
Initial_wait      = 1[s]
Noe               = TRUE
Noe_time          = 2[s]
Recvr_gain        = 60
Relaxation_delay  = 2[s]
Repetition_time   = 3.04333312[s]
Temp_get          = 18.5[dC]
```

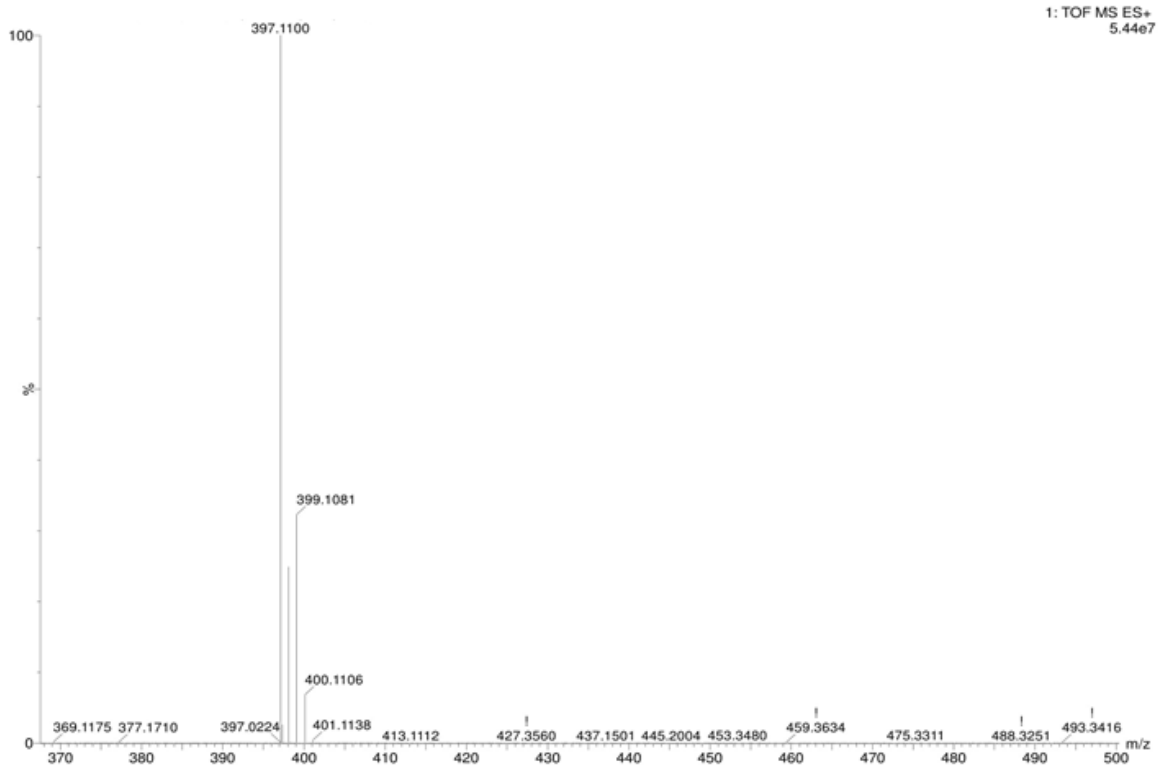
1: TOF MS ES+
5.44e7
100
%
0
397.1100
399.1081
400.1106
369.1175
377.1710
397.0224
401.1138
413.1112
427.3560
437.1501
445.2004
453.3480
459.3634
475.3311
488.3251
493.3416
370
380
390
400
410
420
430
440
450
460
470
480
490
500
m/z

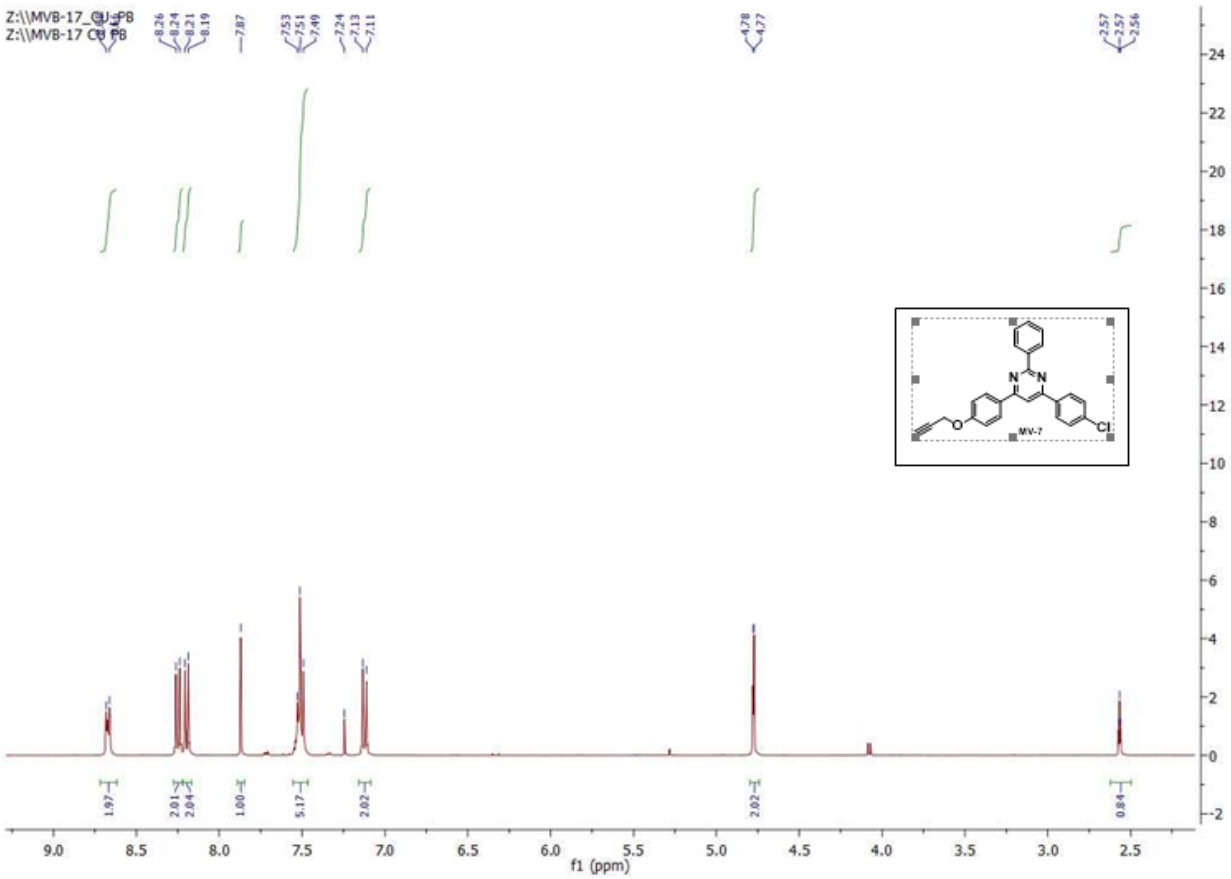
Z:\\MVB-17_CDCl3_P8
Z:\\MVB-17 CDCl3 P8
8.26
8.24
8.21
8.19
7.87
7.53
7.51
7.49
7.24
7.13
7.11
4.78
4.77
2.57
2.57
2.56
MV-7
Cl
1.97
2.01
2.04
1.00
5.17
2.02
2.02
0.84
f1 (ppm)

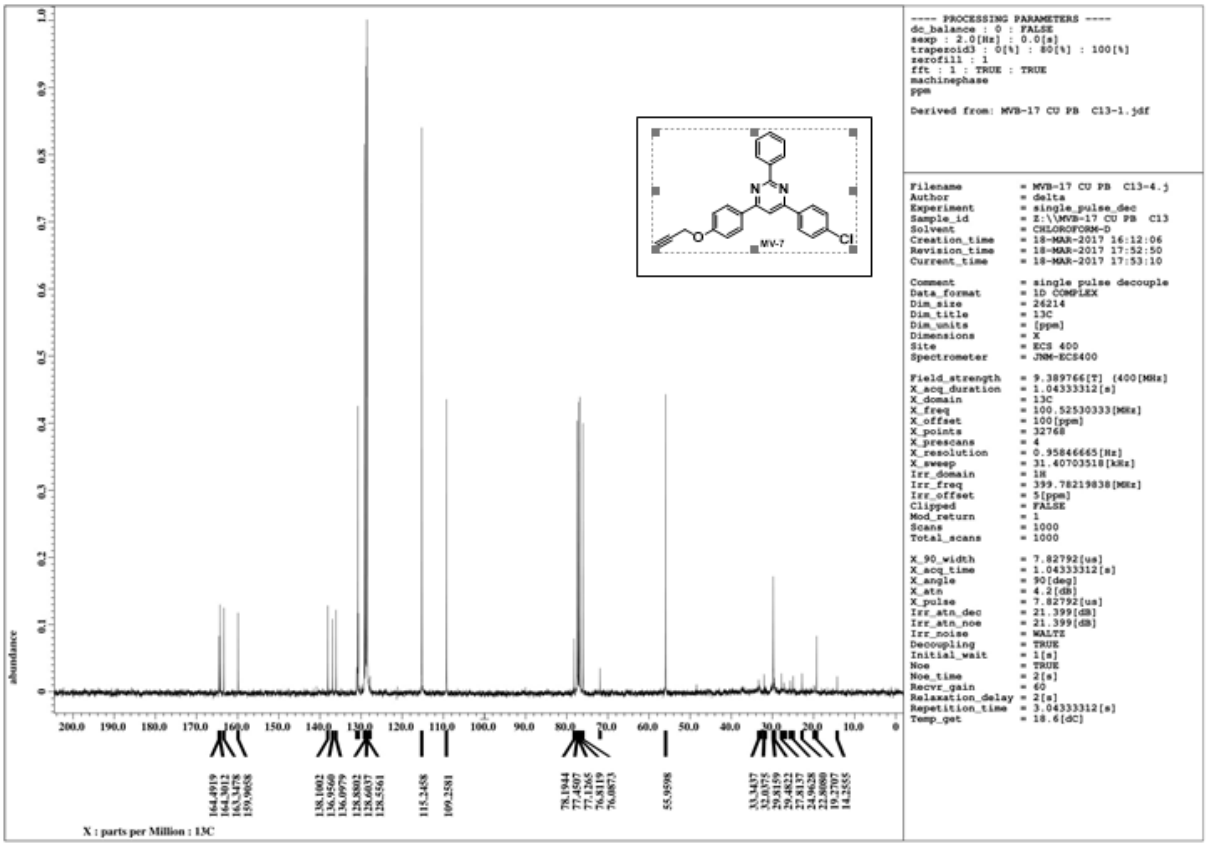
MV-7
Cl
abundance
X : parts per Million : 13C
---- PROCESSING PARAMETERS ----
dc_balance : 0 : FALSE
sexp : 2.0[Hz] : 0.0[s]
trapezoid : 0[%] : 80[%] : 100[%]
zerofill : 1
fft : 1 : TRUE : TRUE
machinephase
ppm
Derived from: MVB-17 CU PB C13-1.jdf
Filename = MVB-17 CU PB C13-4.j
Author = delta
Experiment = single_pulse_dec
Sample_id = I:\\MVB-17 CU PB C13
Solvent = CHLOROFORM-D
Creation_time = 18-MAR-2017 16:12:06
Revision_time = 18-MAR-2017 17:52:50
Current_time = 18-MAR-2017 17:53:10
Comment = single pulse decouple
Data_format = 1D COMPLEX
Dim_size = 26214
Dim_title = 13C
Dim_units = [ppm]
Dimensions = X
Site = ECS 400
Spectrometer = JNM-ECS400
Field_strength = 9.389766[T] (400[MHz]
X_acq_duration = 1.04333312[s]
X_domain = 13C
X_freq = 100.52530333[MHz]
X_offset = 100[ppm]
X_points = 32768
X_prescans = 4
X_resolution = 0.95846665[Hz]
X_sweep = 31.40703518[kHz]
Irr_domain = 1H
Irr_freq = 399.7821983[MHz]
Irr_offset = 5[ppm]
Clipped = FALSE
Mod_return = 1
Scans = 1000
Total_scans = 1000
X_90_width = 7.82792[us]
X_acq_time = 1.04333312[s]
X_angle = 90[deg]
X_atn = 4.2[dB]
X_pulse = 7.82792[us]
Irr_atn_dec = 21.399[dB]
Irr_atn_noe = 21.399[dB]
Irr_noise = WALTZ
Decoupling = TRUE
Initial_wait = 1[s]
Noe = TRUE
Noe_time = 2[s]
Recvr_gain = 60
Relaxation_delay = 2[s]
Repetition_time = 3.04333312[s]
Temp_get = 18.6[dC]

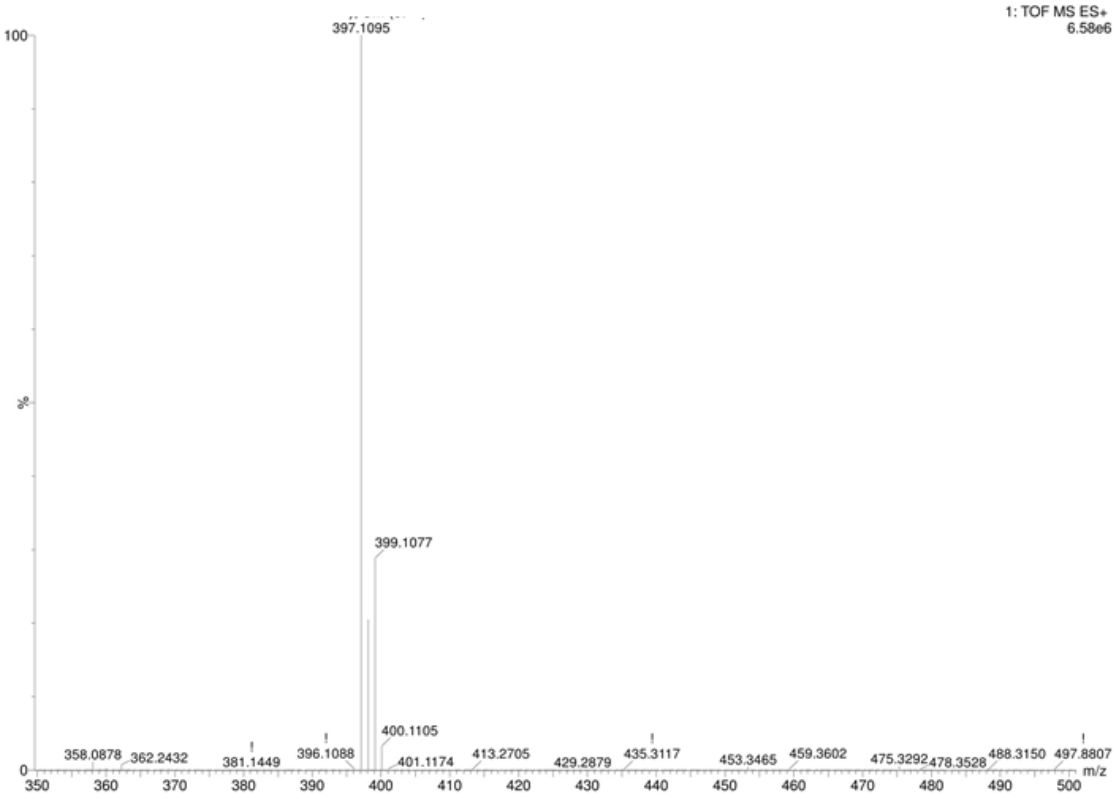
1: TOF MS ES+
6.58e6
100
%
0
397.1095
399.1077
400.1105
358.0878
362.2432
381.1449
396.1088
401.1174
413.2705
429.2879
435.3117
453.3465
459.3602
475.3292
478.3528
488.3150
497.8807
350
360
370
380
390
400
410
420
430
440
450
460
470
480
490
500
m/z

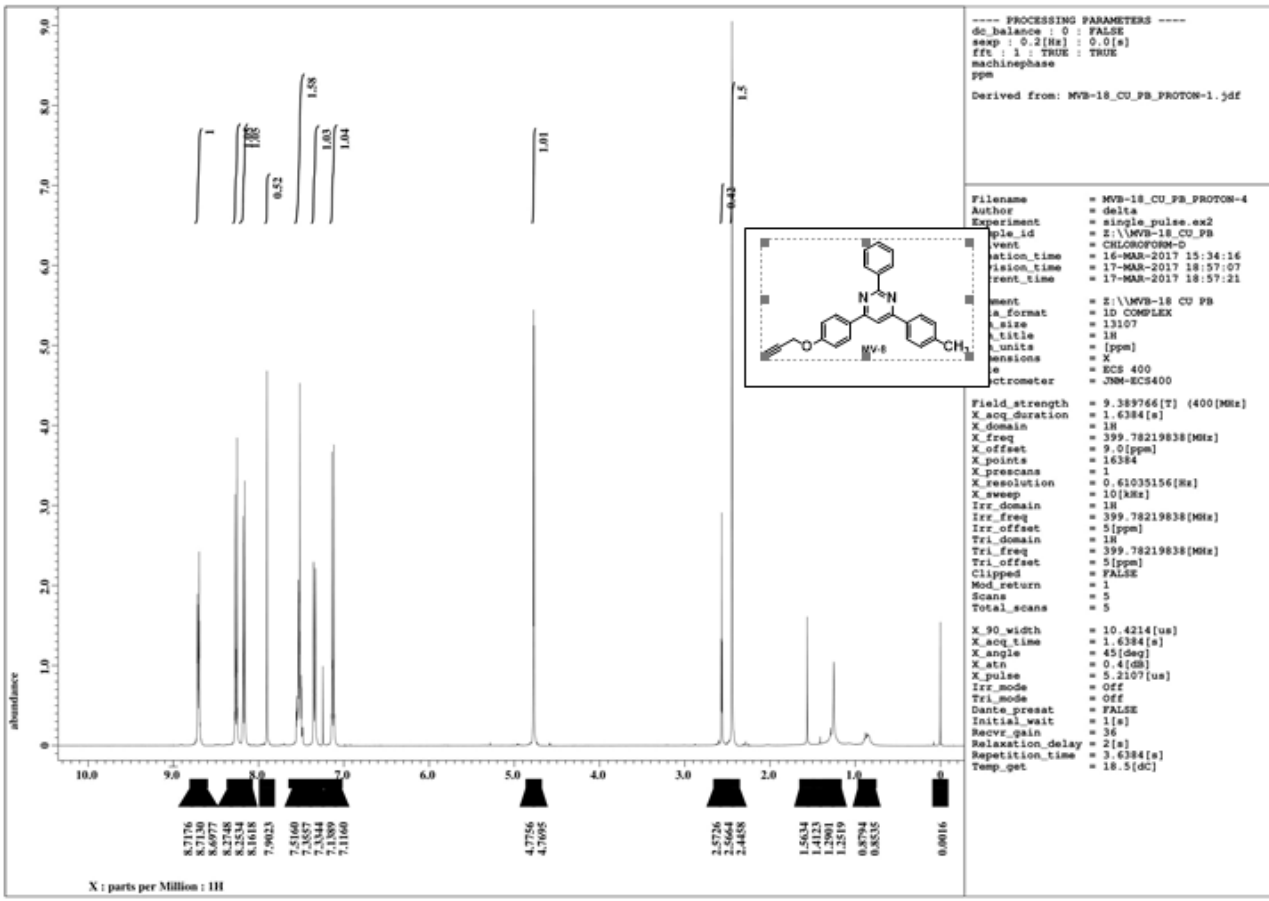
---- PROCESSING PARAMETERS ----
dc_balance : 0 : FALSE
sexp : 0.2[Hz] : 0.0[s]
fft : 1 : TRUE : TRUE
machinephase
ppm
Derived from: MVB-18_CU_PB_PROTON-1.jdf
Filename = MVB-18_CU_PB_PROTON-4
Author = delta
Experiment = single_pulse.ex2
Sample_id = Z:\\MVB-18_CU_PB
Solvent = CHLOROFORM-D
Creation_time = 16-MAR-2017 15:34:16
Revision_time = 17-MAR-2017 18:57:07
Current_time = 17-MAR-2017 18:57:21
Comment = Z:\\MVB-18 CU PB
Data_format = 1D COMPLEX
Data_size = 13107
Data_title = 1H
Data_units = [ppm]
Dimensions = X
Site = ECS 400
Spectrometer = JNM-ECS400
Field_strength = 9.389766[T] (400[MHz]
X_acq_duration = 1.6384[s]
X_domain = 1H
X_freq = 399.78219838[MHz]
X_offset = 9.0[ppm]
X_points = 16384
X_prescans = 1
X_resolution = 0.61035156[Hz]
X_sweep = 10[kHz]
Irr_domain = 1H
Irr_freq = 399.78219838[MHz]
Irr_offset = 5[ppm]
Tri_domain = 1H
Tri_freq = 399.78219838[MHz]
Tri_offset = 5[ppm]
Clipped = FALSE
Mod_return = 1
Scans = 5
Total_scans = 5
X_90_width = 10.4214[us]
X_acq_time = 1.6384[s]
X_angle = 45[deg]
X_atn = 0.4[dB]
X_pulse = 5.2107[us]
Irr_mode = Off
Tri_mode = Off
Dante_presat = FALSE
Initial_wait = 1[s]
Recvr_gain = 36
Relaxation_delay = 2[s]
Repetition_time = 3.6384[s]
Temp_get = 18.5[dC]
MV-8
abundance
X : parts per Million : 1H

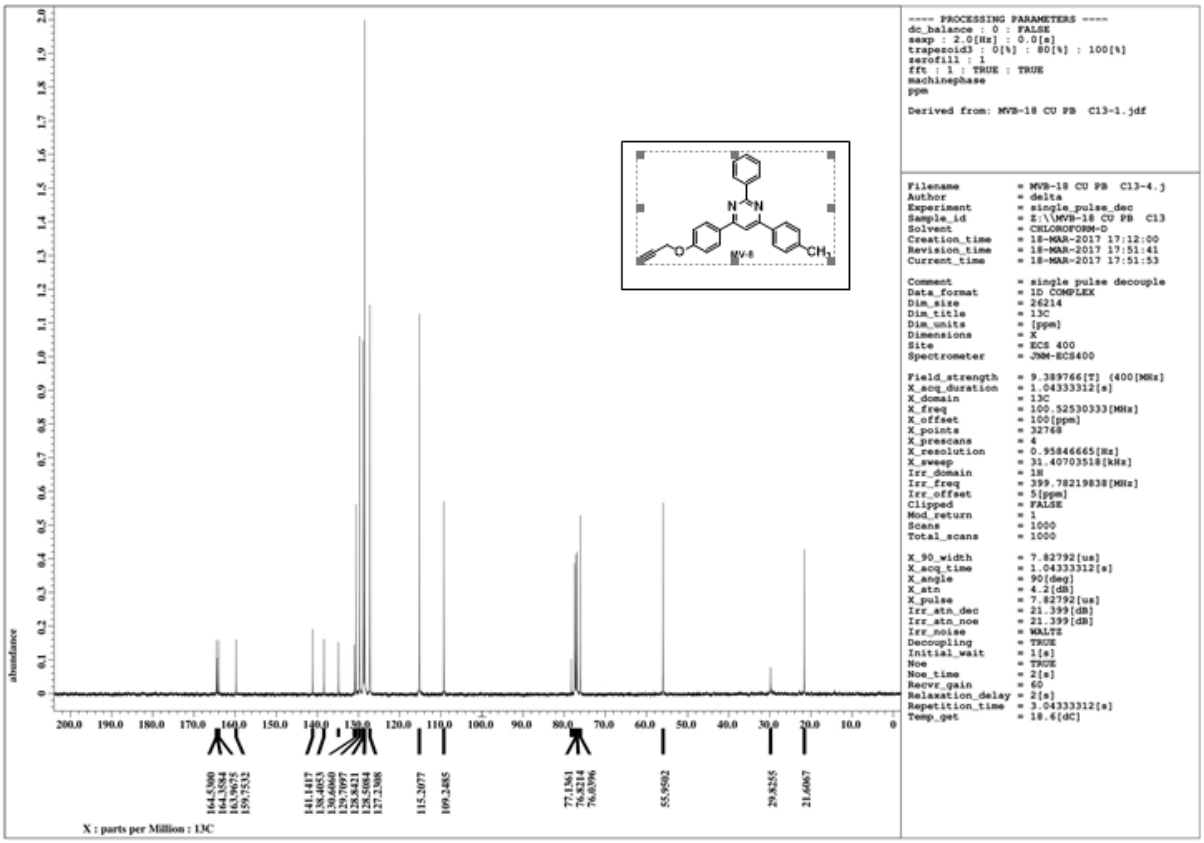
MV-8
abundance
X : parts per Million : 13C
164.5300
164.3584
163.9675
159.7532
141.1417
138.4053
130.6060
129.7097
128.5421
125.5644
123.2308
115.2077
109.2485
77.1361
76.8214
76.8096
55.9502
29.8255
21.6067
---- PROCESSING PARAMETERS ----
dc_balance : 0 : FALSE
sexp : 2.0[Hz] : 0.0[s]
trapezoid3 : 0[%] : 80[%] : 100[%]
zerofill : 1
fft : 1 : TRUE : TRUE
machinephase
ppm
Derived from: MVB-18 CU PB C13-1.jdf
Filename = MVB-18 CU PB C13-4.j
Author = delta
Experiment = single_pulse_dec
Sample_id = Z:\\MVB-18 CU PB C13
Solvent = CHLOROFORM-D
Creation_time = 18-MAR-2017 17:12:00
Revision_time = 18-MAR-2017 17:51:41
Current_time = 18-MAR-2017 17:51:53
Comment = single pulse decouple
Data_format = 1D COMPLEX
Dim_size = 26214
Dim_title = 13C
Dim_units = [ppm]
Dimensions = X
Site = ECS 400
Spectrometer = JNM-ECS400
Field_strength = 9.389766[T] (400[MHz]
X_acq_duration = 1.04333312[s]
X_domain = 13C
X_freq = 100.52530333[MHz]
X_offset = 100[ppm]
X_points = 32768
X_prescans = 4
X_resolution = 0.95846665[Hz]
X_sweep = 31.40703518[kHz]
Irr_domain = 1H
Irr_freq = 399.78219838[MHz]
Irr_offset = 5[ppm]
Clipped = FALSE
Mod_return = 1
Scans = 1000
Total_scans = 1000
X_90_width = 7.82792[us]
X_acq_time = 1.04333312[s]
X_angle = 90[deg]
X_atn = 4.2[dB]
X_pulse = 7.82792[us]
Irr_atn_dec = 21.399[dB]
Irr_atn_noe = 21.399[dB]
Irr_noise = WALTZ
Decoupling = TRUE
Initial_wait = 1[s]
Noe = TRUE
Noe_time = 2[s]
Recvr_gain = 60
Relaxation_delay = 2[s]
Repetition_time = 3.04333312[s]
Temp_get = 18.6[dC]

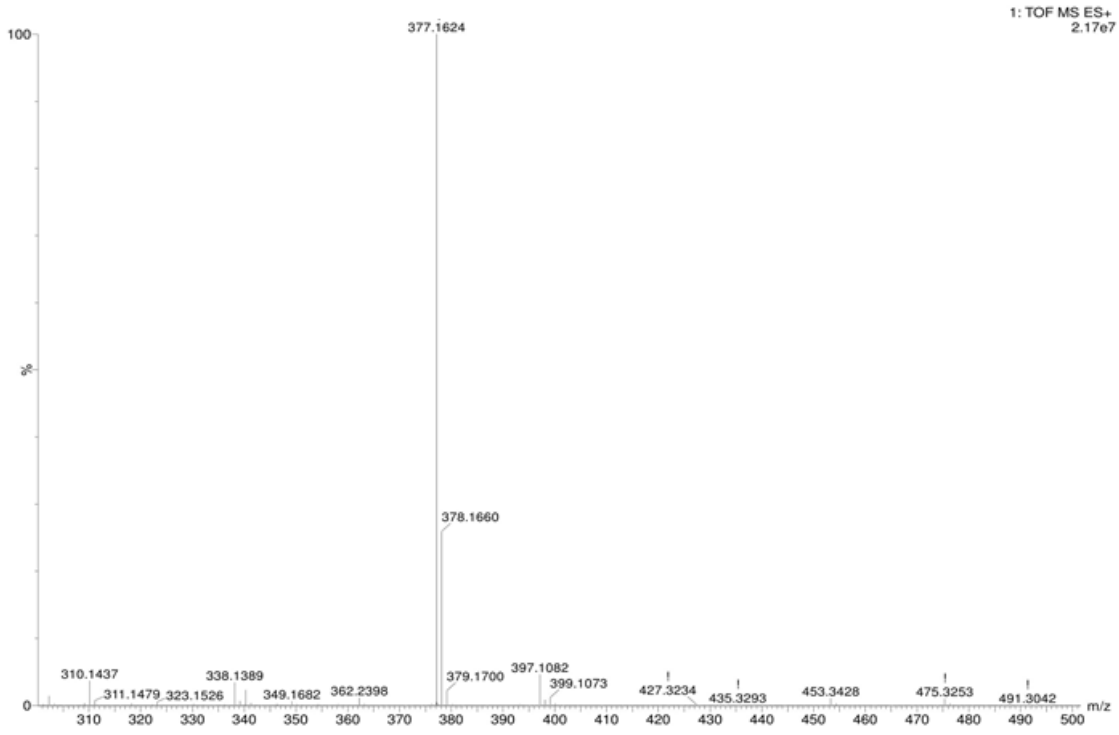
1: TOF MS ES+
2.17e7
100
%
0
377.1624
378.1660
310.1437
311.1479
323.1526
338.1389
349.1682
362.2398
379.1700
397.1082
399.1073
427.3234
435.3293
453.3428
475.3253
491.3042
310
320
330
340
350
360
370
380
390
400
410
420
430
440
450
460
470
480
490
500
m/z

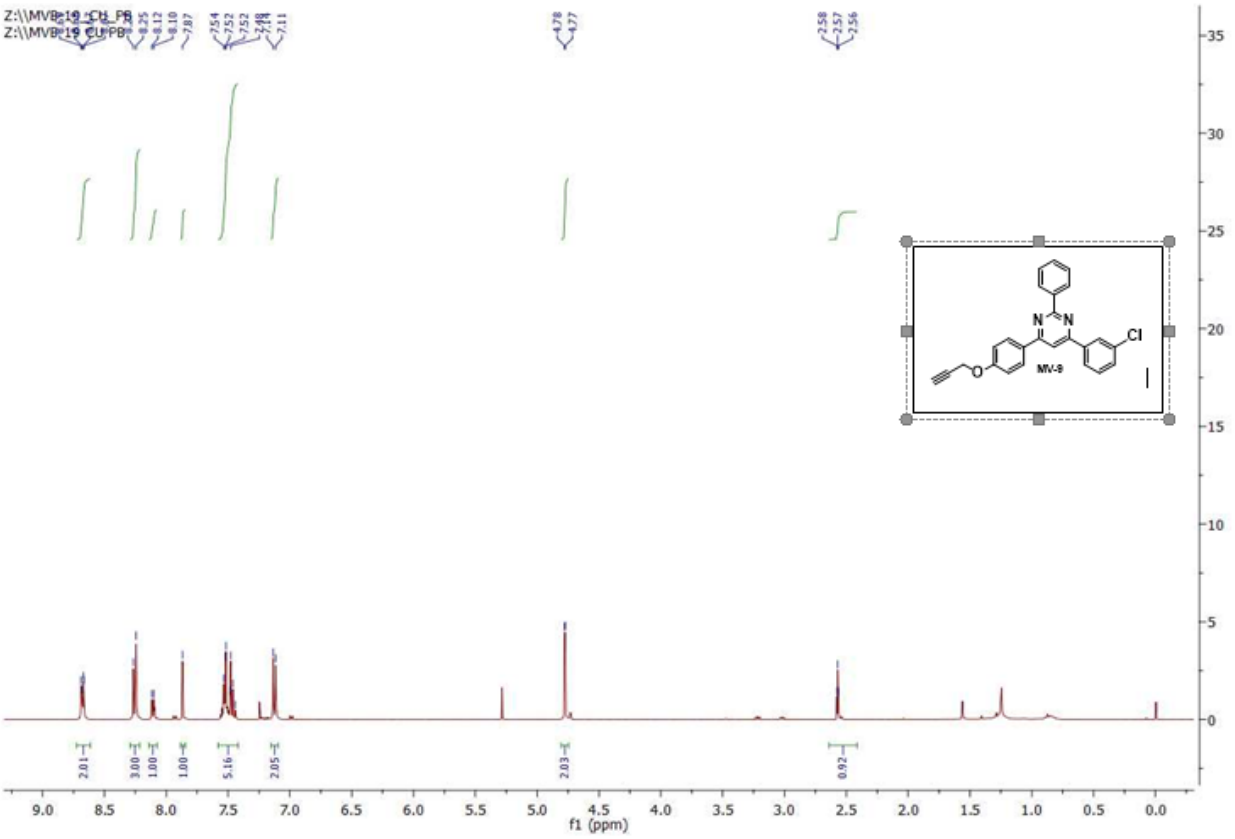
Z:\\MVB-19 CU_PB
Z:\\MVB-19 CU_PB
8.25
8.12
8.10
7.87
7.54
7.52
7.52
7.49
7.48
7.11
4.78
4.77
2.58
2.57
2.56
N
N
Cl
O
MV-9
2.01
3.00
1.00
1.00
5.16
2.05
2.03
0.92
f1 (ppm)

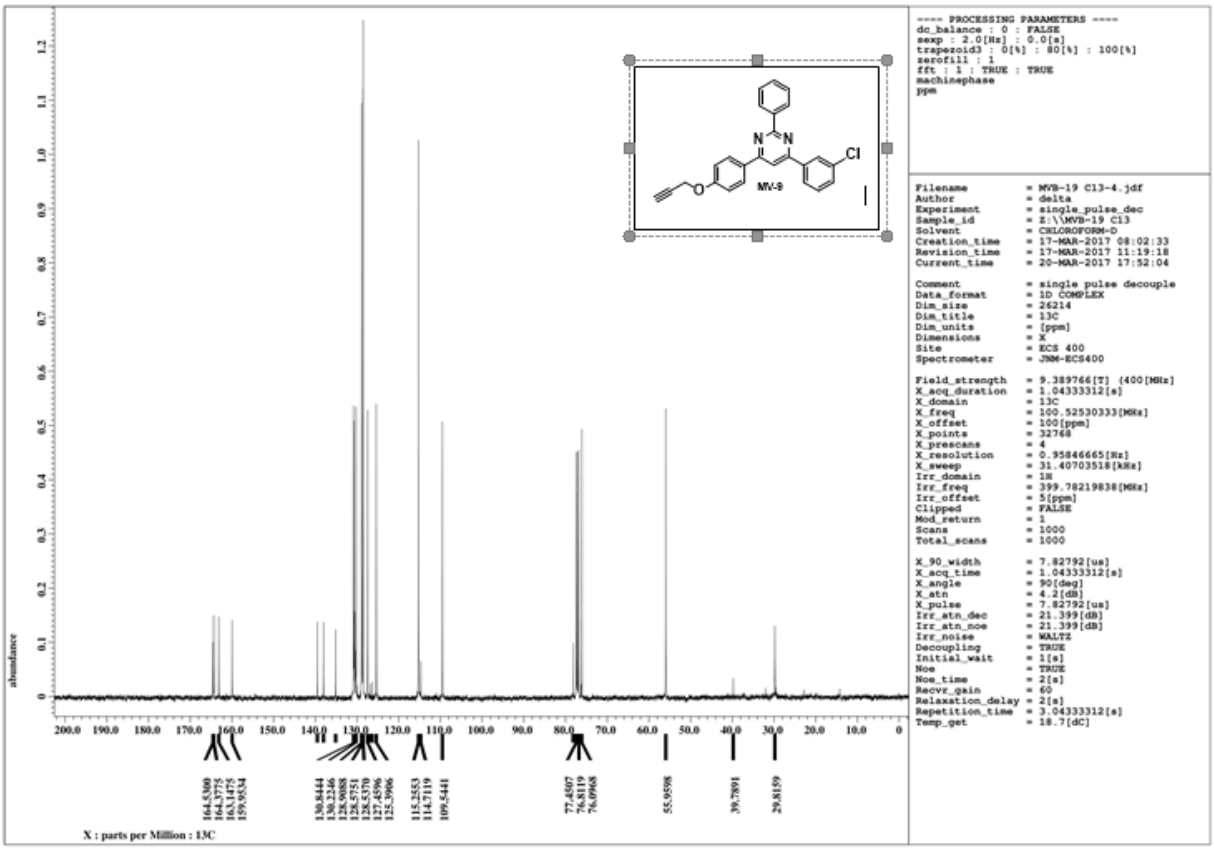
abundance
MV-9
Cl
N
N
O
164.5309
164.3775
163.1475
159.9534
139.8444
138.2244
128.9088
128.5751
128.5370
127.4596
125.5986
115.3553
114.7119
109.5441
77.4507
76.8119
76.0968
55.9598
39.7891
29.8159
X : parts per Million : 13C
==== PROCESSING PARAMETERS ====
dc_balance : 0 : FALSE
sexp : 2.0[Hz] : 0.0[s]
trapezoid3 : 0[%] : 80[%] : 100[%]
zerofill : 1
fft : 1 : TRUE : TRUE
machinephase
ppm
Filename = MVB-19 C13-4.jdf
Author = delta
Experiment = single_pulse_dec
Sample_id = E:\\MVB-19 C13
Solvent = CHLOROFORM-D
Creation_time = 17-MAR-2017 08:02:33
Revision_time = 17-MAR-2017 11:19:18
Current_time = 20-MAR-2017 17:52:04
Comment = single pulse decouple
Data_format = 1D COMPLEX
Dim_size = 26214
Dim_title = 13C
Dim_units = [ppm]
Dimensions = X
Site = ECS 400
Spectrometer = JNM-ECS400
Field_strength = 9.389766[T] (400[MHz]
X_acq_duration = 1.04333312[s]
X_domain = 13C
X_freq = 100.52530333[MHz]
X_offset = 100[ppm]
X_points = 32768
X_prescans = 4
X_resolution = 0.95846665[Hz]
X_sweep = 31.40703518[kHz]
Irr_domain = 1H
Irr_freq = 399.78219838[MHz]
Irr_offset = 5[ppm]
Clipped = FALSE
Mod_return = 1
Scans = 1000
Total_scans = 1000
X_90_width = 7.82792[us]
X_acq_time = 1.04333312[s]
X_angle = 90[deg]
X_atn = 4.2[dB]
X_pulse = 7.82792[us]
Irr_atn_dec = 21.399[dB]
Irr_atn_noe = 21.399[dB]
Irr_noise = WALTZ
Decoupling = TRUE
Initial_wait = 1[s]
Noe = TRUE
Noe_time = 2[s]
Recvr_gain = 60
Relaxation_delay = 2[s]
Repetition_time = 3.04333312[s]
Temp_get = 18.7[dC]

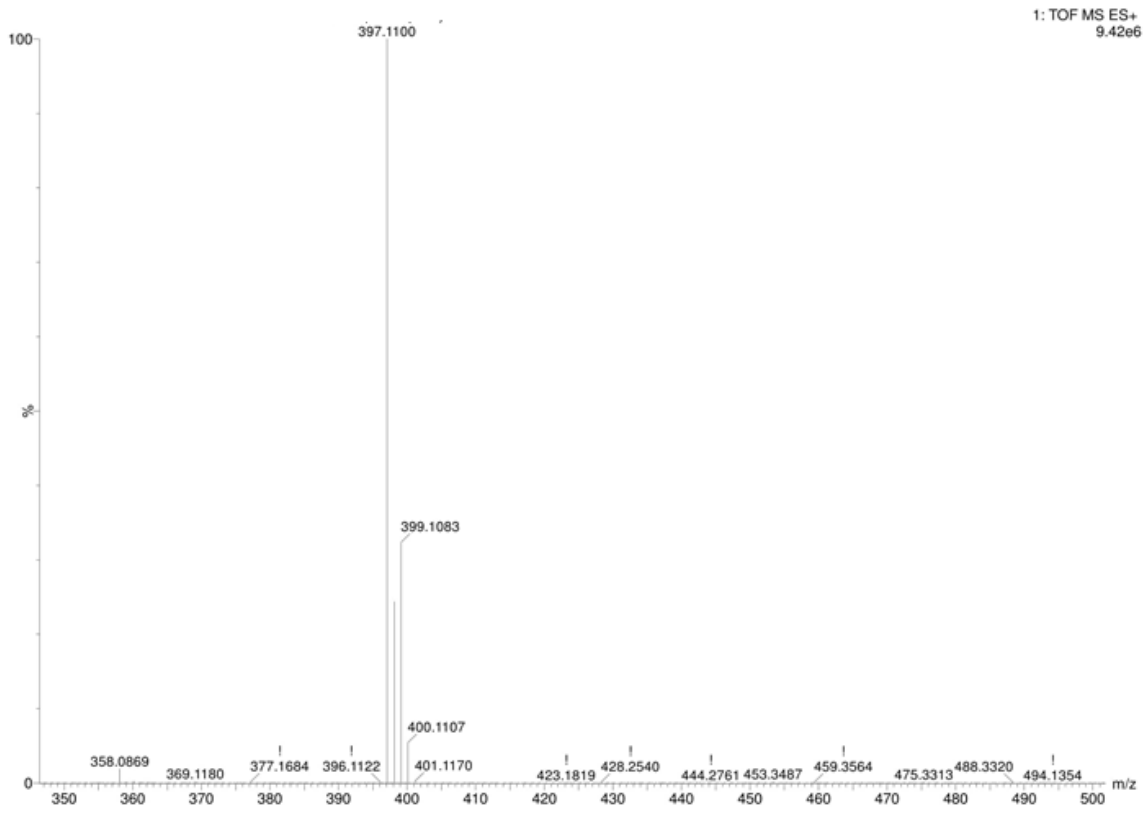
1: TOF MS ES+
9.42e6
100
%
0
397.1100
399.1083
400.1107
358.0869
369.1180
377.1684
396.1122
401.1170
423.1819
428.2540
444.2761
453.3487
459.3564
475.3313
488.3320
494.1354
350
360
370
380
390
400
410
420
430
440
450
460
470
480
490
500
m/z

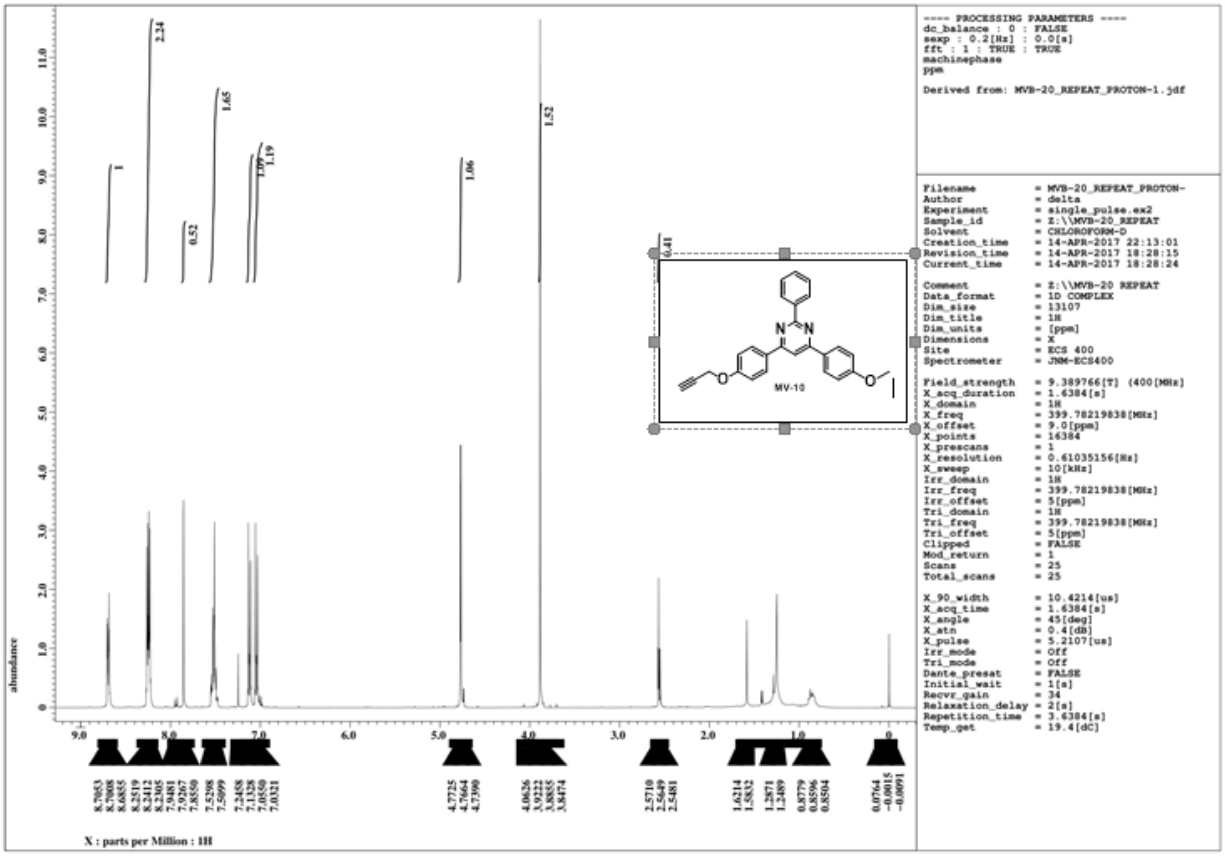
==== PROCESSING PARAMETERS ====
dc_balance : 0 : FALSE
sexp : 0.2[Hz] : 0.0[s]
fft : 1 : TRUE : TRUE
machinephase
ppm
Derived from: MVB-20_REPEAT_PROTON-1.jdf
Filename = MVB-20_REPEAT_PROTON-
Author = delta
Experiment = single_pulse.ex2
Sample_id = E:\\MVB-20_REPEAT
Solvent = CHLOROFORM-D
Creation_time = 14-APR-2017 22:13:01
Revision_time = 14-APR-2017 18:28:15
Current_time = 14-APR-2017 18:28:24
Comment = E:\\MVB-20 REPEAT
Data_format = 1D COMPLEX
Dim_size = 13107
Dim_title = 1H
Dim_units = [ppm]
Dimensions = X
Site = ECS 400
Spectrometer = JNM-ECS400
Field_strength = 9.389766[T] (400[MHz]
X_acq_duration = 1.6384[s]
X_domain = 1H
X_freq = 399.78219838[MHz]
X_offset = 9.0[ppm]
X_points = 16384
X_prescans = 1
X_resolution = 0.61035156[Hz]
X_sweep = 10[kHz]
Irr_domain = 1H
Irr_freq = 399.78219838[MHz]
Irr_offset = 5[ppm]
Tri_domain = 1H
Tri_freq = 399.78219838[MHz]
Tri_offset = 5[ppm]
Clipped = FALSE
Mod_return = 1
Scans = 25
Total_scans = 25
X_90_width = 10.4214[us]
X_acq_time = 1.6384[s]
X_angle = 45[deg]
X_atn = 0.4[dB]
X_pulse = 5.2107[us]
Irr_mode = Off
Tri_mode = Off
Dante_presat = FALSE
Initial_wait = 1[s]
Recvr_gain = 34
Relaxation_delay = 2[s]
Repetition_time = 3.6384[s]
Temp_get = 19.4[dC]
abundance
X : parts per Million : 1H
MV-10

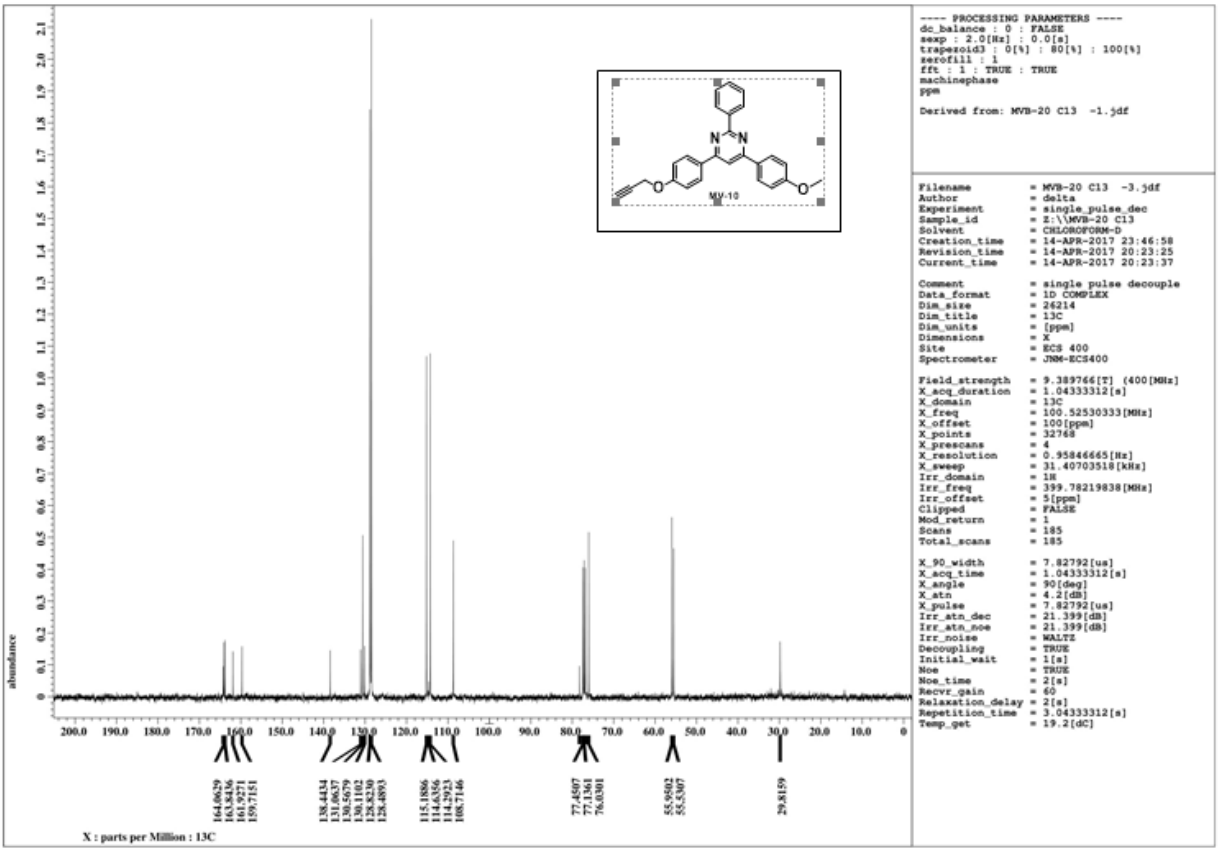


```
---- PROCESSING PARAMETERS ----
dc_balance : 0 : FALSE
sexp : 2.0[Hz] : 0.0[s]
trapezoid3 : 0[%] : 80[%] : 100[%]
zerofill : 1
fft : 1 : TRUE : TRUE
machinephase
ppm

Derived from: MVB-20 C13  -1.jdf
```

```
Filename            = MVB-20 C13  -3.jdf
Author              = delta
Experiment          = single_pulse_dec
Sample_id           = Z:\\MVB-20 C13
Solvent             = CHLOROFORM-D
Creation_time       = 14-APR-2017 23:46:58
Revision_time       = 14-APR-2017 20:23:25
Current_time        = 14-APR-2017 20:23:37

Comment             = single pulse decouple
Data_format         = 1D COMPLEX
Dim_size            = 26214
Dim_title           = 13C
Dim_units           = [ppm]
Dimensions          = X
Site                = ECS 400
Spectrometer        = JNM-ECS400

Field_strength      = 9.389766[T] (400[MHz]
X_acq_duration      = 1.04333312[s]
X_domain            = 13C
X_freq              = 100.52530333[MHz]
X_offset            = 100[ppm]
X_points            = 32768
X_prescans          = 4
X_resolution        = 0.95846665[Hz]
X_sweep             = 31.40703518[kHz]
Irr_domain          = 1H
Irr_freq            = 399.78219838[MHz]
Irr_offset          = 5[ppm]
Clipped             = FALSE
Mod_return          = 1
Scans               = 185
Total_scans         = 185

X_90_width          = 7.82792[us]
X_acq_time          = 1.04333312[s]
X_angle             = 90[deg]
X_atn               = 4.2[dB]
X_pulse             = 7.82792[us]
Irr_atn_dec         = 21.399[dB]
Irr_atn_noe         = 21.399[dB]
Irr_noise           = WALTZ
Decoupling          = TRUE
Initial_wait        = 1[s]
Noe                 = TRUE
Noe_time            = 2[s]
Recvr_gain          = 60
Relaxation_delay    = 2[s]
Repetition_time     = 3.04333312[s]
Temp_get            = 19.2[dC]
```

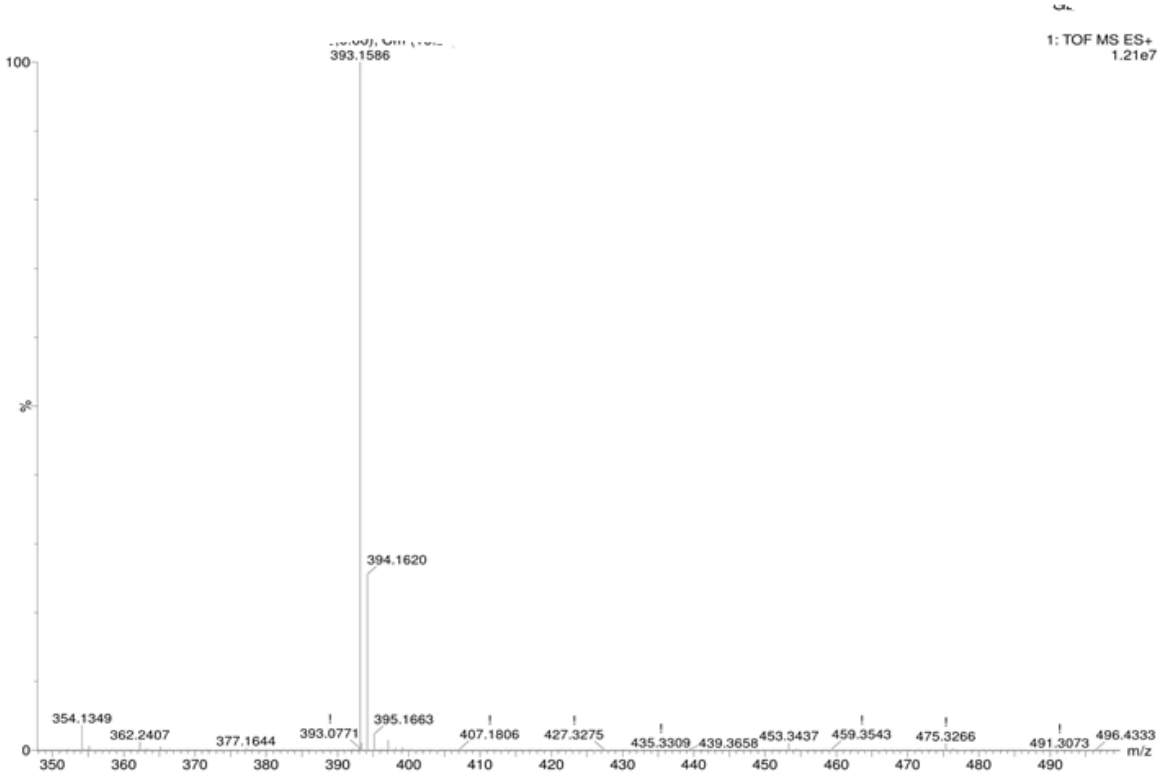
1: TOF MS ES+
1.21e7
393.1586
100
%
0
394.1620
354.1349
362.2407
377.1644
393.0771
395.1663
407.1806
427.3275
435.3309
439.3658
453.3437
459.3543
475.3266
491.3073
496.4333
m/z
350
360
370
380
390
400
410
420
430
440
450
460
470
480
490

URKUND

Urkund Analysis Result

Analysed Document:	plagiarism.docx (D39103781)
Submitted:	5/17/2018 9:14:00 AM
Submitted By:	vpathania18@gmail.com
Significance:	3 %

Sources included in the report:

https://helda.helsinki.fi/handle/10138/41902 https://kundoc.com/pdf-2-heteroarylidene-1-indanone-derivatives-as-inhibitors-of-monoamine-oxidase-.html

https://www.ncbi.nlm.nih.gov/pubmed/27662218

https://www.science.gov/topicpages/s/selective+mao-b+inhibitors

Instances where selected sources appear:

4